Electromagnetic propagation through non-dissipative and dissipative barriers

A thesis presented in partial fulfillment of
the requirements for the degree of
Master of Science
in Physics at
Massey University
Palmerston North, New Zealand

by

Avi Shalav

May 2002

Acknowledgments

There are a number of people whom without their support, this thesis would not have been made possible. Firstly, I would like to thank Neil Pinder my supervisor who has taught me understanding, confidence and ingenuity I had not previously known possible.

Secondly, I would also like to thank my family for their continual love and encouragement.

And finally, I would like to thank my friends and work colleagues who have taught me that persistence does pay off and that 'giving up' is never an option.

Abstract

A Matlab simulation was developed to help visualise and investigate electromagnetic tunnelling through particular non-dissipative and dissipative barriers within a waveguide. The theory behind the simulation is based on a transmission line model that accurately predicts experimental results and is shown to be equivalent to previous numerical and quantum tunnelling models.

A few useful speeds referring to electromagnetic waves have been defined and utilised to calculate the speeds at which different incident time signals penetrate electromagnetic barriers.

Due to bandwidth restrictions, the created incident time signals had wavepacket properties. The importance of resampling an oscillating signal at the appropriate frequency to avoid aliasing has been recognised.

The definition and creation of matched signals that can penetrate long barriers yet remain a single pulse have been investigated. Such signals will have no practical application since the attenuation will deem the transmitted signals immeasurable. However, the speeds through these larger barrier lengths will have a smaller uncertainty since the time delays are longer. Most of the signal distortion depends only on the barrier interfaces rather than the barrier length.

Penetration through dissipative barriers gives speeds below the vacuum speed of light for all barrier lengths investigated. Faster than light speeds are however predicted for penetration through non-dissipative barriers greater than about 4cm.

Contents

List of Figures

Chapter 1

Introduction

1.1 *Tunnelling and the collapse of causality*

Causality allows two different observers to agree on a cause and an effect of a particular event and is a fundamental assumption of modern relativistic physics.

According to Einstein's theory of special relativity, if a signal could travel faster than the speed of light then there would be a violation of causality. Signals would seem to arrive before they departed and they could even appear to travel backwards in time. By making use of superluminal signals it would be possible to communicate with the past, which is not logically possible. To overcome this 'logical disaster' it has been assumed throughout the physics world that no signal may travel faster than c, the speed of light in free space [1]. Speeds greater than c, are defined to be superluminal while speeds less than c are defined to be subluminal.

In recent years, experiments on quantum barrier tunnelling and electromagnetic barrier tunnelling have yielded superluminal speeds creating wide public interest [2, 3]. Experiments in the quantum regime consist of two-photon interferometry [4], or tachyonlike excitations in inverted two level media [5, 6]. Experiments in the electromagnetic regime consist of microwave propagation over short distances using launcher and receiver horns [7], microwave transmission through undersized waveguides [8-11], photonic waveguide/heterostructure tunnelling experiments [12, 13] and more recently total internal reflection in a double prism experiment [14]. Electromagnetic barriers can magnify the time scale up to nanoseconds so microwave experiments can be

compared with theoretical predictions taken from quantum tunnelling which require a less accessible time range [15]. This is because the length of the barrier must be of the order of the wavelength of the radiation for measurable tunnelling to occur. Propagation times in the nanosecond regime can be obtained with microwave barriers (electromagnetic radiation with cm wavelengths).

1.2 *The analogy between quantum and electromagnetic tunnelling*

The analogy between quantum tunnelling and electromagnetic (or photon) tunnelling is well known [16-18]. The analogy is from a similarity between the two fundamental equations governing these seemingly different tunnelling situations. The one dimensional Schrödinger wave equation is the basic relationship for determining wave functions and energy levels of a quantum particle. The time independent Schrödinger equation can be written as

$$\nabla^2\psi + \frac{2m}{\hbar^2}(E-U)\psi = 0 \tag{1.1}$$

Where ψ is the wavefunction, m is the particle mass, $\hbar$ is Planck's constant divided by 2π, E is the particle energy, and U is the uniform potential energy.

The wave equation derived from Maxwell's equations for classical electromagnetic fields is

$$\nabla^2 E = \mu\sigma\frac{\partial E}{\partial t} + \mu\varepsilon\frac{\partial^2 E}{\partial t^2} \tag{1.2}$$

Where μ is the coefficient of permeability of the medium (usually equal to that of free space μ_0), ε is the coefficient of permitivitty of the medium, σ is the conductivity of the medium and in this case, E is the electromagnetic wave function usually a sinusoid of the form $e^{i\omega t-\gamma z}$ where ω is the angular frequency, γ is the complex propagation constant and z is the direction of propagation. If there were no losses (σ =0) then

$$\nabla^2 E = \mu\varepsilon\frac{\partial^2 E}{\partial t^2} \tag{1.3}$$

Doing the differentiation

$$\frac{\partial^2 E}{\partial t^2} = -\omega^2 E \tag{1.4}$$

and substituting in

$$\mu\varepsilon = \frac{n^2}{c^2} \tag{1.5}$$

Where n is the refractive index of the medium and c is the speed of light in a vacuum, Equation (1.3) can be re-written as:

$$\nabla^2 E + \frac{n^2\omega^2}{c^2} E = 0 \tag{1.6}$$

Equations (1.1) and (1.6) are formally identical and if we write:

$$\frac{n^2\omega^2}{c^2} = \frac{2m}{\hbar^2}(E - U) \tag{1.7}$$

Then an electromagnetic wave with frequency ω in a medium with a refractive index of n is analogous to a quantum particle with energy E in a potential U.

Quantum particles are known to 'tunnel' through potential barriers [19-21] and there exist situations where electromagnetic 'tunnelling' also occurs. One situation in the electromagnetic regime where tunnelling occurs is along a waveguide containing a barrier (a region where propagation does not occur). Such a region is said to be evanescent.

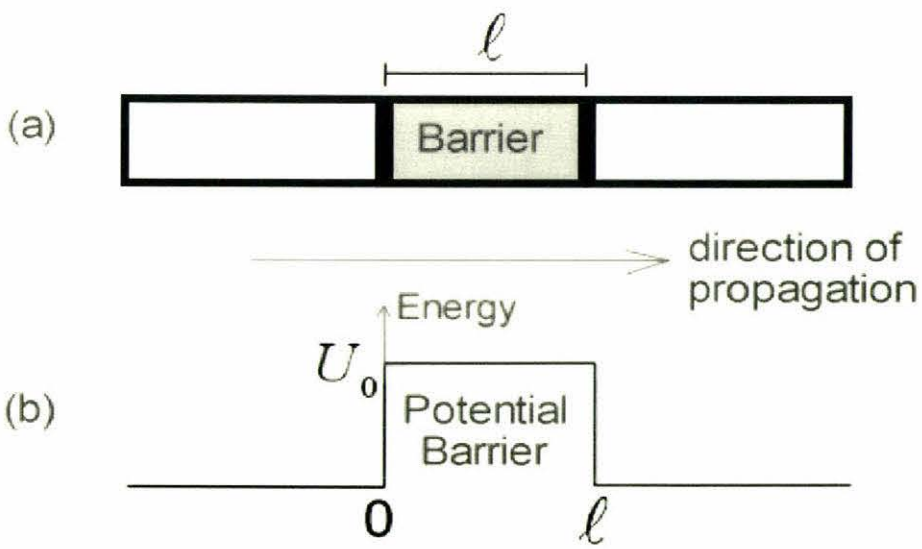

Figure 1.1: Tunnelling analogies. (a) A waveguide with an evanescent barrier of length ℓ. (b) Analogous potential quantum barrier of length ℓ and height U_0.

In this study, the waveguide with a barrier can be considered in 3 sections. It is required that the dominant waveguide mode be freely propagated through the first and third sections, this implies that the signal frequencies f be greater than f_1 (the lower cut-off frequency in regions 1 and 3). It is also required that the dominant mode be evanescent in the second section, this implies that f be less than f_2 (the upper cut-off frequency in region 2), see equation (2.11) in section 2.2.1

1.3 *Tunnelling time and the Hartman effect*

How long does a quantum particle or electromagnetic wave take to tunnel through a barrier region? This question has created much interest and speculation over recent years. In 1962, Thomas E. Hartman published a paper [19] giving analytic expressions for the time spent by a quantum particle tunnelling through a potential barrier. He found that the transmission times were less than the time that would be required for the incident particle to travel a distance equal to the barrier length with speed c. This result leads to a finite tunnelling time that is independent of the barrier length. In the case of electromagnetic tunnelling through a barrier within a waveguide, there is a noticeable time delay. This delay arises from phase changes on transmission through the barrier interfaces and not from the traversal of the barrier. Likewise, studies on the dwell times of a quantum particle tunnelling through a quantum potential barrier have shown that the tunnelling particles spend equal amounts of time near the entrance and exit faces of the barrier, but vanishingly little within the barrier [20, 21]. Because of this, superluminal (faster than light) speeds are predicted for both quantum and electromagnetic tunnelling. Theoretical studies based on the 1-D Klein-Gordon equation show that a Gaussian wavepacket incident on the left side of a barrier, emerges on the right side at an earlier time than would appear to be allowed by causal propagation [22]. It will be shown later in this thesis why a Gaussian signal is the preferred signal to use in such an investigation. The superluminal experiments mentioned in section 1.1 are in accordance with the Hartman effect.

1.4 *Electromagnetic tunnelling through a waveguide*

Throughout the 1990's a group of scientists under the leadership of Günter Nimtz at the University of Cologne carried out 'superluminal' experiments [8-13] using a waveguide with various types of barriers. Their results suggested that for particular barriers, a 'signal' could be sent faster than the speed of light. One of their studies involved the experimental investigation of electromagnetic waveguide tunnelling through both dissipative and non-dissipative barriers [8]. Barrier lengths of 4.9 cm and 6.47 cm were fabricated and the results of this experiment were presented as two graphs, refer to figure 1.2. The first graph showed the modulus of the transmission coefficient as a function of frequency while the second showed the phase shift of the transmission coefficient as a function of frequency. Time domain signals can be constructed from these frequency domain experiments.

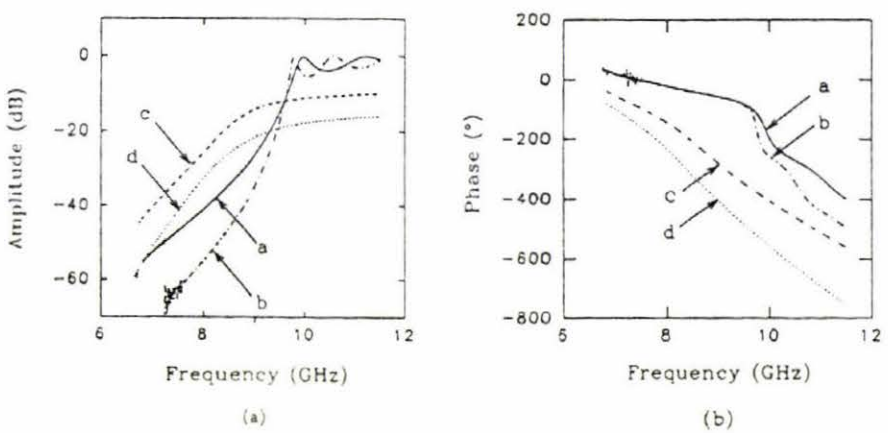

Figure 1.2: Experimental Results. Reproduced from Fig.2, page 1381, Nimtz *et al.* [8]. Transmission coefficient magnitude against frequency (a) and phase against frequency (b) for two barrier lengths a,c=4.9cm and b,d=6.47cm. c and d are filled with a complex dielectric medium.

It was claimed that for the non-dissipative barriers, the traversal time was independent of barrier length resulting in superluminal speeds. The group speeds that were calculated from the phase time for the 7GHz component gave speeds of 1.1c and 1.5c through the 4.9cm and 6.47cm non-dissipative barriers respectively. Their results also showed that with dissipation, the phase shift became dependent on barrier length. The propagation phase change in this case is dominant and the Hartman effect was not observed. Consequently, superluminal speeds were not observed. The group speeds calculated gave speeds of 0.7c for both dissipative barrier lengths (again for the 7GHz component).

Chapter 2

Non-dissipative and dissipative electromagnetic barriers within a waveguide

2.1 *Electromagnetic properties within a waveguide*

2.1.1 *Introduction to the waveguide*

Most undergraduate texts on electromagnetism (for example [23, 24]) have chapters on the propagation of electromagnetic waves through waveguides. Starting with Maxwell's curl equations it is possible to find the intrinsic properties of the dominant wave propagating through a rectangular waveguide, refer to figure 2.1. The results have been summarised below.

Using the axes shown in figure 2.1, a propagating dominant mode will have a transverse electric field component E_x and a transverse magnetic intensity component H_y expressed as

$$\begin{aligned} E_x &= \mid E \mid e^{i\omega t - \gamma z} \\ H_y &= \mid H \mid e^{i\omega t - \gamma z} \end{aligned} \tag{2.1}$$

Where $\mid E \mid$ and $\mid H \mid$ are the electric and magnetic amplitudes respectively, ω is the angular frequency of the component, t is the time and γ is the complex propagation constant. If γ is imaginary, then E_x and H_y are in phase. The ratio of E_x to H_y is called the transverse-wave impedance Z_{xy}.

$$Z_{xy} = \frac{E_x}{H_y} \tag{2.2}$$

Which can be written in terms of γ as

$$Z_{xy} = \frac{i\omega\mu_0}{\gamma} \tag{2.3}$$

γ is a complex number defined as

$$\gamma = \alpha + i\beta \tag{2.4}$$

α is the attenuation constant (real part of γ) and β is the phase constant (imaginary part of γ).

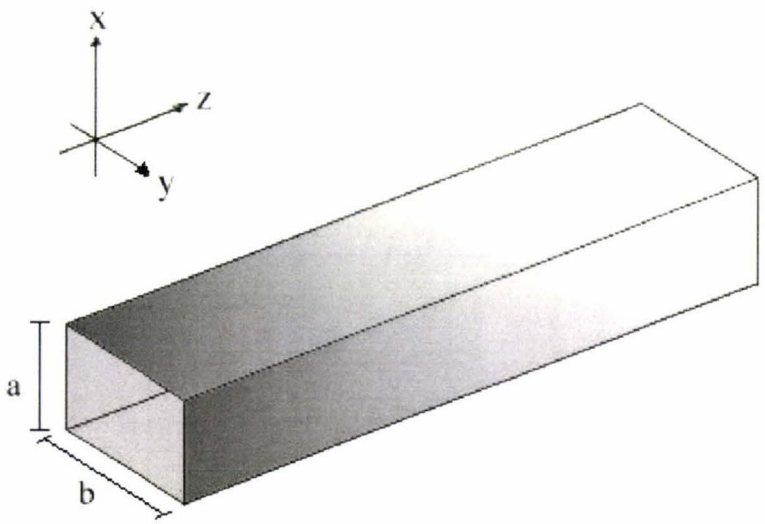

Figure 2.1: A hollow rectangular metallic waveguide. Electromagnetic propagation occurs in the z direction.

For the dominant mode, γ can be written as

$$\gamma = \sqrt{\left(\pi/b\right)^2 + i\omega\mu_0\left(\sigma + i\omega\varepsilon\right)} \tag{2.5}$$

Where σ is the conductivity of the medium in the guide. If this is a lossless dielectric (for example non-dissipative), σ has the value of zero. If $\sigma = 0$, then equation (2.5) simplifies to

$$\gamma = \sqrt{\left(\pi/b\right)^2 - \omega^2\mu_0\varepsilon} \tag{2.6}$$

Notice that if $\left(\pi/b\right)^2 > \omega^2\mu_0\varepsilon$ then γ will be real and consist of only the α component. The wave will therefore be attenuated and propagation is forbidden. This occurs when

the angular frequency ω is 'small'. If $\left(\pi/b\right)^2 < \omega^2\mu_0\varepsilon$ then γ will be imaginary and consist only of the $i\beta$ component. The wave will therefore be propagated without attenuation. This occurs when the angular frequency ω is 'large'. The angular cut-off frequency ω_c occurs when $\gamma = 0$ implying $\left(\pi/b\right)^2 = \omega_c{}^2\mu_0\varepsilon$. Upon rearrangement, the cut-off frequency f_c (in Hz) for the dominant mode in a non-dissipative medium is given by

$$f_c = \frac{1}{2b\sqrt{\mu_0\varepsilon}} \tag{2.7}$$

where $\omega_c = 2\pi f_c$.

2.1.2 *Field configurations within a waveguide*

At low frequencies (but still larger than cut-off) only the dominant H mode can propagate and is characterized by the electric field E_x, and the magnetic intensity H_y, and H_z (which acts in the direction of propagation). Figure 2.2 shows the 'shape' of these fields within a waveguide. The z-axis (direction of travel) goes into the page. The configurations of the transverse fields can be seen in figure 2.3.

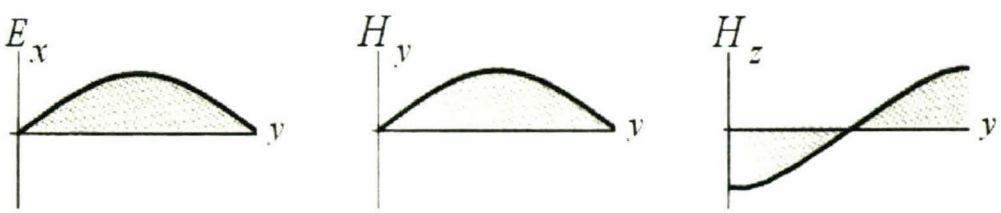

Figure 2.2: Field components of the dominant mode (this diagram is based on Figure 14-11, page 651, Krauss [23])

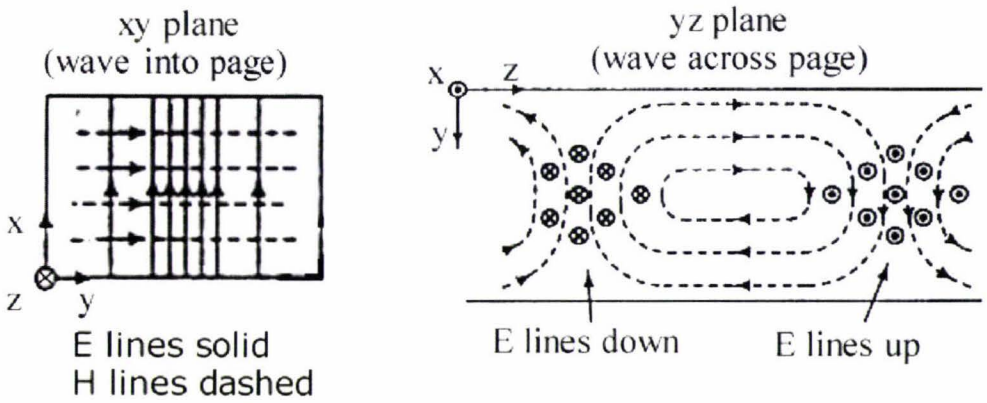

Figure 2.3: Field Configurations for the dominant mode inside a hollow rectangular waveguide (This diagram is based on Figure 14-12, page 651, Krauss [23])

2.2 *Waveguide properties with a potential barrier*

2.2.1 *Design of a waveguide with a potential barrier*

A waveguide similar to that of figure 2.1, can be designed such that a barrier exists within the guide. Such a waveguide would have 3 separate regions. Regions 1 and 3 would have the same electrical properties and dimensions so that only the dominant mode could propagate through them. Since $n = \sqrt{\varepsilon/\varepsilon_0}$ (where n is the refractive index and ε is the permittivity of the appropriate region) and $c = 1/\sqrt{\mu_0\varepsilon_0}$, equation (2.7) can be re-written in terms of the refractive index n of the medium and vacuum speed of light c as

$$f_c = \frac{c}{2bn} \quad \text{(For the non-dissipative dominant mode)} \tag{2.8}$$

Region 2 would be made to act as an electromagnetic barrier. This can be done in one of two practical ways. Firstly by decreasing the width of the guide (reducing the cross-section). In this case, the refractive index is the same through all 3 regions. Secondly by keeping the dimensions the same and changing the medium in region 2. This is the more sensible approach, first because it is easier to manufacture but more importantly because the boundary conditions on the electric and magnetic fields at the barrier interfaces are

easier to apply. A medium must be chosen such that the refractive index in region 2 is smaller than the two regions on either side of it, refer to figure 2.4.

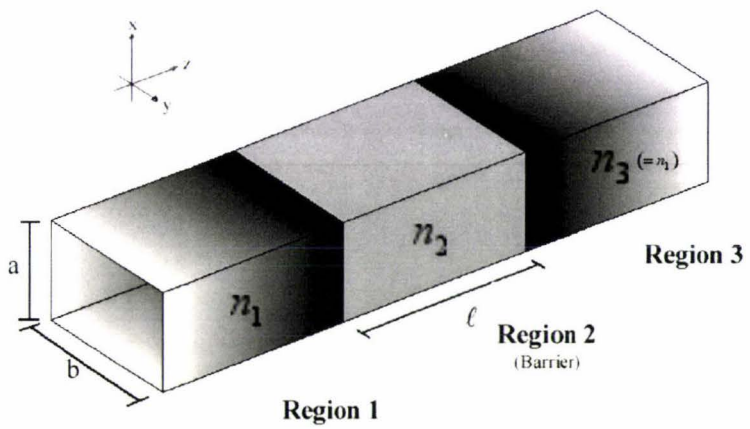

Figure 2.4: A Waveguide with a barrier of length ℓ. Regions 1 and 3 have the same refractive index. Region 2 can act as a barrier if $n_2 < n_1$.

This system will act as a waveguide barrier to the dominant mode if the frequency range f obeys

$$f_1 < f < f_2 \tag{2.9}$$

Where $f_1 = \frac{c}{2bn_1}$ allowing propagation in regions 1 and 3 and $f_2 = \frac{c}{2bn_2}$ forbidding propagation in region 2.

2.2.2 *Penetration through non-dissipative and dissipative waveguide barriers*

Both dissipative ($\sigma \neq 0$) and non-dissipative ($\sigma = 0$) barriers have been fabricated and investigated experimentally [8] by changing the refractive index of region 2 (leaving the dimensions unchanged). This section outlines the important properties of the experimental set-up of the paper presented by Nimtz *et al.* [8].

A waveguide similar to figure 2.4 was used. Regions 1 and 3 were filled with paraffin wax (a dielectric) which has a refractive index of 1.5 (implying $n_1 = n_3 = 1.5$). The lower cut-off frequency of these regions was calculated to be 6.33GHz. This is the lowest frequency at which propagation can occur through an infinitely long section and is called the lower frequency cutoff. Propagation without attenuation occurs in regions 1 and 3 implying that the propagation constant consists only of the imaginary phase constant part. That is

$$\gamma_1 = \gamma_3 = i\beta \tag{2.10}$$

γ_1 and γ_3 are the propagation constants in regions 1 and 3 respectively.

For the non-dissipative case, region 2 was filled with air ($n_2 = 1$), which implies that propagation cannot occur through an infinitely long section at frequencies less than 9.49GHz, regions 1, 2 and 3 constitute a barrier for frequencies f constrained such that

$$6.33GHz < f < 9.49GHz \tag{2.11}$$

Comparison of equation 2.11 with equation 2.9 yields $f_1 = 6.33GHz$ and $f_2 = 9.49GHz$.

For the dissipative case, region 2 was filled with carbon loaded urethane foam which had a complex refractive index ($n_2 = 1.16 + i0.07$). Because the refractive index has an imaginary component, the cut-off frequency is also complex and the allowed frequencies f are no longer clearly defined.

For the non-dissipative barrier, only attenuation occurs and the propagation constant in region 2 (γ_2) will only consist of the attenuation constant.

$$\gamma_2 = \alpha \tag{2.12}$$

For a dissipative barrier, the propagation constant is complex implying γ_2 is of the form

$$\gamma_2 = \alpha_2 + i\beta_2 \tag{2.13}$$

where α_2 and β_2 are the attenuation and phase constants respectively in region 2.

For each barrier type, two barrier lengths ℓ, 4.9cm and 6.47cm were investigated by Nimtz *et al.* [8]. The width *b* of the guide was 1.58cm. The height *a* is not important since the experiment only relies on the presence of the dominant mode. The results of this experiment have already been presented in figure 1.2.

2.2.3 *The Frequency Constraints*

As mentioned in the previous section, the relevant frequencies f were constrained between the lower-cutoff (6.33GHz) and upper-cutoff (9.49GHz) frequencies. For the non-dissipative barrier, these cutoff frequencies were calculated using equation 2.8 but using the appropriate refractive index (depending on the region). Figure 2.5 shows the Brillouin diagram (graph of f against β) for regions 1 and 3 of a selected waveguide. Only the dominant mode ($m=1$) propagates between 6.33GHz and 12.65GHz. Higher order modes are shown in figure 2.5 although they were not allowed in this study. In general,

$$\beta = \sqrt{(2\pi f)^2 \mu_0 \varepsilon - m\pi^2 / b^2} \tag{2.14}$$

If the frequency were to be increased, more modes could start to propagate. The shape of the curves which make up a Brillouin diagram are dependent on the refractive index n. Decreasing n increases the lower cutoff frequency, refer to figure 2.6. The lower-cutoff frequency for the non-dissipative barrier is 9.49GHz. Frequencies above this allow the dominant mode to propagate through the barrier.

The lower-cutoff frequency for region 2 acts as the upper-cutoff frequency for the allowed frequencies since propagation through this region is to be forbidden. Strictly speaking, propagation does occur since the barrier is not infinitely long and reflections play a significant role, as will be discussed in section 2.3.3.

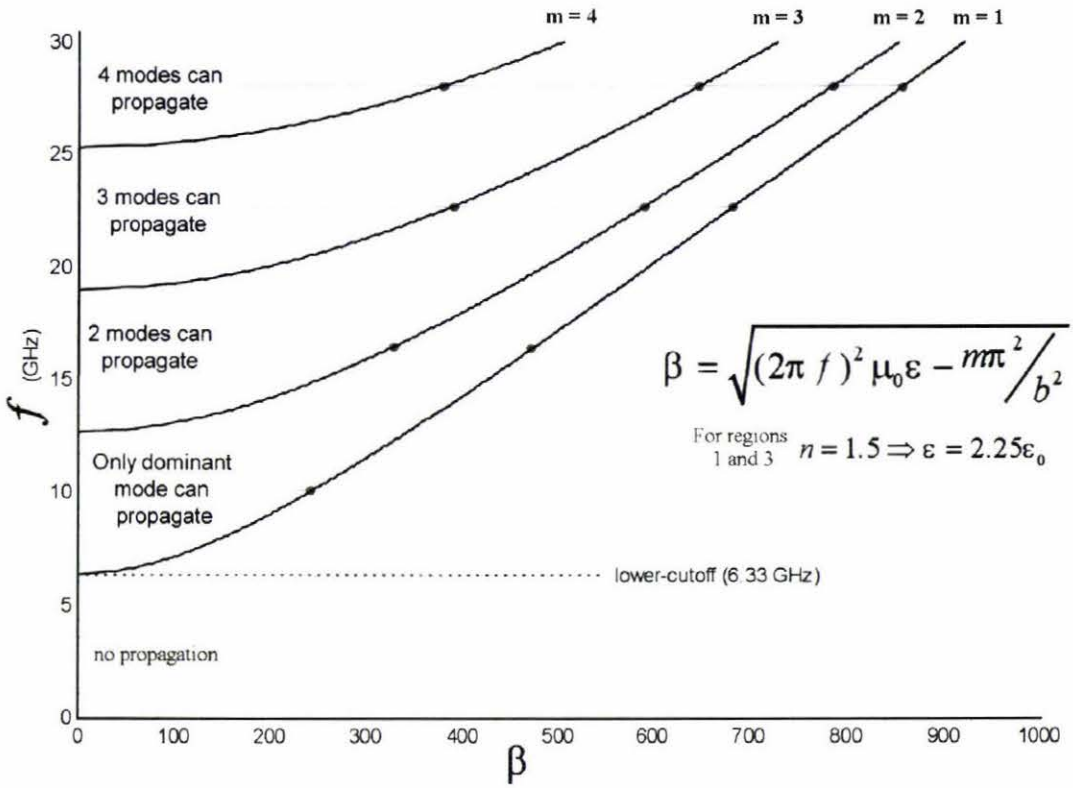

Figure 2.5: Brillouin Diagram for the propagation in a rectangular dielectric filled waveguide. The coefficient of permittivity is $2.5\varepsilon_0$ and the guide width b is 1.58cm.

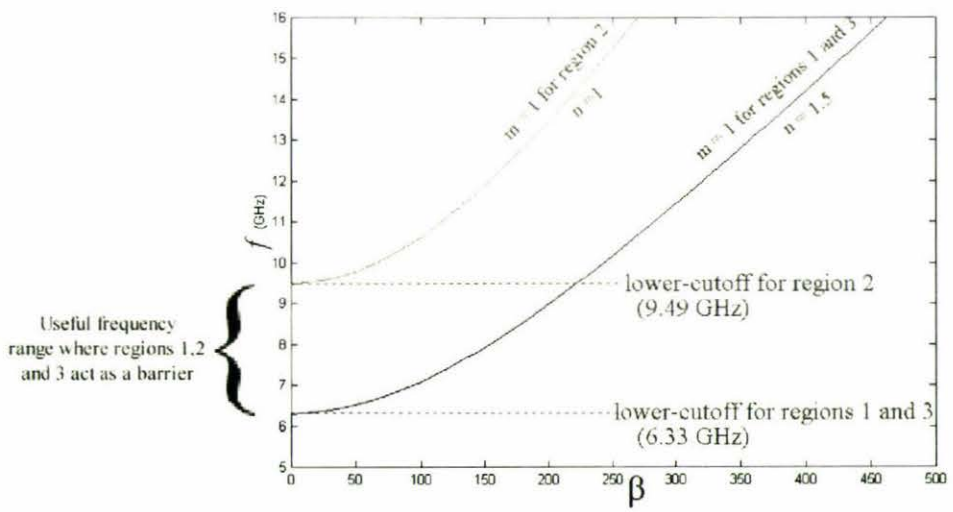

Figure 2.6: Brillouin Diagram comparing dominant mode frequency bands through a waveguide with a non-dissipative barrier.

2.2.4 *Electromagnetic properties of a non-dissipative barrier*

Figure 2.6 shows that at frequencies between 6.33GHz and 9.49GHz the propagation constant through both regions 1 and 3 (γ_1 and γ_3 respectively) are purely imaginary. Solving for β from equation (2.6) gives

$$\beta = \sqrt{\omega^2 \mu_0 \varepsilon - \pi^2 / b^2} \tag{2.15}$$

Implying

$$\gamma_1 = \gamma_3 = i\sqrt{\omega^2 \mu_0 \varepsilon - \pi^2 / b^2} \tag{2.16}$$

The traverse fields are in phase and the wave impedance of both regions 1 and 3 (Z_1 and Z_3 respectively) are real. From equation (2.3) it can be shown

$$Z_1 = Z_3 = \frac{\omega \mu_0}{\beta} \tag{2.17}$$

Similarly figure 2.6 shows that the propagation constant through region 2 (γ_2) through the non-dissipative barrier between 6.33GHz and 9.49GHz is real and α is given by

$$\alpha = \sqrt{\pi^2 / b^2 - \omega^2 \mu_0 \varepsilon} \tag{2.18}$$

Equation (2.13) implies

$$\gamma_2 = \sqrt{\pi^2 / b^2 - \omega^2 \mu_0 \varepsilon} \tag{2.19}$$

The wave impedance through region 2 (Z_2) is inductive (imaginary) and given by

$$Z_2 = \frac{i\omega \mu_0}{\alpha} \tag{2.20}$$

2.2.5 *Electromagnetic properties of a dissipative barrier*

Strictly speaking, the dissipative barrier is not a barrier at all. This is because the propagation constant is complex which implies that a signal is not only attenuated but also propagated, a condition which is not allowed if the region is to act as a barrier. Nimtz *et al.* [8] considered the region to act as a barrier if $\alpha_2 > \beta_2$. It was found that the allowed frequencies were further restricted such that

$$6.33GHz < f < 8.20GHz \tag{2.21}$$

Nevertheless, important properties relating to the effect the dissipative 'barrier' has on the signal can be calculated and analysed.

Regions 1 and 3 are the same as for the non-dissipative investigaiton since these regions are left unaltered. The propagation constant through region 2 is complex and comprises of real α_2 and imaginary β_2 components. The attenuation constant α_2 for the dissipative barrier is calculated to be

$$\alpha_2 = \frac{1}{2}\left\{\frac{\pi^2}{b^2} - \omega^2\mu_0\varepsilon_2 + \sqrt{\left(\frac{\pi^2}{b^2} - \omega^2\mu_0\varepsilon_2\right)^2 + (\omega\mu_0\sigma)^2}\right\}^{1/2} \tag{2.22}$$

And the phase constant through the barrier β_2 is calculated to be

$$\beta_2 = \frac{\omega\mu_0\sigma}{2\alpha_2} \tag{2.23}$$

Details of these calculations can be found in appendix A.1.

The wave impedance is also complex and is given by

$$Z_2 = \frac{i\omega\mu_0}{\gamma_2} \tag{2.24}$$

2.3 *Numerical and analytical models for the transmission coefficient through non-dissipative and dissipative barriers*

2.3.1 *A Quantum model*

By suppressing the time variation, Gasiorowicz [25] defines an analytical solution for the transmission coefficient T through a quantum potential barrier identical to the diagram shown in figure 1.1(b). Assuming z to be the direction of propagation, the general solution of Schrödinger's equation (1.1) within the barrier will be

$$\psi(z) = Ae^{-\kappa_1 z} + Be^{\kappa_1 z} \qquad |z| < \ell/2 \tag{2.25}$$

where A and B are constants, ℓ is the barrier length and $\kappa_1 = \sqrt{2mE/\hbar^2}$ is also a constant.

The general solutions outside the barrier are

$$\begin{aligned} \psi(z) &= e^{i\kappa_1 z} + Re^{-i\kappa_1 z} && z < -\ell/2 \\ \psi(z) &= Te^{i\kappa_1 z} && z > \ell/2 \end{aligned} \tag{2.26}$$

where R and T are the reflection and transmission coefficients respectively. The constants are found by matching the boundary conditions at $z = \pm \ell/2$.

Working through the algebra results in a transmission coefficient given by

$$T = \frac{2\kappa_1\kappa_2}{2\kappa_1\kappa_2 \cosh(\kappa_2\ell) + i(\kappa_1^{\,2} - \kappa_2^{\,2})\sinh(\kappa_2\ell)} \tag{2.27}$$

where $\kappa_2 = \sqrt{2m(U-E)/\hbar^2}$.

This implies the magnitude of T can be written as

$$|T| = \frac{1}{\sqrt{1 + \left[\frac{(\kappa_1^{\,2} + \kappa_2^{\,2})}{(2\kappa_1\kappa_2)}\sinh(\kappa_2\ell)\right]^2}} \tag{2.28}$$

2.3.2 *Previous waveguide models*

An accurate waveguide model was devised by taking the propagation constant to be an eigenvalue of the fundamental mode. Theoretical equations relating to the phase and amplitude have been published [26] and compared [17] and are in full agreement with the experimental results. By resolving the required coefficients using the characteristic determinant method, precise expressions for the transmission and reflection coefficients were constructed for a multi-layered structure. The characteristic determinant D of a multi-layered structure with N interfaces written in terms of the propagation constants (γ_1 and γ_2) through a guide of length ℓ was calculated by Cuevas *et al.* [26] to be:

$$D = e^{\gamma_1\ell}\left\{\cos\left(\frac{Nqb}{2}\right) - i\frac{\sin\left(Nqb/2\right)}{\sin(qb)} \times \sqrt{\sin^2(qb) + \left(-\frac{1}{2}\left(\frac{\gamma_2}{i\gamma_1} + \frac{i\gamma_1}{\gamma_2}\right)\sinh(-\gamma_2\ell)\right)^2}\right\} \tag{2.29}$$

where b is the waveguide width and q plays the role of 'quasimomentum' of the system and is defined by

$$\cos(qb) = \cos(i\gamma_1)\cosh(-\gamma_2 d) - \frac{1}{2}\left(\frac{i\gamma_1}{\gamma_2} - \frac{\gamma_2}{i\gamma_1}\right)\sin(\gamma_2 \ell)\sinh(-i\gamma_2 d) \tag{2.30}$$

where d is the separation of the layers of the multi-layered structure.

The transmission coefficient T is the inverse of the characteristic determinant implying

$$T = 1/D \tag{2.31}$$

This expression for the transmission coefficient is true for both the non-dissipative and dissipative barriers.

For a single barrier, $N = 2$ and $d = 0$ (no distance between the barriers since only one barrier exists) and equation (2.29) is greatly simplified. Using this result for the non-dissipative case, and re-writing γ_1 and γ_2 in terms of the constants α and β one finds

$$|T| = \frac{1}{\sqrt{1 + \left[\left(\frac{\alpha^2 + \beta^2}{2\alpha\beta}\right)\sinh(\alpha\ell)\right]^2}} \tag{2.32}$$

These theoretical results for a single barrier (two interfaces) agree with experiment over the whole frequency range considered (even at frequencies above cut-off). This model for the transmission coefficient agrees with the experimental results for the non-dissipative case, but not for the dissipative case.

This model is based on Maxwell's equations yet agrees with the non-causal results from the experiment described in section 1.4. Another model using Maxwell's theory but based on the time dependent Green's function for a simplified model has also been studied [27]. The solutions obtained also agree with the experimental results from section 1.4.

2.3.3 *A transmission line model*

As mentioned earlier, there exists a time delay when an electromagnetic signal passes through a barrier within a waveguide. This delay is due to a phase change at each of interfaces. Relative amplitudes (including the phase change) of the reflected and transmitted waves can be calculated by matching the boundary conditions at the interfaces. This is quite difficult to do since the effect of multiple reflections must be included, refer to appendix A.2. Simplification occurs if a transmission line approach is used. Such an approach has been discussed by Rulf [28]. By considering the interactions between plane electromagnetic waves and a dielectric medium Rulf derives an expression (from Maxwell's equations) relating to the transmission through an arbitrary number (N) of plane parallel layers having varying thickness and dielectric properties. Rulf obtains a 2x2 matrix (called W) which provides a linear relationship between input and output amplitudes

$$\begin{pmatrix} A_0 \\ B_0 \end{pmatrix} = \begin{pmatrix} w_{11} & w_{12} \\ w_{21} & w_{22} \end{pmatrix} \begin{pmatrix} A_{N+1} \\ B_{N+1} \end{pmatrix} \tag{2.33}$$

where A_i and B_i are the amplitudes of the waves that propagate in the growing and diminishing z directions respectively and w_{11}, w_{12}, w_{21} and w_{22} are the components of W. The transmission coefficient will be given as

$$T = {A_{N+1}}/{A_0} = {1}/{w_{11}} \tag{2.34}$$

As an example, the transmission through a single homogeneous slab was calculated giving the following equation for the transmission coefficient in terms of the characteristic impedance of the two media, the length of the slab and the propagation constant through the slab:

$$T = \frac{4Z_1Z_2}{(Z_1+Z_2)^2 \exp(\gamma_2 \ell) - (Z_2 - Z_1)^2 \exp(-\gamma_2 \ell)} \tag{2.35}$$

This model can be used to describe the transmission through a barrier within a waveguide in which case, Z_1 is the wave impedance of region 1 (and 3), Z_2 is the wave impedance of region 2, γ_2 is the propagation constant of region 2 and ℓ is the barrier length. Z_1 and Z_2 are defined in sections 2.2.4 and 2.2.5. Similar to the Cuevas *et al.* model, it is also complex and has both magnitude and phase information.

2.3.4 *Model similarities*

Non-dissipative barriers can be included by re-writing the impedance in terms of α and β and applying appropriate exponential trigonometric identities, in this case equation (2.35) can be re-written as

$$T = \frac{2\alpha\beta}{2\alpha\beta\cosh(\alpha\ell) + i(\beta^2 - \alpha^2)\sinh(\alpha\ell)} \tag{2.36}$$

which is formally identical to equation (2.27) describing the transmission coefficient of a quantum barrier. Using a quantum model, we may find the waveguide equivalent by replacing $\sqrt{2m(U-E)/\hbar^2}$ with the attenuation constant α and $\sqrt{2mE/\hbar^2}$ with the phase constant β. This is only true for a non-dissipative barrier where the propagation constants in each region are either real or imaginary but not both.

Using the quantum analogy, it is easy to verify that the magnitude of the transmission coefficient $|T|$ will be that of equation (2.32) once the substitutions have been made. appendix A.3 verifies this by calculating $|T|$ from equation (2.35). Not only does this show that the waveguide and transmission line models for a single barrier (double interface) are equivalent, but also that a quantum model yields the same numerical result. Both the waveguide and the transmission line models theoretically predict the transmission coefficient through a multi-layered structure within a waveguide. Showing that these theories are numerically identical would be mathematically intensive. The magnitude of the transmission coefficient for a single barrier has been calculated using both theories and their agreement demonstrated, refer to appendix A.3 for details.

2.4 *Speeds of Light*

Many theoretical studies of the speed of propagation of electromagnetic energy through dispersive regions have been investigated. The studies by Brillouin [29], Oughstun and Sherman [30], and Loudon [31] are particularly useful. Smith [32] summarises the definitions, physical significance, interrelationships and the observability of seven different speeds of light.

The seven speeds discussed are:

1) The phase speed
2) The group speed
3) The energy speed
4) The signal speed
5) The relativistic speed constant
6) The ratio of units speed
7) The centrovelocity

Bloch [33] introduces another useful definition:

8) The correlation speed

When testing causality, the most useful speeds are the group/phase, energy, signal and correlation speeds.

2.4.1 *Phase and Group speeds*

The phase speed v_p and group speed v_g for the dominant mode in a rectangular waveguide are given by [7] as

$$\frac{c}{v_p} = \frac{v_g}{c} = \sqrt{1-\left(\frac{\lambda}{2b}\right)^2} \tag{2.37}$$

where λ is the free-space wavelength and b is the waveguide width. The phase speed is greater than c, but the signal propagates with the group speed is always less than c.

For a monochromatic plane wave, propagation through a dispersive but non-absorbing dielectric, the phase speed is usually given by

$$v_p = \frac{\omega}{k} \tag{2.38}$$

where ω is the angular frequency and k is the wavenumber of the signal.

The phase speed is the result of a calculation and has no physical quantity associated with it. The waveform being investigated must also be monochromatic since the phase speed is dependent on frequency.

The group speed is given by

$$v_g = \frac{d\omega}{dk} \tag{2.39}$$

This definition can not be used to describe propagation through regions of gain or absorption (dissipation). In such regimes, negative, zero or infinite group speeds occur due to large distortions. Bosov *et al.* [34] have shown that the group speed is a function of the absorption, the length of the path and the pulse shape. Klapka [35], introduced a new definition for the group speed. He proposed that the group speed be the speed of motion of the temporal centre of gravity of the amplitude of the wave packet. The group speed could be written as

$$v_g = \left| \nabla \left(\int_{-\infty}^{\infty} t \,|\, E(z,t) \,|\, dt \Big/ \int_{-\infty}^{\infty} |\, E(z,t) \,|\, dt \right) \right|^{-1} \tag{2.40}$$

Where $|\, E(z,t) \,|$ is the amplitude of the signal. Equation (2.40) reduces to equation (2.43) if the attenuation is negligible. Equation (2.40) is similar to the centrovelocity that describes the motion of the center of gravity of the intensity rather than amplitude. The indefinite integrals of equation (2.40) will give null or infinite results for periodic signals.

The speed of propagation through barriers has been theoretically investigated by Hartman [19] and suggests that the phase speed and group speed can be identified from the phase shift suffered by a wave crossing the barrier. Hartman adopts a phase-time approach that has been used successfully in both quantum and electromagnetic regimes [36], [15]. According to this model, a phase time delay t_p is given by

$$t_p = \frac{\Delta\phi}{\Delta\omega} \tag{2.41}$$

where $\Delta\phi$ is the phase change and $\Delta\omega$ is the frequency variation.

Using this delay, the Hartman phase speed after traversing a barrier of length ℓ, can be written as

$$v_{Hp} = \frac{\ell\omega}{\phi} \tag{2.42}$$

and the group speed can be written as

$$v_{Hg} = \ell \frac{d\omega}{d\phi} \tag{2.43}$$

v_p and v_g depend on the guide width b whereas v_{Hp} and v_{Hg} depend on the barrier length ℓ. Also, v_p and v_g depend on the permittivity of the region whereas v_{Hp} and v_{Hg} depend upon the phase change upon traversing the region. However, both models predict the phase and group speeds to depend on the frequency.

2.4.2 *The Energy Speed*

The energy velocity is defined by

$$v_e = \frac{P}{U_t} \tag{2.44}$$

where P is the net power flow density and U_t is the stored energy density associated with propagation. P can be determined experimentally, but U_t cannot. Olum [37] has investigated superluminal travel and suggests that negative energy densities are required. The energy speed, like the phase speed, does not correspond to the propagation of a real observable physical quantity since it is not known when it leaves or when it arrives. It is however an important concept which can be calculated theoretically.

2.4.2.1 Energy speed through non-dissipative barriers

Huxley [38] has shown that the complex Poynting vector can be used to approximate the power flow through a non-dissipative barrier. The average power flow density is given by

$$P = \frac{1}{2}\mathrm{Re}(E_x H_y^*) \tag{2.45}$$

Since $H_y^* = E_x^*/Z_1^*$ (complex conjugating and re-arranging Equation (2.2)). Equation (2.45) can be re-written as

$$P = \frac{1}{2Z_1}|E_t|^2 \tag{2.46}$$

Since the transmission coefficient T has been calculated, P can be expressed in terms of the incident electric field by substituting TE_i for E_t. Using Fresnel's equations for fields which are incident to non-dissipative media, the average power flow density through the waveguide is

$$P = \frac{\int P da}{\int da} = \frac{2\alpha_2^2 \beta_1}{\omega \mu_0 (\alpha_2^2 + \beta_1^2)} \int_A E_2{}^2 da \tag{2.47}$$

where E_2 is the electric field amplitude incident on the second interface and the integrals are over the cross-sectional area A of the waveguide. α_2 is the attenuation constant in region 2, and β_1 is the phase constant in region 1.

U_ℓ will be the sum of the energy stored in the barrier by the electric and magnetic fields. The energy stored per unit volume by an electric field E is given by

$$U_E = \frac{1}{2} \varepsilon_0 E^2 \tag{2.48}$$

and the energy stored per unit volume by a magnetic field H is given by

$$U_H = \frac{1}{2} \mu_0 H^2 \tag{2.49}$$

Pinder [39] has calculated the energy stored per unit volume for the transverse electric field, transverse magnetic field and a longitudinal magnetic field by calculating the additional electric and magnetic energy stored due to propagation by using the phase shift ϕ to account for power flow. If ϕ were zero, there would be no power flow. Using equations (2.48) and (2.49) Pinder calculates the total energy stored in a non-dissipative barrier to be

$$U_\ell = \ell \int_A da = \frac{\alpha^2 (1 - \cos(\phi))}{\omega^2 \mu} \int_A E_2{}^2 da \tag{2.50}$$

Applying the boundary conditions at the second interface, ϕ can be calculated in terms of α and β since

$$\cos\phi = \frac{\alpha^2 - \beta^2}{\alpha^2 + \beta^2} \tag{2.51}$$

Using this result and substituting equations (2.47) and (2.50) into (2.44) and simplifying yields

$$v_e = \frac{\omega}{\beta} \tag{2.52}$$

Notice this is equal to the phase speed in regions 1 and 3 and this can be greater than c (superluminal).

2.4.2.2 Energy speed through dissipative barriers

The energy speed through a dissipative barrier must be calculated using a different method than that used to calculate the energy speed through a non-dissipative barrier. The reflected wave is not needed for energy transport and due to the complex propagation constant, the barrier does not strictly represent a region in which tunnelling must occur. The energy density stored in the dielectric U_d must be added to that stored in the electric and magnetic fields U_t. Equation (2.44) becomes

$$v_e = \frac{P}{U_t + U_d} \tag{2.53}$$

Finding U_d is not trivial. Loudon [31] discusses a classical model representing an absorbing dispersive dielectric as an ensemble of damped non-interacting oscillators of mass m, charge e, resonant angular frequency ω_0 and displacement r. The equation of motion of such an oscillator is

$$eE = m(r + \Gamma r + \omega_0^2 r) \tag{2.54}$$

where E is the electric field and Γ is the damping coefficient. The refractive index is strongly frequency dependent and complex. It can be written as

$$n + i\kappa = \sqrt{\frac{\varepsilon}{\varepsilon_0}} \tag{2.55}$$

where κ is the imaginary part of the complex refractive index.

Loudon [31] also showed that the energy density stored in the fields plus that stored in the medium of a TEM wave propagating through an infinite dispersive, dissipative medium is given by

$$\frac{|E|^2}{2}\left(n^2 + 2\omega\kappa/\Gamma\right) \tag{2.56}$$

Detailed knowledge of the electrical properties of the dielectric is required to calculate the energy density stored and since this is not usually available the stored energy density cannot be calculated.

Pinder [39] obtains the maximum possible energy speed by using the energy density stored in the electric and magnetic fields, since these can be found. The maximum possible energy speed is given by

$$v_{eMAX} = \frac{2\beta_2\omega}{\omega^2\mu_0\varepsilon_0 + \alpha_2^2 + \beta_2^2 + \frac{\pi^2}{b^2}} \tag{2.57}$$

This is similar to the result obtained by Loudon [31].

2.4.3 *Signal speed*

The signal speed is given by

$$v_s = \frac{\ell}{t_s} \tag{2.58}$$

where t_s is the propagation delay across the barrier. Experimentally, an ideal detector of infinite sensitivity is required to detect the first non-zero part of the signal. Since such a detector does not exist, another criterion is required. The signal is said to have arrived when it reaches a significant fraction of the maximum input signal. Brillouin [29] suggests about a third. The signal speed cannot be unambiguously defined since the speeds depend on the value of the fraction chosen. If attenuation or gain are present, the value of this fraction and therefore the signal speed are ambiguous and problematical. The signal speed is also strongly dependent on distortion. The transmitted signal will need to be normalised so that it can be compared with the incident signal. If the value of the fraction is taken as unity then the transmitted signal is defined to have arrived when the peak of the incident signal has been detected. Time delay studies in the quantum tunnelling regime [40] suggest that there is no causative relationship between incident peaks and the transmitted signals since the transmitted signals arise primarily from the front end of the incident signal.

2.4.4 *The correlation speed*

The correlation speed is given by

$$v_c = \frac{\ell}{t_c} \tag{2.59}$$

where t_c is the transit or delay time found by using the cross-correlation function. The cross-correlation function for periodic functions is given by

$$R_{1,2}(t_c) = \frac{1}{\tau}\int_0^{\tau} E_1(t)E_2(t+t_c)dt \tag{2.60}$$

where τ is the period of E_1 and E_2. E_1 is one waveform and $E_2(t+t_c)$ is another waveform shifted by the delay or transit time. The correlation function essentially is based on an idea of 'pattern matching' by sliding one object over another. The maximum of the cross-correlation function occurs when E_2 is shifted so that it most closely matches E_1. If E_1 is equal to E_2, then equation (2.60) yields the auto-correlation function. The transit time t_c will be the time between the peaks of the auto and cross-correlation functions. Bloch [33] has shown that useful results can be obtained from highly dispersive and absorptive media in which the original signal becomes highly distorted, and even unrecognisable. This technique is used to locate earthquakes from seismic records and also to detect nuclear explosions.

When cross-correlating two time signals which have been sampled at a different frequency, one of the signals will need to be interpolated so that at a given time, both signals will have a particular magnitude. Alternatively, both signals could be interpolated. For example, let signal *A* be sampled *a* times in time *t* and let signal *B* be sampled *b* times in time *t*. Interpolating each signal so that *A* is *b* times larger and *B* is *a* times larger will result in the signals *A* and *B* both being sampled *ab* times in time t.

When cross-correlating two signals, it is important that the signal amplitudes are close to zero at the start and end of the signal. These small amplitudes define the 'start' and 'finish' of the signal. In this study, the signals used for cross-correlation purposes will be 'padded' with zeros. This is done by adding a 'block' of zeros equal to the signal length to the beginning and end of the signal. The signal length used for cross-correlation will therefore be three times longer than the original signal.

Cross-correlation of incident and transmitted signals of a dispersive medium must be approached with caution. The frequency shift between incident and transmitted signals can cause the cross-correlation function to be zero. The envelopes of the incident and transmitted signals must be cross-correlated to avoid a null result [41]. For similar reasons, the envelope must be used when calculating the signal speeds.

Chapter 3

A theoretical study of non-dissipative and dissipative barrier penetration within a waveguide

3.1 *Creating an incident signal*

3.1.1 *The Discrete Fourier Transform (DFT)*

Any signal which is tunnelled through a waveguide with a barrier is necessarily frequency band limited due to the frequency constraints which allow for propagation (see section 2.2.3). The Fourier Transform (FT) gives a direct relationship between the time domain and the frequency domain of a given signal and for this reason has been used to model many physical applications [42].

The FT is used to construct time domain signals which are aperiodic. Ideally, the signal that is to be created for use in this study will consist of only one pulse. This is not practically possible due to the frequency constraints, and a truncated FT must be used. For this reason, the Discrete Time Fourier Transform (DFT) must be taken of the time signal instead. A consequence of this is that the signal created will be periodic in nature. Although the FT and DFT transform are numerically different they are very similar and can be easily associated with each other [43]. A fast computer algorithm called the Fast Fourier Transform (FFT) is often used to calculate the DFT.

Usually the FFT is written in two-sided, complex representation as

$$X_a(m) = \sum_{k=0}^{N-1} x_a(k) \exp\left(\frac{-i2\pi mk}{N}\right) \qquad (3.1)$$

And its inverse $$x_a(k) = \frac{1}{N}\sum_{m=0}^{N-1} X_a(m)\exp\left(\frac{+i2\pi mk}{N}\right) \tag{3.2}$$

$X_a(m)$ are evenly spaced samples in the frequency domain, $x_a(k)$ are evenly spaced samples in the time domain, N is the number of samples of the signal, m and k are integers which relate $X_a(m)$ and $x_a(k)$ back to the actual frequency and time domains of $X(f)$ and $x(t)$ respectively. For example, $x(k) = x_a(k\Delta t)$ for a sampling interval Δt. The equations (3.1) and (3.2) are very similar and only differ by the scaling factor $1/N$ and the exponential part being replaced by its complex conjugate. The DFT can be also written as a sum of phase shifted cosine terms

$$x_a(k) = \frac{1}{N}\sum_{k=0}^{N-1} |X_a(m)|\cos\left(\frac{2\pi mk}{N} + \phi_a\right) \tag{3.3}$$

where $|X_a(m)|$ and ϕ_a represent the magnitude and phase of $X_a(m)$ respectively.

Writing $X(f)$ and $x(t)$ in the form of equation (3.1) and (3.2) we find

$$X(f) = \sum_{t=t_i}^{t_f} x(t)\exp(-i2\pi ft) \tag{3.4}$$

and $$x(t) = \frac{\Delta f \Delta t}{nN}\sum_{t=t_i}^{t_f} X(f)\exp(+i2\pi ft) \tag{3.5}$$

This time, Δt is the time range of the signal and Δf is the frequency interval (or allowed bandwidth) of the signal components. In this study, we will construct a pulse which is 4ns wide so Δt equals 4ns and Δf equals 3.16GHz (a result obtained by subtracting 6.33GHz from 9.49GHz). n is the number of time samples taken over Δt. N is the number of components required over Δf and f are N equally spaced frequencies within Δf.

$x(t)$ written in terms of phase-shifted cosine terms is

$$x(t) = \frac{\Delta f \Delta t}{nN}\sum_{t=0}^{n-1} |X(f)|\cos(2\pi ft + \phi) \tag{3.6}$$

where $|X(f)|$ and ϕ represent the magnitude and phase of $X(f)$ respectively. The number of samples n is important if a particular pulse is to be constructed. For example, substituting $k = 0$ into equation (3.3) refers to the DC component of $x(t)$.

For waveguide barrier penetration, the allowed frequencies lie between 6.33GHz and 9.49GHz and not Δf. Using Δf to define f results in frequencies between zero and 3.16GHz being used when in reality, frequencies between 6.33GHz and Δf + 6.33GHz are required. Unfortunately, using the DFT model described and 'adding' 6.33GHz to Δf to define f has an adverse effect on the created time domain signal $x(t)$. Adding a constant frequency to Δf results in 'wavepacket' type signal being created for $x(t)$. Increasing the frequency (which is being added), increases the frequency within the wave-packet. Refer to figure 3.1 which shows the constructed signals $x(t)$ when greater frequencies f are used to re-construct a Gaussian signal. The wave-packet shape is the result of modifying the DFT to utilise the frequencies between 6.33GHz and 9.49GHz. Using this model allows for the investigation of wave-packet signals and emphasises the importance of selecting an appropriate time sampling frequency.

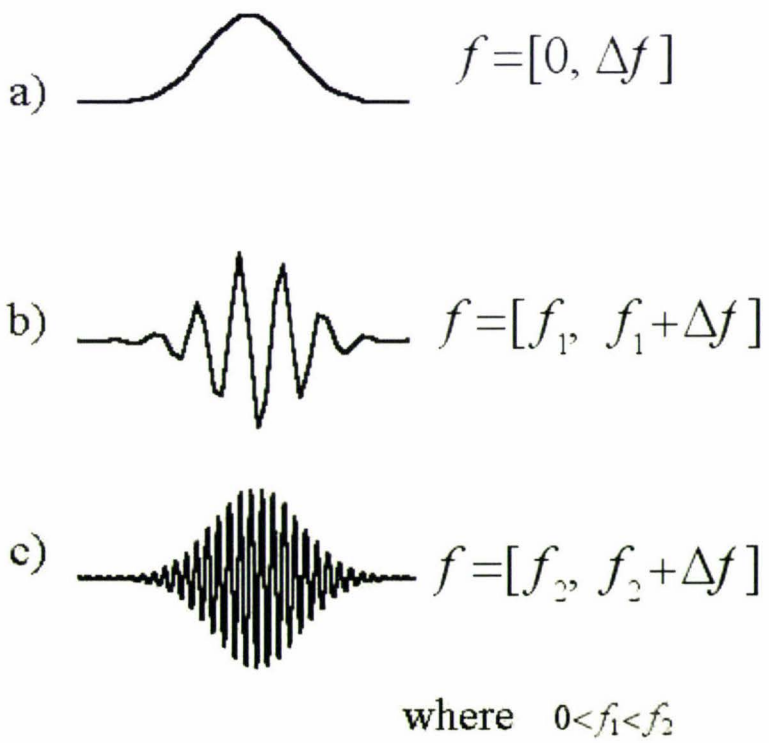

Figure 3.1:The time domain wave-packet reconstruction of a Gaussian signal. a) This is the ideal case, where a DC (0Hz) frequency exists. b) and c) show the effect of increasing the minimum frequency to f_1 and f_2.

3.1.2 *Time-sampling of a wave-packet signal*

The envelope of the wave-packet created is important, especially for cross-correlation and signal speed purposes. The envelope of the signal can be approximated by re-sampling the wave-packet at a certain 'carrier' frequency f_s so that only the points at the peak of each 'wave' within the wave-packet are chosen.

The function $X(f)$ defines the frequency spectrum of the desired signal. It is symmetrical and has a dominant central frequency. This central frequency is the carrier frequency and is given by

$$f_s = \frac{f_1 + f_2}{2} \tag{3.7}$$

Where f_1 and f_2 are the lower cutoff and upper cutoff frequencies respectively. The sampling rate t_s required is that of the carrier frequency f_s, given by

$$t_s = \frac{1}{f_s} \tag{3.8}$$

The number of time samples n over the time range Δt given by

$$n = \frac{\Delta t}{t_s} \tag{3.9}$$

3.2 *Incident time signal construction*

As already mentioned, the created signal will be periodic (for example, a series of pulses is created) due to the DFT model used to define the signal. Using a value of 4ns for Δt results in a time difference of about 80ns between each pulse, which is temporally long enough to prevent interference from either an earlier or a later pulse. Refer to figure 3.2 which shows this time difference between pulses for a Gaussian signal.

Various signals (Gaussian and non-Gaussian) were constructed over a 4ns time domain Δt for both the non-dissipative and dissipatve barrier situations, refer to appendix E and the Matlab EBP toolbox. The way this was done is outlined below using a logarithmic Gaussian as an example. A logarithmic Gaussian has a short rise time and a longer decay time and is a useful signal to analyse.

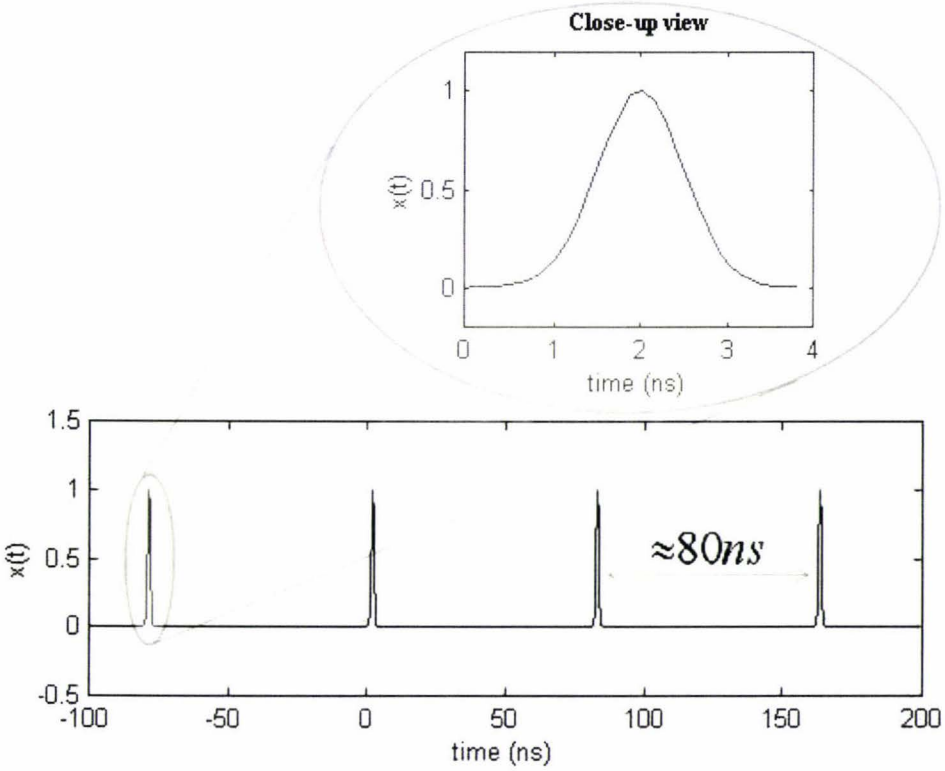

Figure 3.2: A periodic Gaussian signal created from the DFT

1) Define the shape of the pulse required.

A logarithmic Gaussian is of the form $x(t) = \exp(-[\log(at+b)]^2)$ where, this time, a and b are constants allowing the signal to 'fit' within the time window Δt. The values for t have been selected such that the spacing between each consecutive time value is t_s with a total of n sample points. n is calculated from equation (3.9) and is rounded to the nearest integer, taken to be 32 and 29 for the non-dissipative and dissipative cases respectively. These values are different since n depends on the different frequency constraints of the two barrier types, refer to figure 3.3.

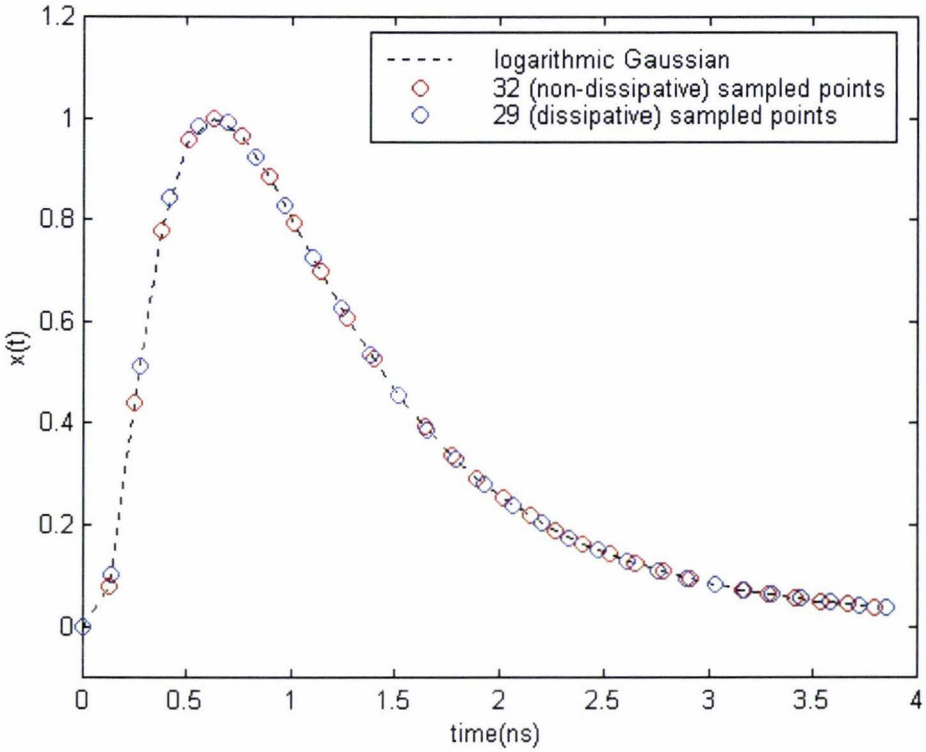

Figure 3.3: The required (logarithmic Gaussian) signal shape to be created using the DFT

2) Take the DFT of x(t) to find X(f).

N is not restricted whereas n is. N needs to be relatively large but a value of 256 ($=2^8$) has proven ample. Taking N to be equal to 2^q for some integer q greatly reduces the computing time of a FFT algorithm. Using equation (3.4), 256 equally spaced values of $X(f)$ can be calculated over the frequency range $\triangle f$, refer to figure 3.4.

The 'shape' of the amplitude spectrum for both barrier cases are identical except for a frequency shift and a magnitude change. They both are representations of the same required time domain signal so this similarity is to be expected.

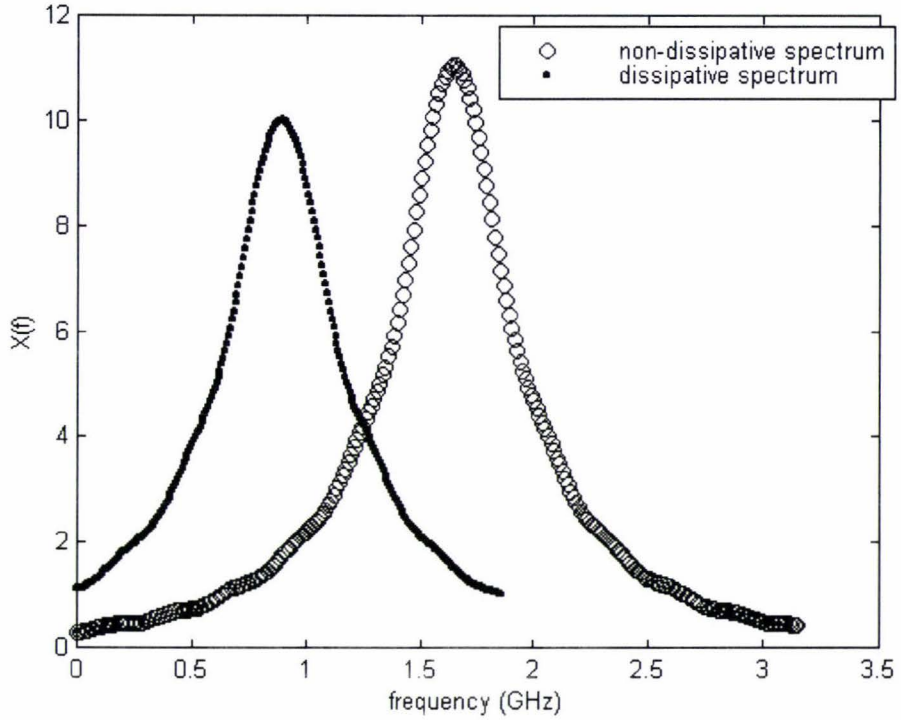

Figure 3.4: Amplitude spectra for a log-Gaussian incident signal

3) Re-construct x(t) using cosine components.

Although we have values of $X(f)$ over a frequency domain $\triangle f$ we actually want a frequency domain of $6.33GHz + \triangle f$. By adding $6.33GHz$, low frequency components are lost, and the signal assumes wave-packet properties. The envelope of the wave-packet is important since it will be the envelope which will be used to calculate the cross-correlation and signal speeds, refer back to section 2.44. Time-sampling the wave-packet at the central frequency is done to obtain the required envelope for analysis. Figure 3.5 shows this sampling for the non-dissipative case.

Referring back to figure 3.4 the amplitude spectrum is symmetrical about a central maximum carrier frequency. This frequency is calculated to be 7.91GHz for a non-dissipative barrier and 7.26GHz for a dissipative barrier. It is from these values that n has been calculated.

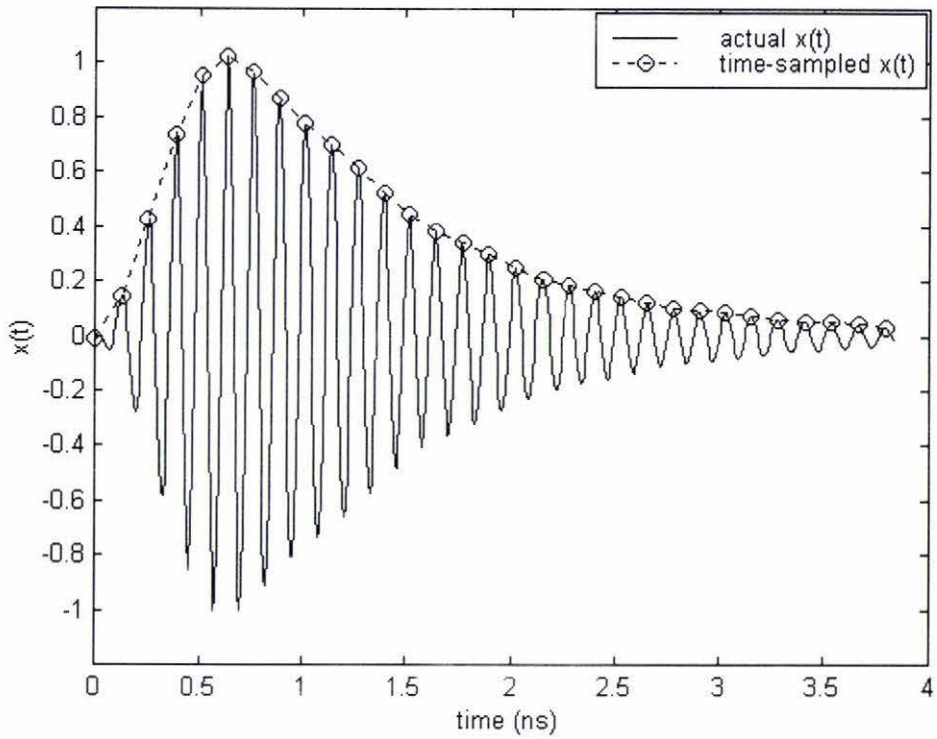

Figure 3.5: The created and time-sampled (envelope) signals of x(t) required for a non-dissipative analysis.

For the non-dissipative barrier, the carrier frequency is calculated to be 7.91 GHz but due to an integer number of samples being used in this example, rounding occurs resulting in a carrier frequency of 8.00 GHz. The time-sampled components do not appear truly representative of the allowed frequencies. For example, the 8.00 GHz component appears to be a DC component and all other components have a far greater period than expected, refer to figure 3.6. This result can lead to artifacts being produced and is a direct result of sampling at intervals too great to permit faithful replication of he original signal. This phenomenon is known as aliasing.

Since symmetry exists about f_s, the components with frequencies $f_s \pm df$ for some small change in frequency df will have the same time-sampled waveform. This is also due to aliasing.

In any case, $X(f)$ now has a domain over the frequency range required and by using equation (3.6), $x(t)$ can be reconstructed using cosine components.

The reconstructed logarithmic Gaussian pulse for the dissipative case appears slightly 'bumpy' or 'wavy'. This is because the frequency domain Δf for the dissipative case is 'narrower' than that for the non-dissipative case, refer to figure 3.7.

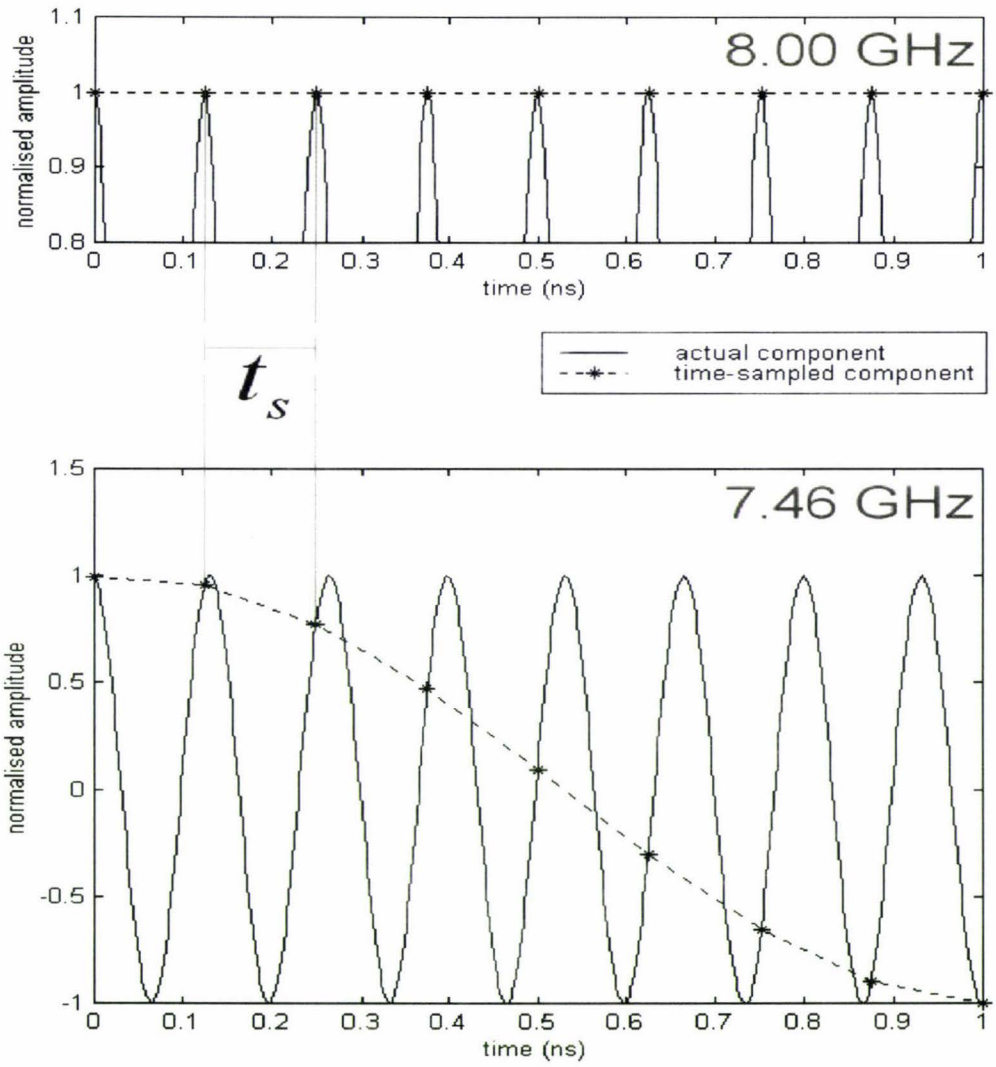

Figure 3.6: Change in apparent period. This diagram shows how the 8GHz component appears to be DC and how the 7.46 GHz component will appear to have half its period in 1ns. This is an effect of aliasing.

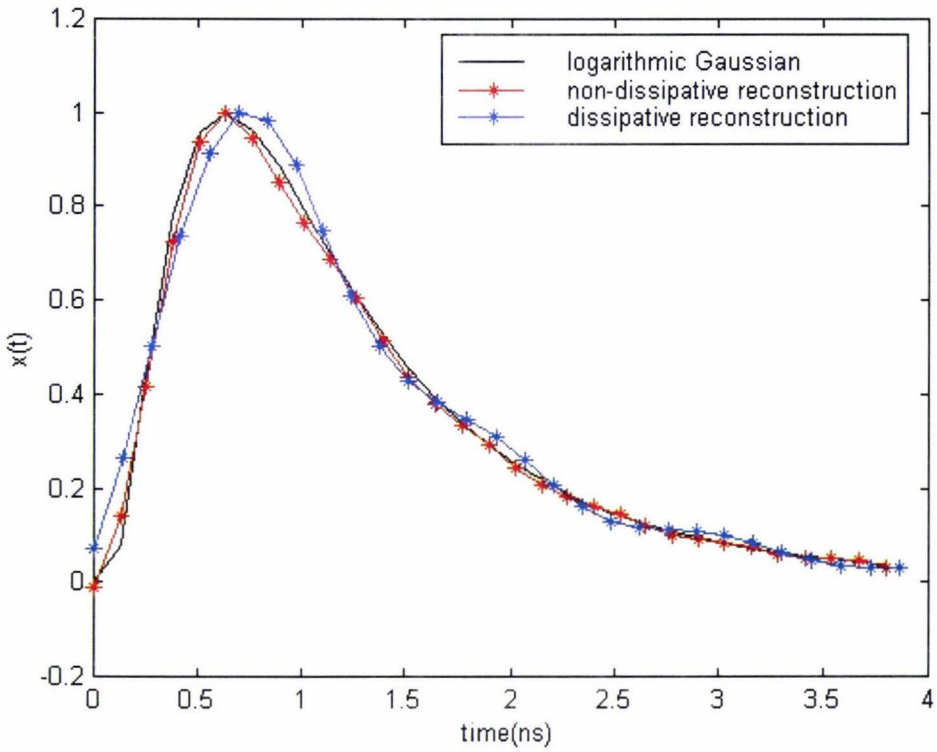

Figure 3.7: Re-constructed envelopes of log-Gaussian time signals. These signals are the envelopes of the time signals which have been re-constructed by adding together all the cosine components obtained from the DFT.

The reconstructed pulses are similar enough to allow the comparison between the propagation effects through the two different barriers. Enough information is now known about the incident signal for it to be investigated when penetrating an electromagnetic barrier within a waveguide.

3.3 *Non-dissipative barrier penetration using the transmission line model*

3.3.1 *Attenuation and phase as a function of frequency*

From equation (2.35) it is possible to find the attenuation and phase change for each cosine component of an incident signal. $|T|$ gives the magnitude of the transmission coefficient as a function of frequency while the phase of T gives the phase shift as a function of frequency. These theoretical results can be directly compared with the experimental results from [8]. The first graph showing the experimental results plots $|T|^2$ (in dB) against frequency. The frequency range can be easily extended to cover the frequencies presented by Nimtz *et al.* [8], but only the frequencies within the window of Δf are used to reconstruct the transmitted signal. Refer to figure 3.8 which is an overlaid plot comparing these theoretical results with the previously published experimental results from Nimtz *et al.* [8] for the 4.9cm and 6.47cm non-dissipative barrier lengths.

As figure 3.8 shows, lower frequencies suffer greater attenuation than the higher frequencies. As ℓ increases, more frequencies become 'highly' attenuated and only frequencies close to f_2 survive. For example, when ℓ=15cm, frequencies between 9.00 and 9.49 GHz have attenuation ranging between less than $-70dB$ to $-10dB$ respectively. Frequencies less than that are highly attenuated well below $-70dB$.

Figure 3.9 shows the phase of T plotted against frequency for both the experimental data from Nimtz *et al.* [8] and the theoretical results obtained from equation (2.35).

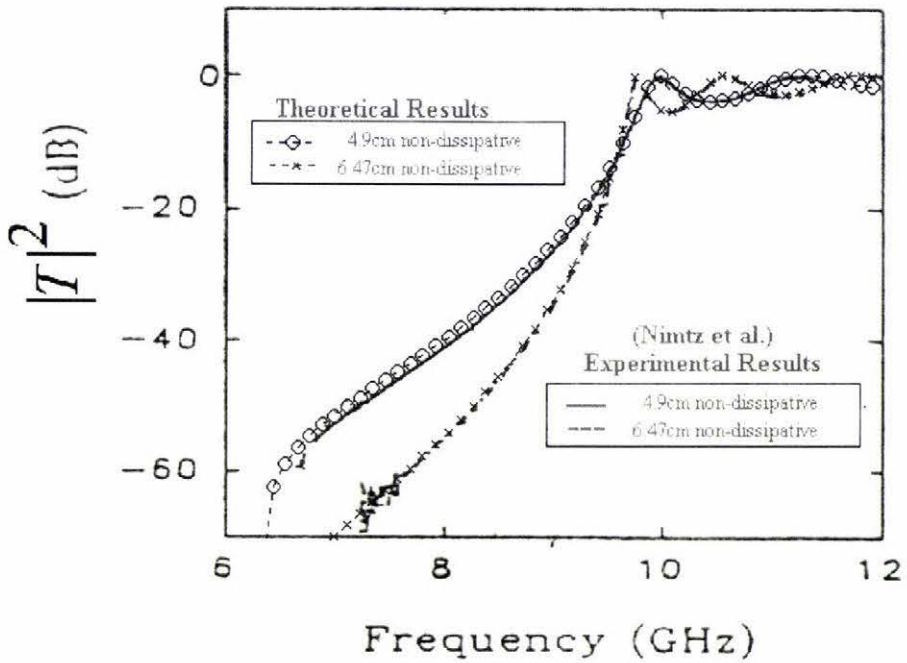

Figure 3.8: $|T|^2$ against frequency for penetration through a non-dissipative barrier. The theoretical results have been laid over the results presented by Nimtz *et al.* [8] (as shown in figure 1.2).

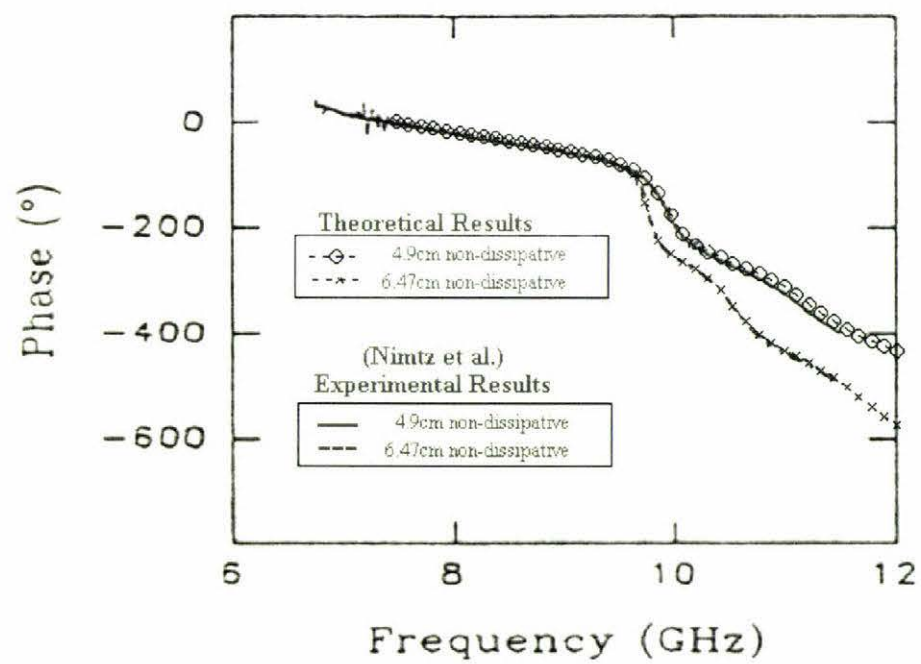

Figure 3.9: Phase against frequency for penetration through a non-dissipative barrier. The theoretical results have been laid over the results presented by Nimtz *et al.* [8] (again, shown in figure 1.2).

The phase change becomes larger in magnitude for increasing barrier length between 0cm and about 2cm for all frequencies examined. Frequencies below 7.44GHz suffer a positive phase shift while those greater than 7.44GHz suffer a negative phase shift, refer to figure 3.10.

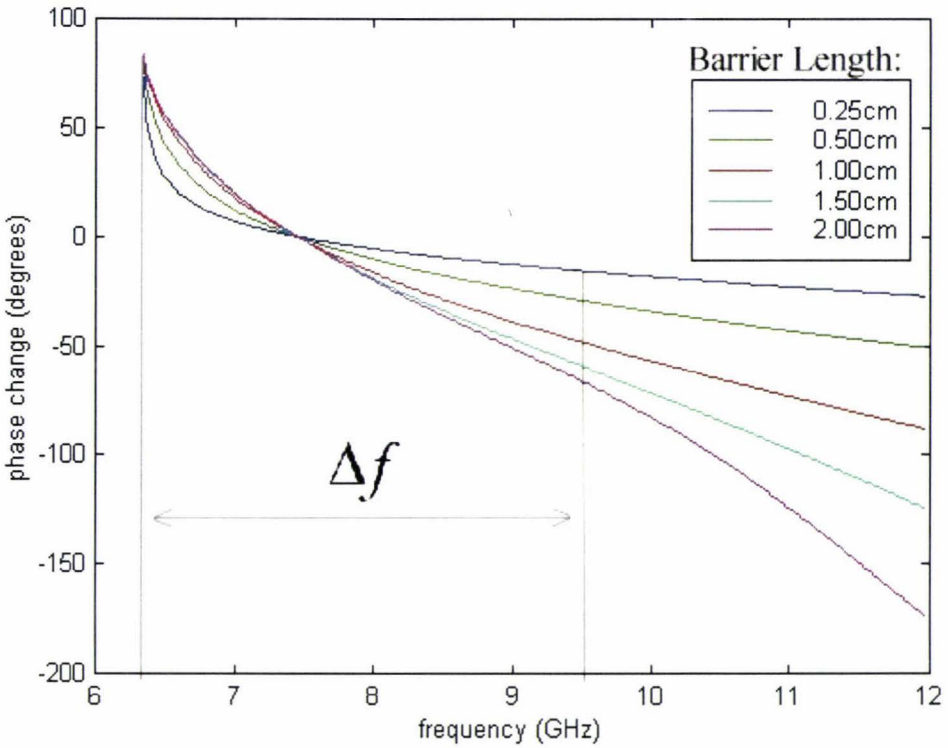

Figure 3.10: Phase against frequency for penetration through a short (<2cm) non-dissipative barrier

For larger barrier lengths ($\ell \geq$ 2.5cm) the phase change appears to be identical for frequencies restricted to Δf. Again both positive and negative phase shifts occur, refer to figure 3.11.

T is the ratio of the transmitted field amplitude in region 3 (E_t) to the incident field amplitude of region 1 (E_i). Since the magnitude and phase of T over the frequencies required is now known, it is possible to reconstruct the signal transmitted through the barrier by multiplying E_i by T. This gives the transmitted signal as a function of time.

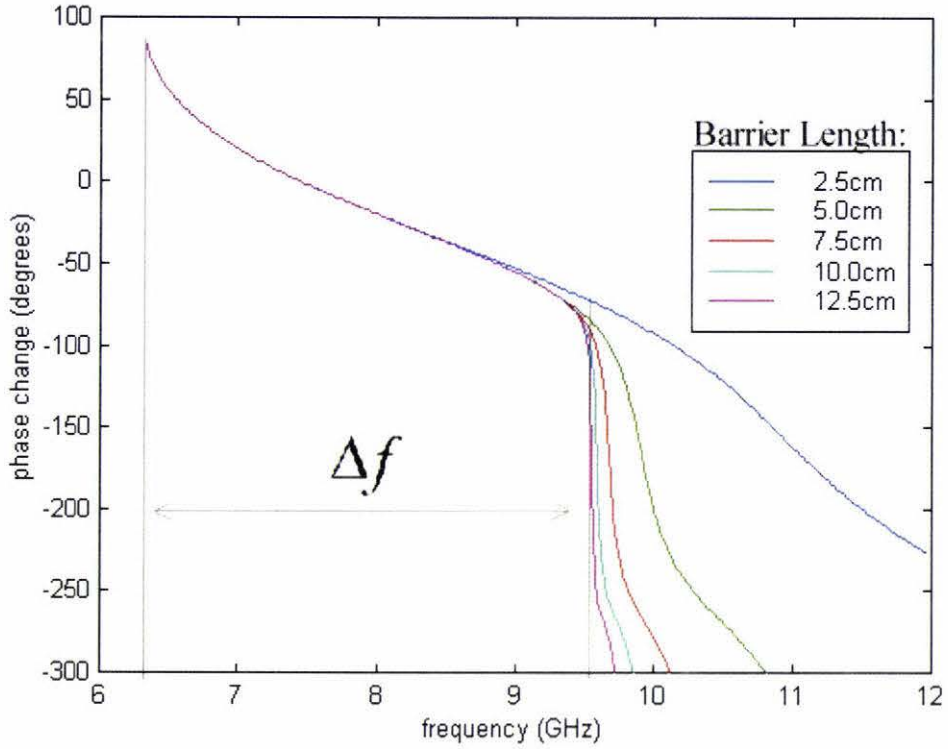

Figure 3.11: Phase against frequency for penetration through a long (>2cm) non-dissipative barrier

3.3.2 *The Transmitted Amplitude Spectrum*

The amplitude spectrum is a graph of the magnitude of the amplitude of the cosine components against frequency. The amplitude spectrum has no phase information about the cosine components. The amplitudes of the cosine components at particular frequencies $X(f)$ is obtained from the DFT of the time domain signal $x(t)$, refer to equation (3.4).

A Gaussian time domain signal is useful to analyse since the FT results in a Gaussian amplitude spectrum. A 'stretched' Gaussian time domain signal results in a 'narrowed' Gaussian amplitude spectrum whereas a 'narrowed' Gaussian time domain signal results in a 'stretched' Gaussian amplitude spectrum.

Appendix C shows the incident ($\ell = 0$) and transmitted amplitude spectra of six signal shapes investigated for increasing barrier lengths, refer also to the Matlab EBP

simulation. The amplitude spectra of the investigated signals shift to higher frequencies with increasing barrier length, refer to appendix C.1-C.6. The relative amplitudes have been investigated. These amplitudes have been normalised by dividing by the maximum. This maximum is taken to be the local maximum that is closest to the maximum of the incident signal amplitude spectrum. Figure 3.12 shows the amplitude spectra at different barrier lengths for a Gaussian incident signal. More complex signals such as the 'double' Gaussian and the sinc also exhibit a shift to higher frequencies with increasing barrier length, but this shift is more complicated, refer to appendix C.5,C.6. The double Gaussian amplitude spectrum consists of a number of peaks. These peaks change in magnitude (but not in frequency) and so a magnitude shift to higher frequencies is observed. The sinc has quite a broad spectrum with three local peaks. As the barrier length increases, the two peaks on the left decrease more quickly than the higher frequency peak. Nevertheless, at large barrier lengths (>10cm), for all signals, only high frequencies close to f_2 remain and the amplitude spectrum no longer has a shape similar to that of the incident signal amplitude spectrum.

The Gaussian's amplitude spectrum, although shifted, is mostly unchanged in shape up to barrier lengths just over 10cm. For this reason, it is expected that the 'shape' of the transmitted time domain signal for a Gaussian will be conserved. All other amplitude spectra distort significantly between barrier lengths of 5cm and 7.5cm. A significant distortion of the amplitude spectrum will result in significant distortion of the time domain signal. Frequencies higher than the central frequency dominate the amplitude spectrum and the original shape of the time signal is lost.

The barrier acts as a high-pass filter and the longer the barrier, the greater the filter effect. As the barrier length increases, the attenuation increases and the signal migrates to higher frequencies just like the treble control on a stereo system. As the knob is turned, the audio output becomes 'tinnier' since the signal migrates to higher frequencies.

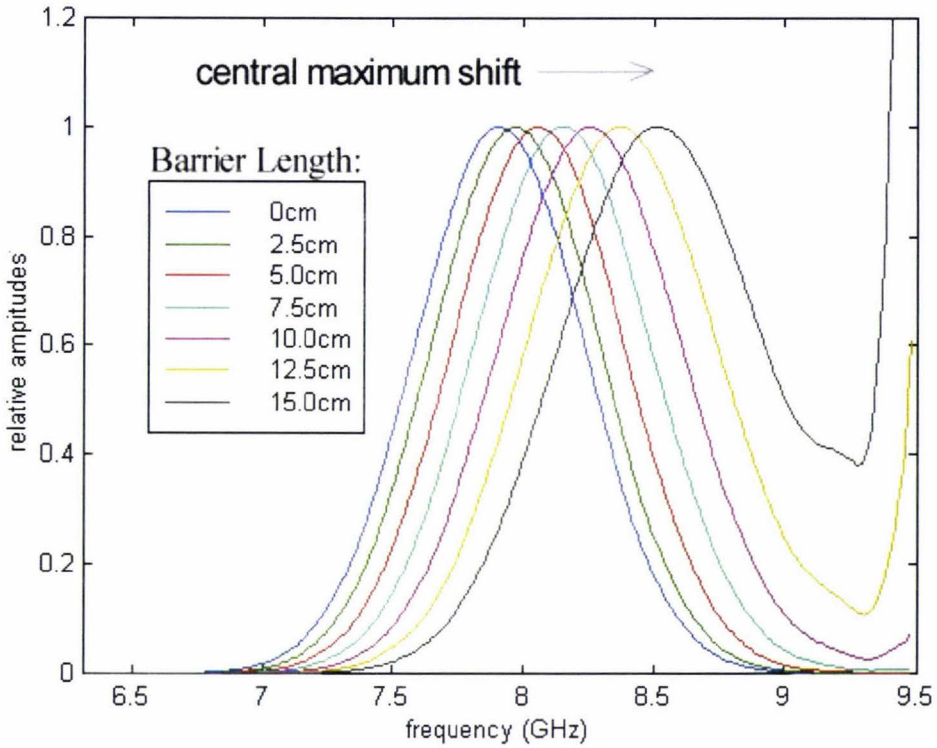

Figure 3.12: The transmitted normalised amplitude spectrum for an incident Gaussian signal traversing a non-dissipative barrier.

3.3.3 *Attenuation and phase as a function of time*

The transmitted pulse is calculated by multiplying each DFT frequency component by the appropriate value of $|T|$, adding the appropriate phase change and then summing all the components.

The large attenuation that occurs for most of the frequencies results in a large attenuation of the transmitted signal. For example, a barrier length of about 2.5cm results in an attenuation of the transmitted signal amplitude by a factor of about 10, a 10cm long barrier length has a transmission amplitude more than 10,000 times less (-80dB) than the incident signal.

The average attenuation over the allowed frequency range increases linearly as barrier length increases. There is a -8.6 ± 0.2 dB/cm average attenuation. This value was calculated using the ratio $|T|$ and is true for all pulse shapes, refer to figure 3.13. Due to

the linearity of graph, the average intensity (and therefore magnitude of the signal components) decays exponentially with increasing barrier length. The different attenuation for different frequencies 'distorts' the transmitted signal. The amount of the distortion depends upon the shape of the incident signal.

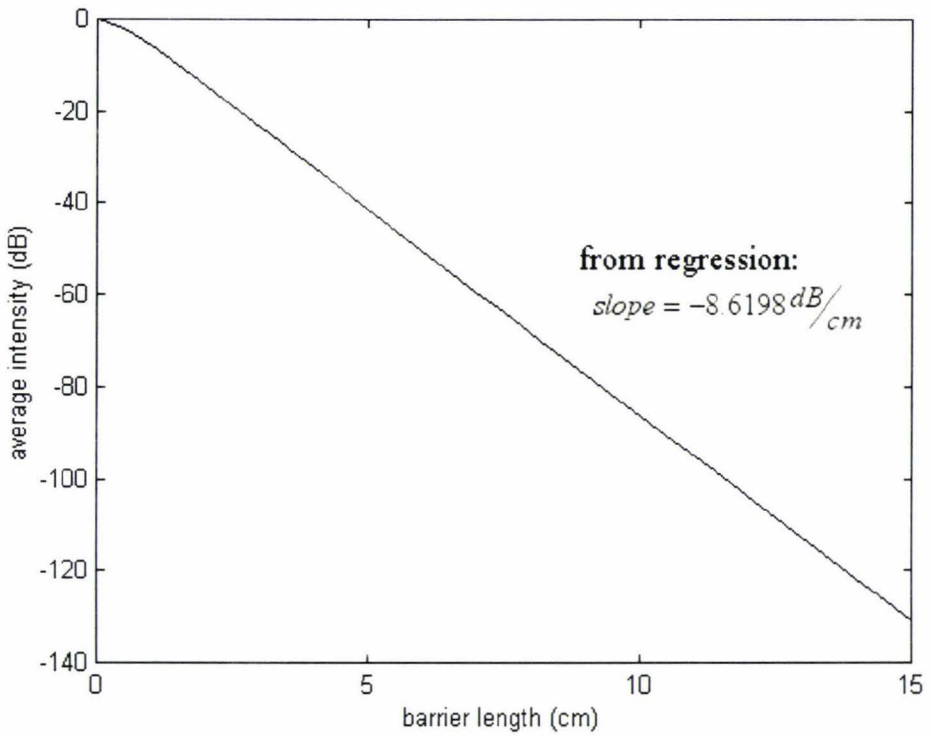

Figure 3.13:Graph showing the linearity between the average intensity and barrier length for non-dissipative barriers.

Each component of the incident signal obtained from the DFT undergoes a phase shift as well as an attenuation. From Figure 3.10 shown earlier, a negative phase shift occurs for frequencies greater than about 7.44GHz. This negative phase shift causes a positive time shift for the transmitted frequency components. A positive phase shift occurs for frequencies less than about 7.44GHz. The positive phase shift causes a negative time shift for the transmitted frequency components. The amplitudes have been normalised so that only the phase changes can be compared, refer to figure 3.14.

A negative time shift would imply that the component arrived before it was sent. This is not 'physically' possible and can be explained by understanding the periodic nature of the component. The component is a sinusoid that temporally extends to $\pm\infty$. It is periodic

in nature and repeats its phase every 2π radians. Because of this, a negative time delay from a positive phase shift, say $\triangle\phi$, is exactly the same as a positive time delay from a negative phase shift $2\pi - \triangle\phi$. This is 'physically' possible. A negative time delay of a sinusoid does not cause concern since it can be described as a positive time delay of the same sinusoid.

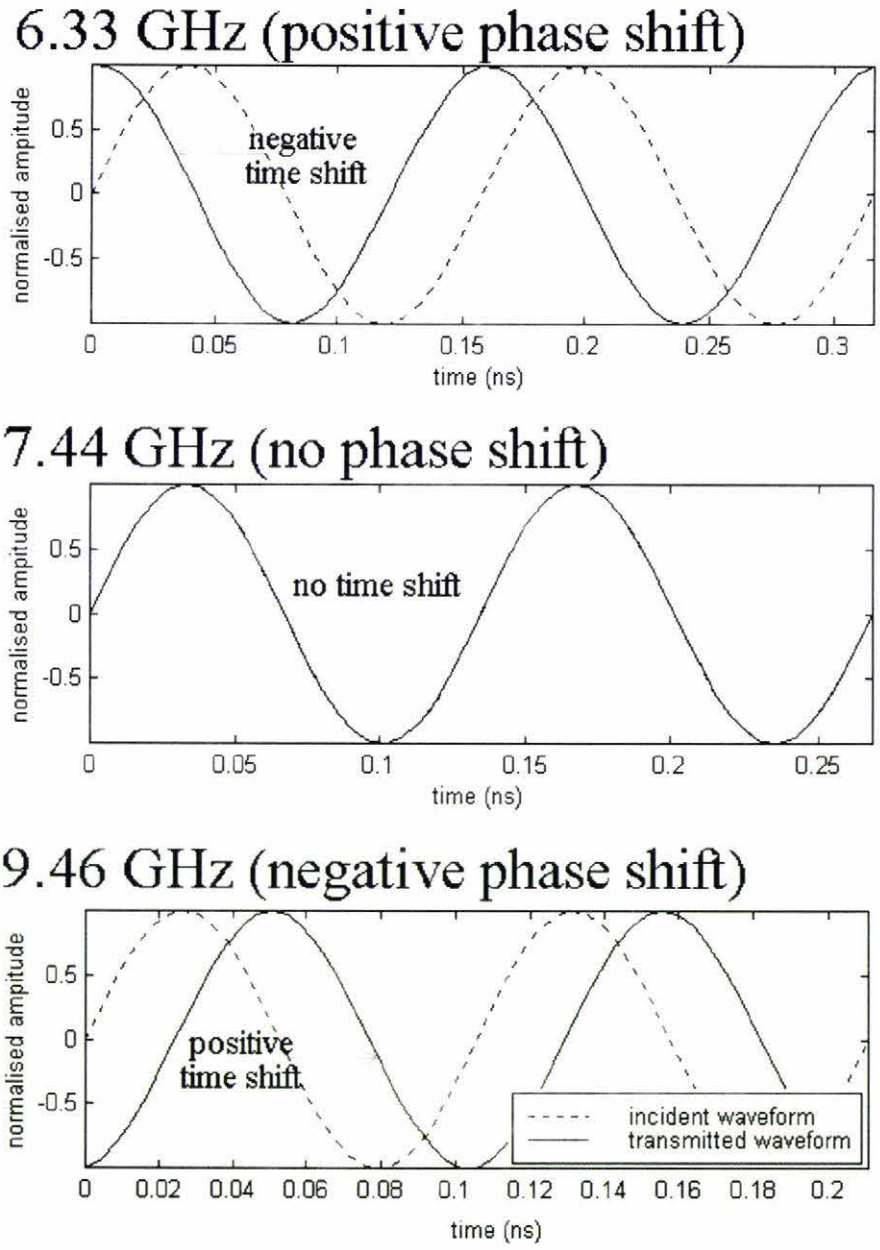

Figure 3.14: Phase shift for a few selected frequencies. Frequencies below 7.44GHz suffer a negative time shift while those greater than 7.44GHz suffer a positive time shift.

About 35% of the components are positively phase shifted. The remaining 65% are negatively phase shifted. The components which are positively phase shifted are more highly attenuated and so it is no surprise that the transmitted time signal as a whole suffers a positive time delay, due to the 'dominant' negative phase shifts.

The phase shift becomes approximately constant for barrier lengths greater than about 2.5cm demonstrating the Hartman effect. The phase shifts do not significantly alter the transmitted signal shape for barrier lengths greater than 2.5cm. Distortion of the amplitude spectrum causes most of the distortion of the transmitted time signal for barrier lengths greater than 2.5cm. This is because only the high frequency components 'survive'.

3.3.4 *The Transmitted Time Signal*

Six transmitted signal 'shapes' were investigated. These shapes are mostly Gaussian in nature except for the sinc shaped signal, refer to appendix B and the Matlab EBP simulation for the transmitted time signals for all investigated signal shapes. The Gaussian however, maintains most of its shape beyond barrier lengths of about 10cm (see Appendix B.1). All other shapes become highly distorted for barrier lengths between 5cm and 7.5cm, refer to appendix B.2-B.6. Guassian shape preservation can be explained by analysing the amplitude spectrum of the transmitted signal, see section 4.2.

3.3.4.1 Wavepacket peak time differences

The transmitted wavepacket time signal depends on the phase shift and attenuation of each cosine component and is created from the superposition of these components. For larger barrier lengths, the superposition of all the components results in a wavepacket signal whose peaks do not have a constant time difference. This implies different sampling times will be required to find the envelope of the wavepacket. This is not practical and the envelope of such a signal cannot be found, as aliasing will undoubtedly occur. The time differences between the peaks for a given signal depend on the signal shape, refer to appendix A. For most signals, at larger barrier lengths, the time differences between the peaks at the beginning and end of the signal are affected the

most. Figure 3.15 shows the time differences between adjacent peaks for a Gaussian transmitted time signal. Ideally, the plotted points will be horizontal and equal to t_s.

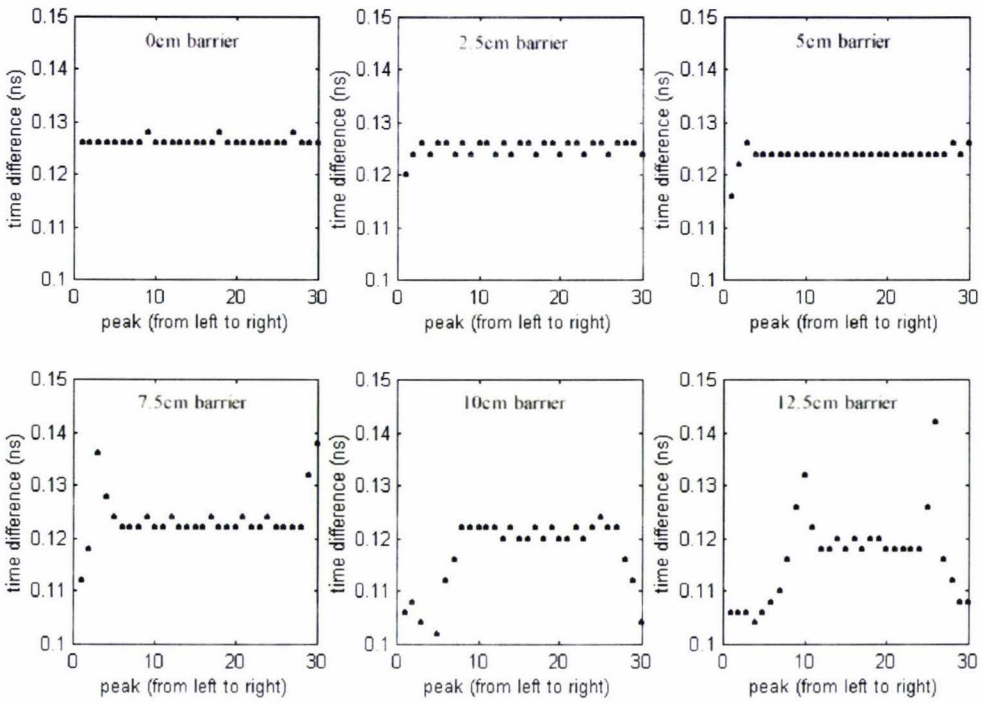

Figure 3.15: Time differences between adjacent carrier peaks for a Gaussian wavepacket after penetrating different non-dissipative barrier lengths. The x-axis refers to the increment between the an *i*th and an *i*th+1 peak for some peak i. It can be seen that as the barrier length increases, most of the time differences occur at the beginning and end of the signal. Ideally, the plotted points will be horizontal implying a constant time difference between adjacent peaks.

This result occurs independently of the number of cosine components N and sampling rate at which the wavepacket signal was sampled. The envelope of the transmitted signals at larger barrier lengths cannot be found, as aliasing will occur. However, it is possible to delay the aliasing effect by starting the sampling at a later peak. For example, by choosing to start the sampling at the seventh peak for the 5cm barrier, refer once more to figure 3.15. In this case, the transient peak differences have been ignored resulting in a truncated envelope. This introduces the concept of a sampling delay. The sampling delay for the previous example will be the time (from 0ns) it takes to reach the seventh peak of the wavepacket.

3.3.4.2 Sampling the envelope of the transmitted time signal

Figure 3.16 shows the normalised incident time signal and transmitted time signal of a Gaussian shaped wavepacket after penetrating a barrier length of 5cm. The Gaussian shape has been preserved since the amplitude spectrum has not been significantly distorted. Although the transmitted and incident signals look similar, there are subtle differences that need to be recognised if the envelope of the transmitted signal is to be found.

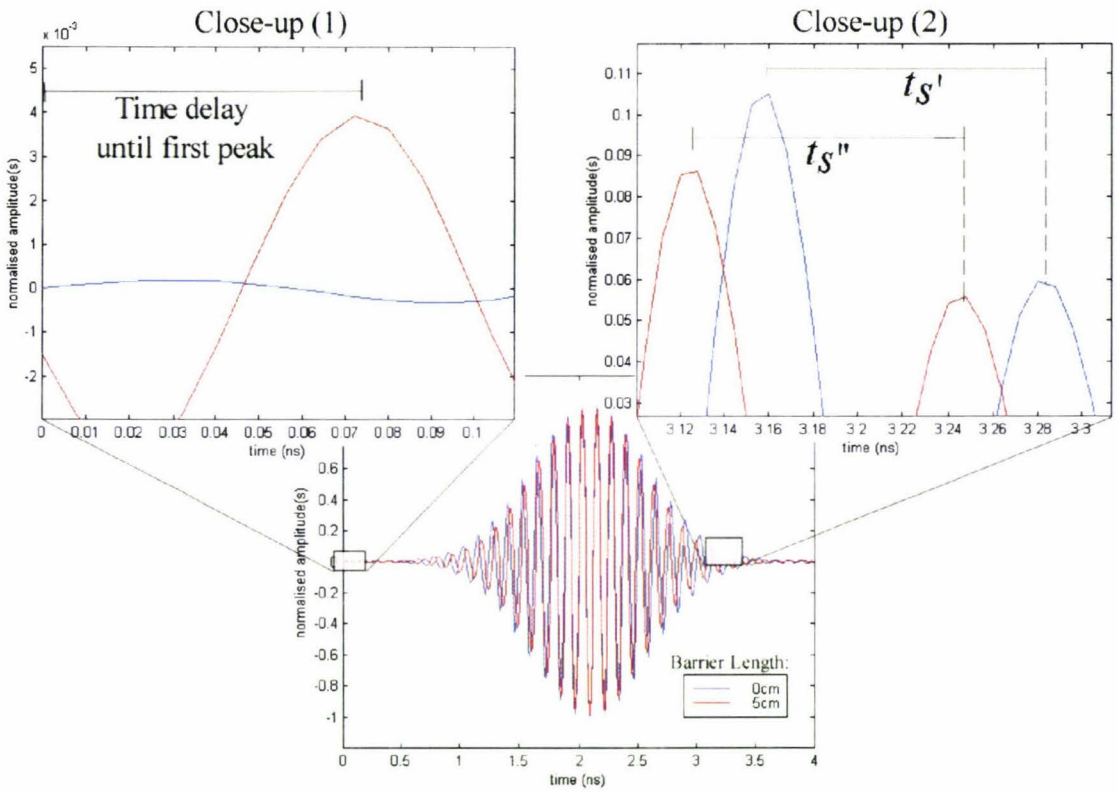

Figure 3.16: The incident and transmitted time signal for a Gaussian shaped wavepacket. The incident signal is characterised by a barrier length of 0cm whereas the transmitted time signal has penetrated a barrier length of 5cm. Close-up (1) and (2) show the subtle yet important differences between the two signals

The incident signal was sampled at the central frequency obtained from the amplitude spectrum, refer to section 3.2. Using the required sampling frequency f_s, refer to equation (3.7), the peaks of the wavepacket are 'selected', resulting in the transmitted envelope signal shape. The sampling time t_s can be thought of as the time difference between successive peaks of the wave packet. The time between successive peaks for the incident signal is shown to be t_s', refer to Close-up (2) of figure 3.16.

For any of the incident time signals investigated, there is an insignificant time sampling delay. This implies that the first peak of the wavepacket occurs at 0ns.

Close-up (1) of figure 3.16 shows that there exists a significant time delay before the first peak of the transmitted time signal appears. Also, the time between peaks is now t_s'', which can be approximated from the central frequency of the 'shifted' amplitude spectrum, refer once more to Close-up (2) of figure 3.15. The transmitted central frequency is now higher than the incident central frequency, implying $t_s'' < t_s'$. Sampling at the inappropriate frequency or not allowing for the time delay will result in significant aliasing. If the time difference between the first and second peak is not representative of the time difference between all peaks, then a longer time delay will be needed to prevent aliasing, see section 3.3.4.1.

Figure 3.17 shows the normalised transmitted time signal envelopes found by sampling at the correct frequency and using the appropriate time sampling delay. The time difference between the first and second peak of the wavepacket can be considered representative of t_s''. Sampling of the transmitted envelopes obtained in figure 3.17 began at the first peak of the Gaussian wavepacket.

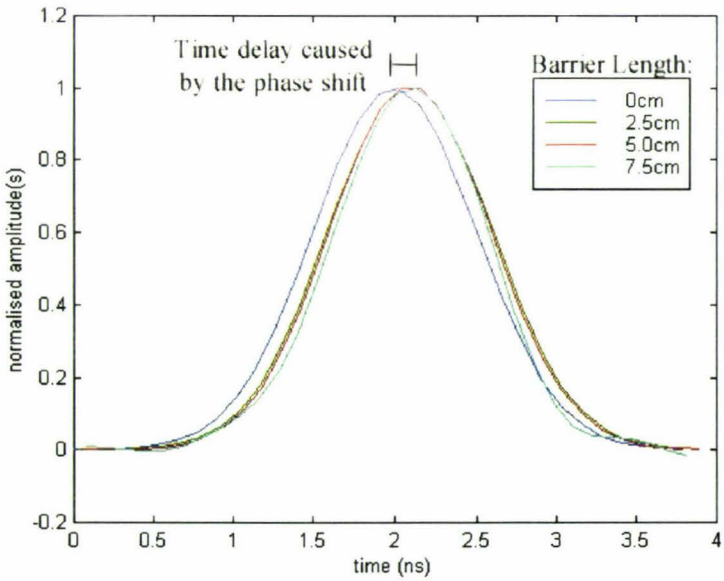

Figure 3.17: The normalised transmitted time signal envelopes for a Gaussian shaped incident signal penetrating various barrier lengths. After barrier lengths of about 2.5cm, the phase shift, and therefore time delay, appears constant.

3.3.5 *Speeds through a non-dissipative barrier*

Although the incident signal is not monochromatic, using the DFT results in a number of monochromatic cosine waves being used to construct the incident waveform. The phase speed of each of these components can be calculated using equation (2.38). The phase speed outside the barrier (in regions 1 and 3) will be real and given by

$$v_p = \frac{\omega}{\beta} \tag{3.10}$$

Figure 3.18 shows the phase speed through the region 1 and 3. The group speed outside the barrier will also be real and given by

$$v_g = \frac{d\omega}{d\beta} \tag{3.11}$$

Refer to figure 3.19 for the group speeds through regions 1 and 3.

Equation (2.52) states that the energy speed inside the barrier region is equal to the phase speed of the signal outside the barrier region.

To find the phase and group speeds inside the barrier, the Hartman values must be used. A plot of the Hartman phase speed against frequency has an asymptote at the frequency which does not suffer a phase shift (7.44GHz). Frequencies less than this have a positive Hartman phase speed (positive phase shift) while those greater have a negative Hartman phase speed (negative phase shift). These phase speeds are greater than c and increase for increasing barrier lengths.

Figure 3.20 shows the absolute Hartman phase velocity divided by c as a function of frequency. The Hartman phase speed diverges at 7GHz so is not considered relevant.

The waveform is not monochromatic and each cosine component suffers a different phase shift, resulting in different Hartman group speeds being calculated for each frequency, refer to figure 3.21.

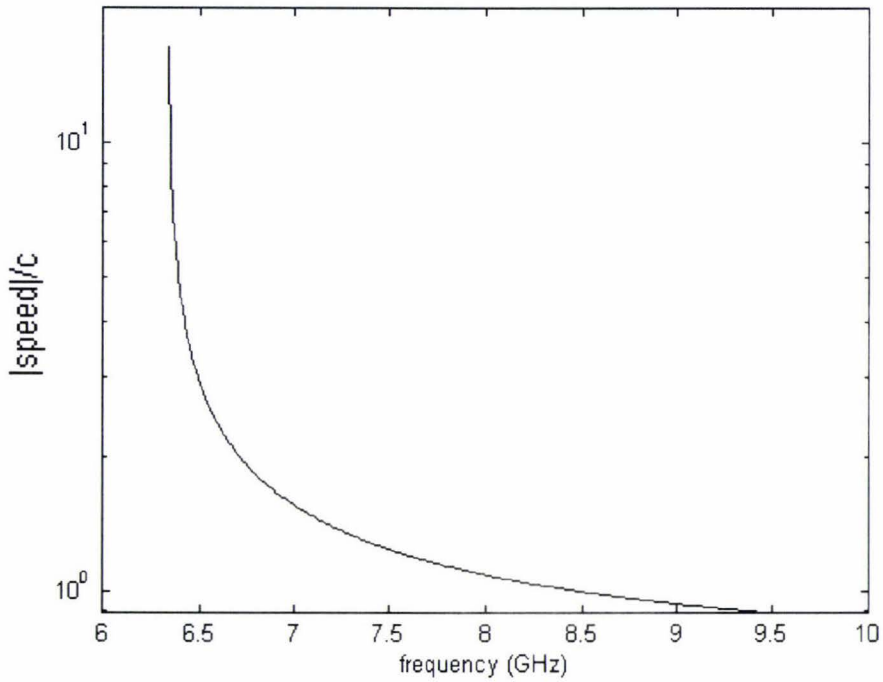

Figure 3.18: Phase speed through the waveguide as a function of frequency. The phase speed through region 1 is the same as that through region 3. This is also the energy speed through region 2, see equation 2.54.

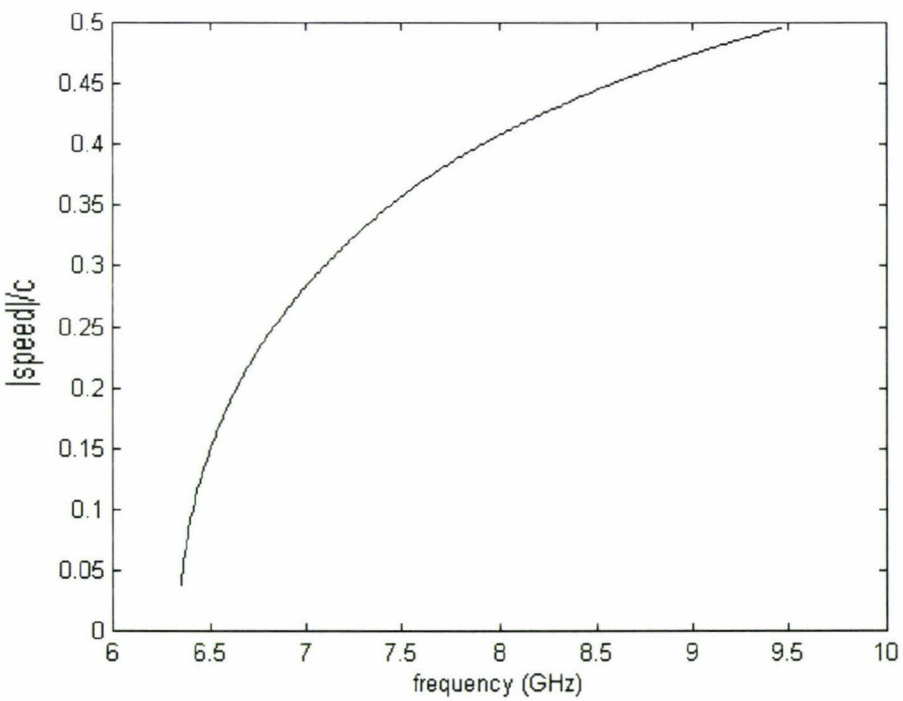

Figure 3.19: Group speeds through the waveguide as a function of frequency. The group speed through region 1 is the same as that through region 3.

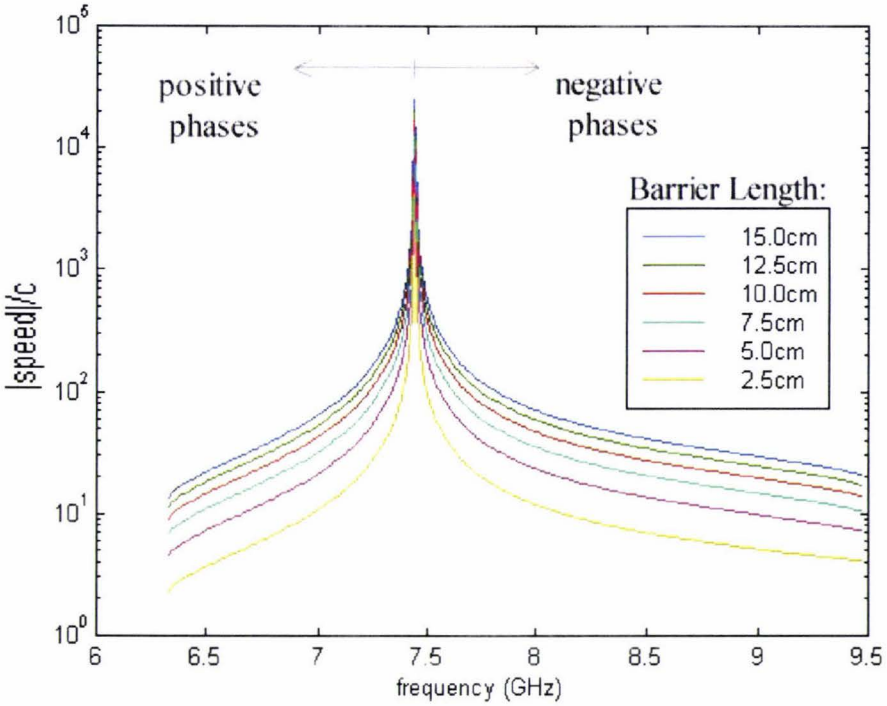

Figure 3.20: Hartman phase speed as a function of frequency for non-dissipative barriers.

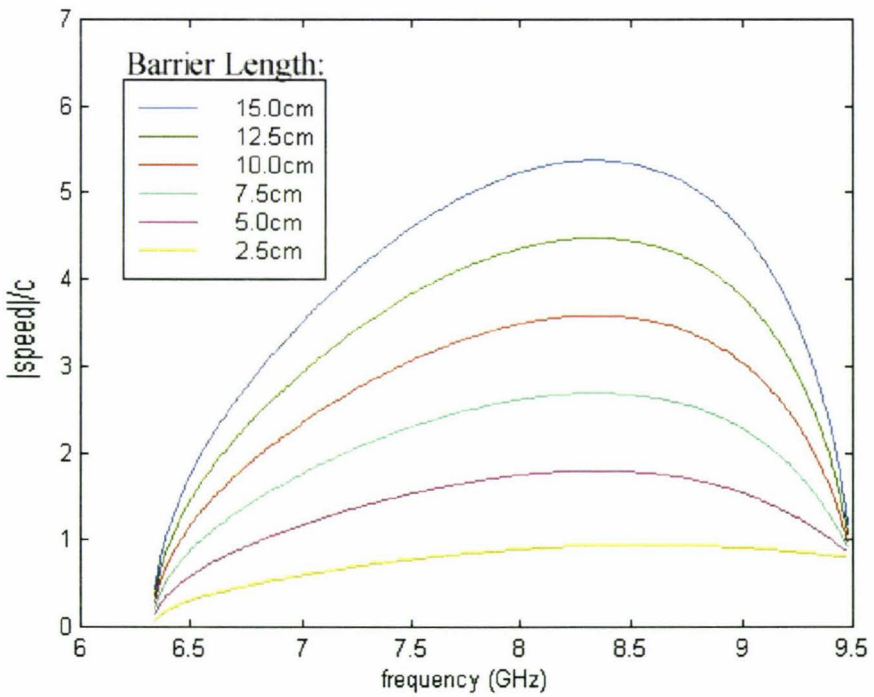

Figure 3.21: Hartman group speed as a function of frequency for non-dissipative barriers.

Nimtz *et al.* [8] used the phase shifts to calculate the group speeds of 1.1 and 1.5 times the vacuum velocity of light for the 4.9cm and 6.47cm barriers respectively at a frequency of 7GHz. These values are the Hartman group speeds and are in total agreement with the results shown in figure 3.21. The Hartman group speeds increase in magnitude with increasing barrier length. Refer once more to figure 3.21 showing the absolute group speed divided by c as a function of frequency. For short barrier lengths (less than about 2cm), superluminal speeds are not observed. For barrier lengths above 2.5cm, most of the Hartman group speeds are superluminal. The greatest Hartman group speed at barrier lengths greater than about 2cm occurs at a frequency about 8.3GHz. This frequency occurs at the point of inflection of the phase versus frequency graph.

At short barrier lengths (less than 2cm), the Hartman group speed is similar to the group speed of the signal outside the barrier as defined by equation (3.11). However, the Hartman group speed increases with increasing barrier length. Neither the Hartman phase nor group speeds depend on the shape of the incident signal since they only depend on the frequencies present and not the amplitudes of the frequency components.

The time sampling delay as described in section 3.3.4.2 must be properly accounted for when investigating the correlation and signal speeds. Truncating the longer of the incident or transmitted time signals so that both the signals exist within the same time window does this.

The padded incident and transmitted envelopes used to find the auto and cross-correlation curves are shown in figure 3.22. Although padding of the signal mitigates the effect of non-zero amplitudes at the end and beginning of the time signal, it will not totally account for significant truncation, refer to close-up of figure 3.22. Significant truncation at the beginning or end of the transmitted time envelope signal will result in smaller or larger delay times respectively when cross-correlating. The cross-correlation speed was found by finding the time delay between the peak of the auto-correlation of the padded incident time signal and the peak of the cross-correlation of the padded incident time signal with the padded transmitted time signal, refer to figure 3.23.

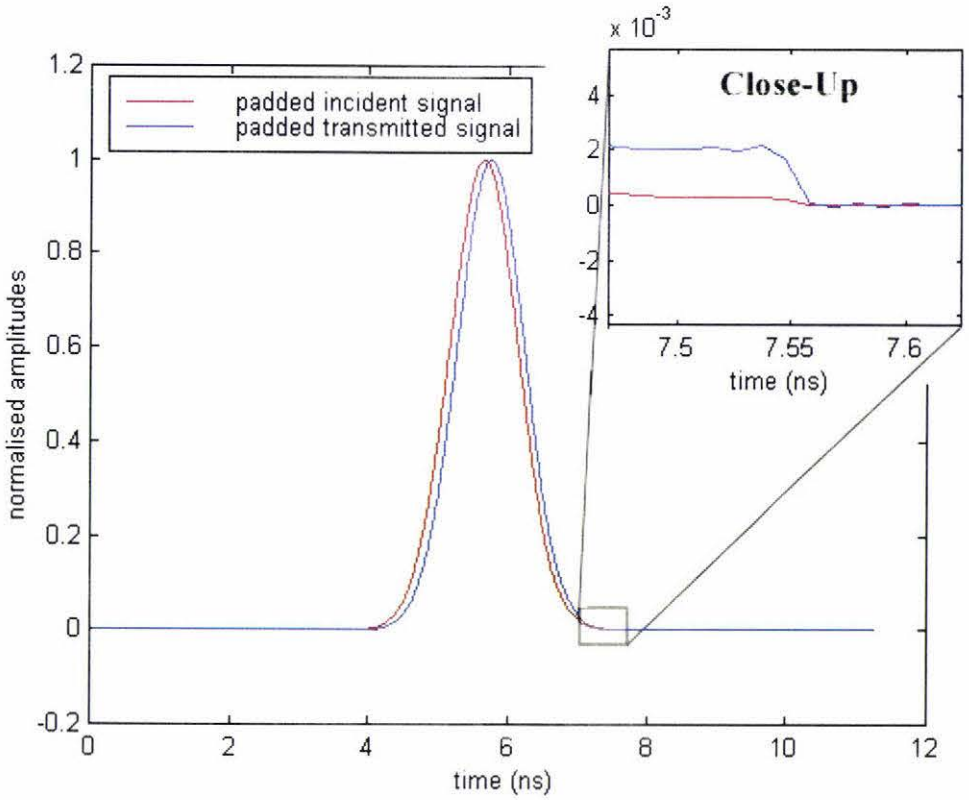

Figure 3.22: Padded incident and transmitted time envelopes used to find the cross-correlation speed. The close-up shows a slightly clipped transmitted time signal.

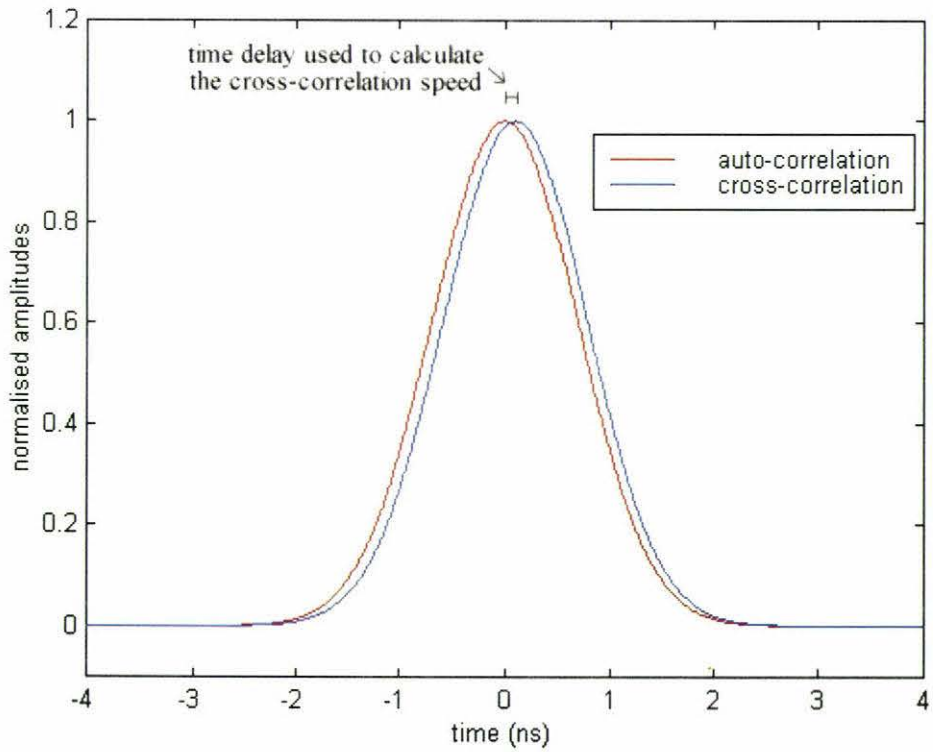

Figure 3.23: Auto and cross-correlation curves. The difference between the peaks is defined to be the delay time.

Figure 3.24 shows the cross-correlation, signal and average Hartman group speeds for barrier lengths between 0cm and 8cm for a Gaussian shaped time signal. There is an approximate linear relationship for increasing barrier lengths for the speeds shown in figure 3.24. Using linear regression, the cross-correlation speed can be given by $(0.240 \pm 0.004)c\ell$ and is within uncertainty to the signal speed $(0.245 \pm 0.006)c\ell$ when the fraction of one (fraction=1) is chosen to signify the arrival of the transmitted signal. The average Hartman group speed is given by $(0.257 \pm 0.002)c\ell$ and is similar to the cross-correlation and signal speed (when the fraction=1), but not within uncertainty. It could still be used to approximate an upper-estimate for the cross-correlation and signal speed (fraction=1). Superluminal cross-correlation and signal speeds (fraction=1) are predicted at barrier lengths greater than about 4cm. Using a fraction of a third (as suggested by Brillouin) yields subluminal signal speeds for all barrier lengths investigated.

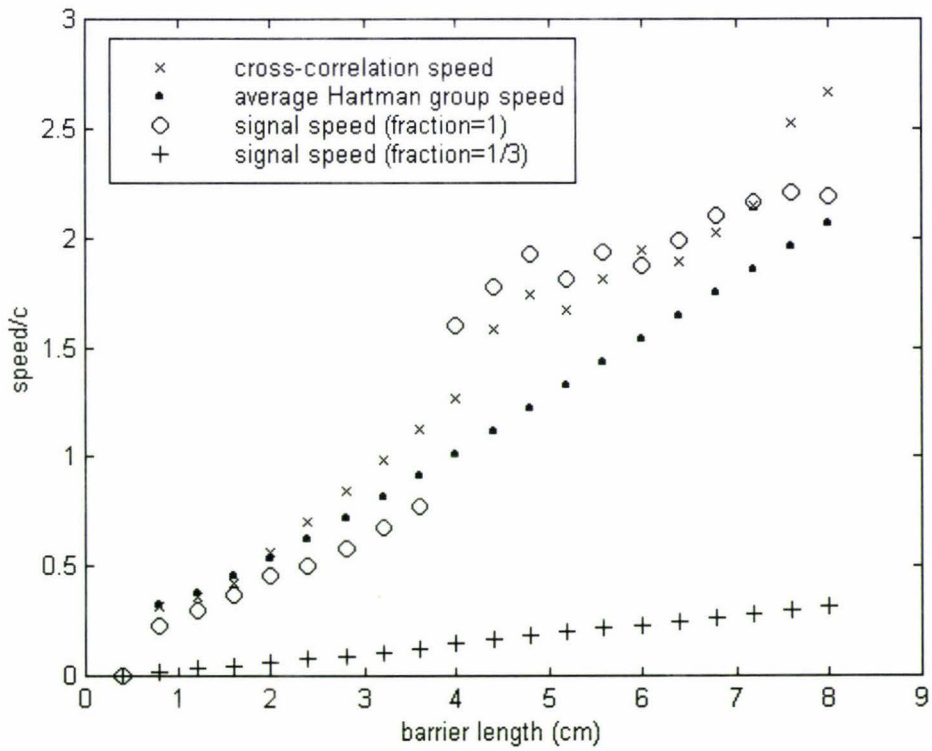

Figure 3.24: Speed as a function of barrier length for a Gaussian shaped time signal penetrating a non-dissipative barrier. Similar results can be obtained from other investigated signals but not up to the barrier lengths shown above (due to significant signal distortion).

Both the cross-correlation and signal speed (fraction=1) curves of figure 3.24 appear to increase abruptly at a barrier length of about 4cm. For increasing barrier lengths, more peaks exist within the wavepacket signal due to the migration of the amplitude spectrum to higher frequenices. Significant truncation of the transmitted time envelope occurs since an integer number of peaks will be sampled within the allowed time window. It is this truncation which causes smaller delay times and therefore faster cross-correlation and signal (fraction=1) speeds.

3.4 *Dissipative barrier penetration using the transmission line model*

3.4.1 *Attenuation and phase as a function of frequency*

By changing the properties of region 2, theoretical results can be obtained for the dissipative barrier and compared with the experimental results of Nimtz *et al.* [8]. An overlaid plot of $|T|^2$ against frequency comparing the theoretical and experimental results are shown in figure 3.25. Although the frequency range has been extended to cover the frequencies presented by Nimtz *et al.* [8], only the frequencies between 6.33GHz and 8.20GHz are used to reconstruct the transmitted signal. The allowed frequencies have been further limited by traversing a dissipative barrier compared to that of a non-dissipative barrier.

The theoretical and experimental results for the 4.9cm barrier are very similar and an agreement between theory and experiment is verified. However, the 6.47cm barrier results differ significantly and do not agree within the experimental and theoretical uncertainties. This discrepancy is probably due to imperfect fabrication of the longer dissipative barrier. The authors of the experimental paper [8] have actually stated that: "...the foamy material was pushed into the longer waveguide with a relatively high pressure leading to a higher density on one side. The transmission of radiation through such a non-symmetric structure is known to depend on the direction of incidence, an effect seen in our experiments" [44].

The attenuation is less but of the same order as that for a non-dissipative barrier. The average attenuation over the allowed frequency range for increasing barrier lengths is

linear, similar to non-dissipative barrier traversal. Using regression, an average attenuation of a signal traversing a dissipative barrier is calculated to be negative 7.6 ± 0.2 dB/cm (again independent of signal shape), which is less than the negative 8.6dB/cm acquired from non-dissipative penetration.

Figure 3.26 shows the phase as a function of frequency comparing the theoretical and experimental results through a 4.9cm and 6.47cm dissipative barriers.

Due to the imperfect fabrication of the longer barrier length, a discrepancy once more exists between the theoretical and experimental results for the 6.47cm barrier.

Negative phase shifts are observed over the whole frequency range investigated. The phase shift becomes larger (negatively) with increasing barrier lengths for all frequencies. This implies that there is no frequency at which the phase remains constant for increasing barrier lengths. The Hartman effect is therefore not dominant.

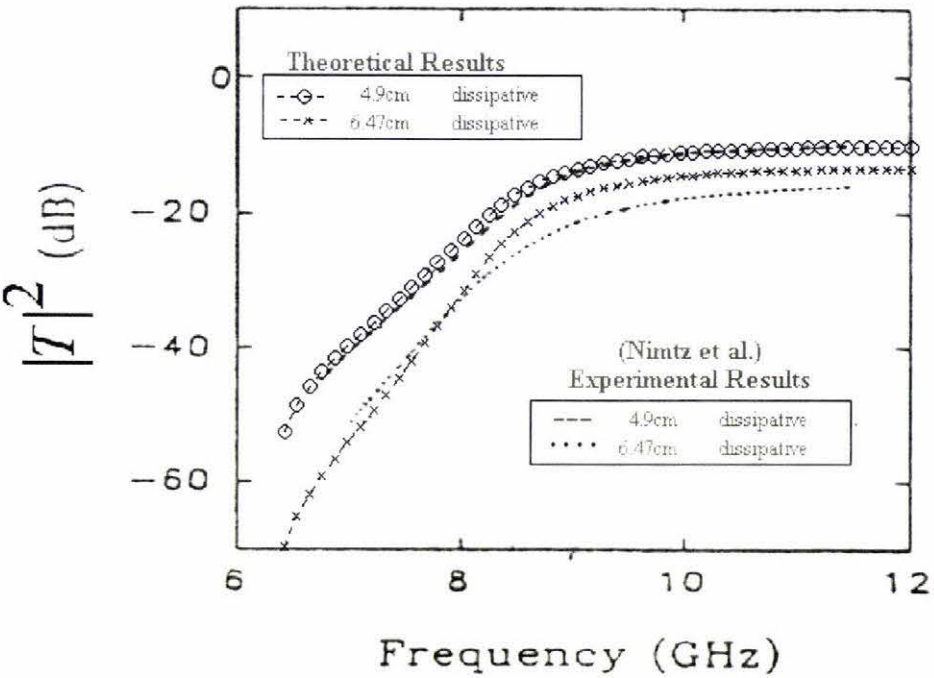

Figure 3.25: $|T|^2$ against frequency for penetration through a dissipative barrier. The theoretical results have been laid over the results presented by Nimtz *et al.* (as shown in Figure 1.2).

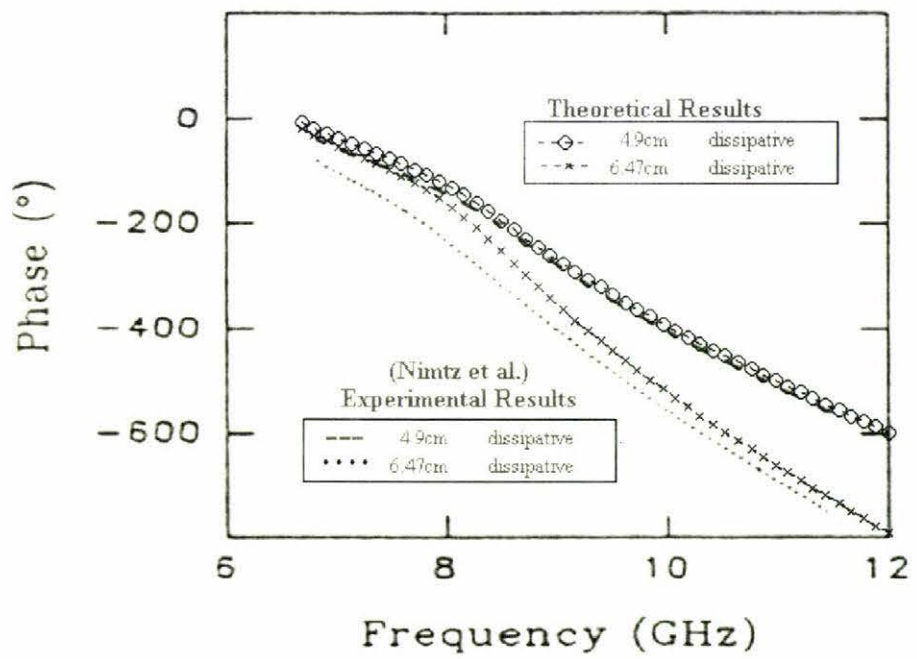

Figure 3.26: Phase against frequency for penetration through a non-dissipative barrier. The theoretical results have been laid over the results presented by Nimtz *et al.* (again, also shown in Figure 1.2).

3.4.2 *The Transmitted amplitude spectrum*

The response of the transmitted power spectrum when the barrier length is increased is similar to that of a non-dissipative barrier except of one major exception: the shape of the spectrum is 'conserved' for quite large barrier lengths. There is a shorter frequency range Δf, implying higher frequencies (whose amplitudes are large) do not traverse the barrier and do not play a part in the construction of the transmitted signal. Figure 3.27 shows these properties for a Gaussian amplitude spectrum for increasing barrier lengths. Again, the barrier acts as a high-pass filter. Other transmitted spectra can be investigated using the Matlab EBP simulation.

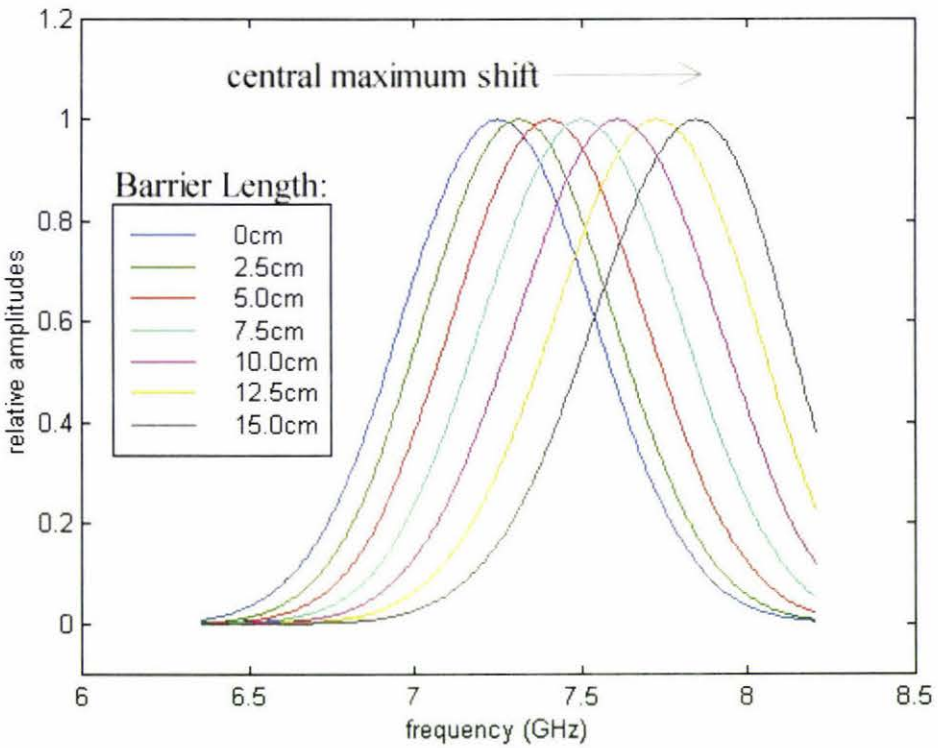

Figure 3.27: The normalized transmitted amplitude spectra of a Gaussian signal penetrating a dissipative barrier.

3.4.3 *Attenuation and phase as a function of time*

The effect of the attenuation on various incident signals is similar to that of a non-dissipative barrier. 70% to 100% of the components making up the transmitted signal suffer a negative phase shift (for all barrier lengths greater than 0cm). The 30% which suffer a positive phase shift are at the lower end of the spectrum and are more attenuated. The Hartman effect is not observed because it is negligible compared with the phase shifts due to propagation. The phases for each component become increasingly negative for increasing barrier lengths.

3.4.4 *The transmitted time signal*

Unlike the non-dissipative barrier, the phase plays a more significant role in the transmitted signal shape. Both attenuation and phase contribute to the distortion of the transmitted signal through the dissipative barrier.

The same signal shapes that have been investigated when traversing the non-dissipative barrier can also be investigated when traversing a dissipative barrier using the Matlab EBP simulation.

3.4.4.1 Wavepacket peak time differences

Like the transmitted wavepacket time signals through the non-dissipative barrier, the peaks within the wavepacket do not have a constant time difference. Again, different sampling times will be required to find the envelope of the wavepacket at larger barrier lengths. For most signals, at larger barrier lengths, the time differences between the peaks is at the beginning of the signal. Figure 3.28 shows the time differences between adjacent peaks for a Gaussian transmitted time signal after penetrating a dissipative barrier. Once again, the ideal curve should be horizontal implying the time difference between the peaks are the same.

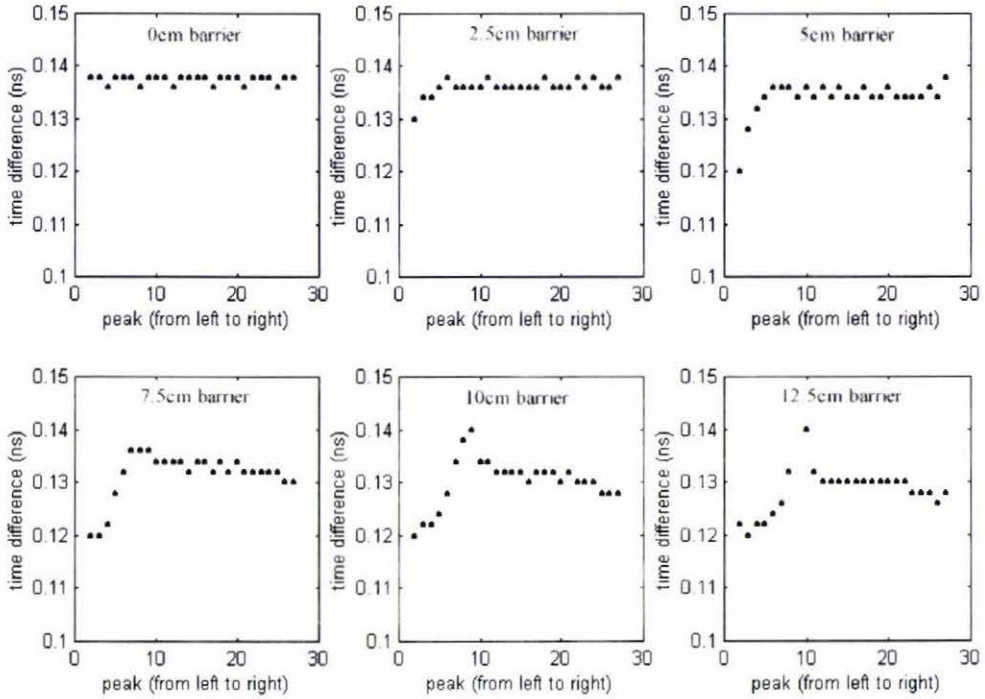

Figure 3.28: Time differences between adjacent peaks for a Gaussian wavepacket after penetrating different dissipative barrier lengths. It can be seen that as the barrier length increases, most of the time differences occur at the beginning and end of the signal. Ideally, the plotted points will be horizontal implying a constant time difference between adjacent peaks.

3.4.4.2 Sampling the envelope of the transmitted time signal

Figure 3.29 shows the normalised envelope of the transmitted time signal for a Gaussian shaped incident time signal after penetrating a dissipative barrier. Sampling began at the seventh peak of the wavepacket since significant transient peak time differences exist. For barrier lengths greater than about 7.5cm, a larger sampling time delay will be required since the seventh peak also becomes non-representative of the required sampling time, refer to figure 3.28. A truncated envelope is a result of the sampling time delay, again refer to figure 3.29. The sampling frequency is found once more from the central frequency of the shifted amplitude spectrum. It can be seen that the larger phase shifts at larger barrier lengths result in larger time delays.

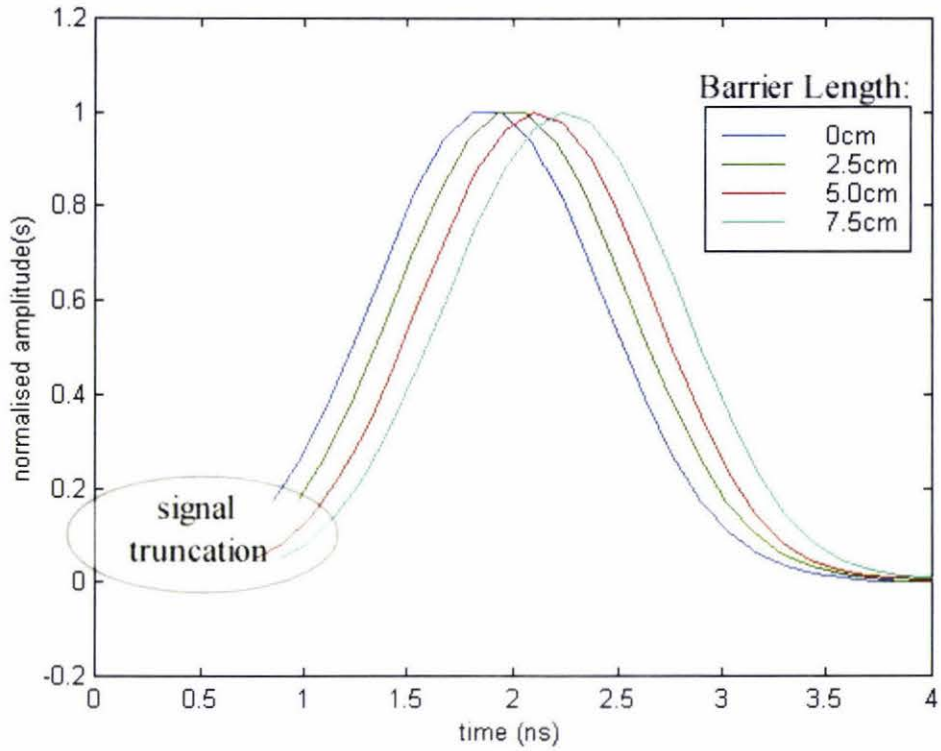

Figure 3.29: The normalised transmitted time signal envelopes for a Gaussian shaped incident signal penetrating various dissipative barrier lengths. Notice how the time delay increases with increasing barrier length. The signals have all been truncated due to required sampling delays (ignoring transient peak differences).

3.4.5 *Speeds through a dissipative barrier*

Since regions 1 and 3 of the waveguide are left unchanged, the phase speed outside the barrier is the same as given for the non-dissipative case. The propagation constant through a dissipative barrier is complex resulting in a phase speed in region 2. Figure 3.30 shows the phase speed through all three regions of the waveguide.

The group speed outside the barrier is same as that mentioned previously, but there is now a group speed through the barrier region. Figure 3.31 shows the group speeds through all three regions of the waveguide. A plot of the magnitude of the Hartman phase speed against frequency has a similar shape as that obtained for a non-dissipative barrier.

One important difference is that as the barrier length is increased, more and more frequencies suffer a negative phase shift. For barrier lengths over 10cm, all frequencies suffer a negative phase shift. Refer to Figure 3.32 which shows the magnitude (absolute value) of the Hartman phase speed divided by c as a function of frequency. This is a result of phase being dependent on barrier length. From these Hartman phase speeds, it is again possible to calculate the Hartman group speeds. Nimtz *et al.* [8] calculated that at a frequency of 7GHz, the group speeds through the dissipative barrier was 0.7c for both the 4.9cm and 6.47cm barriers. The 4.9cm result agrees with the experimental, but the 6.47cm result differs (but not considerably) from that shown in figure 3.33. This discrepancy is due to the differences between the experimental results and the theoretical model for the 6.47cm barrier. Although propagation at all frequencies is subluminal at short barrier lengths, it can be superluminal at larger barrier lengths. For example, the 7GHz component becomes superluminal at barrier lengths greater than 10cm. At short barrier lengths, the group speed is similar to the Hartman group speed, but the Hartman group speed strongly depends on barrier length and increases accordingly.

Figure 3.34 shows the signal (fraction=1 and 1/3) and average Hartman group speeds for barrier lengths between 0cm and 8cm for a Gaussian time signal. Unlike the non-dissipative barrier case, a linear relationship does not exist. The signal speed (fraction=1) is close however to the average Hartman group speed. Although penetration through all the barrier lengths investigated give subluminal speeds, an upper limit of $1.5c$ can be predicted at very long barrier lengths.

The signal speed depends on the signal shape yet follows a curve similar to that produced from the average Hartman group speed which is independent of signal shape. At higher barrier lengths, a larger part of the envelope is truncated. This results in underestimated signal speeds. Cross-correlation speeds have not been investigated since significant truncation of the envelope at the beginning of the signal results in negative time delays and therefore negative cross-correlation speeds.

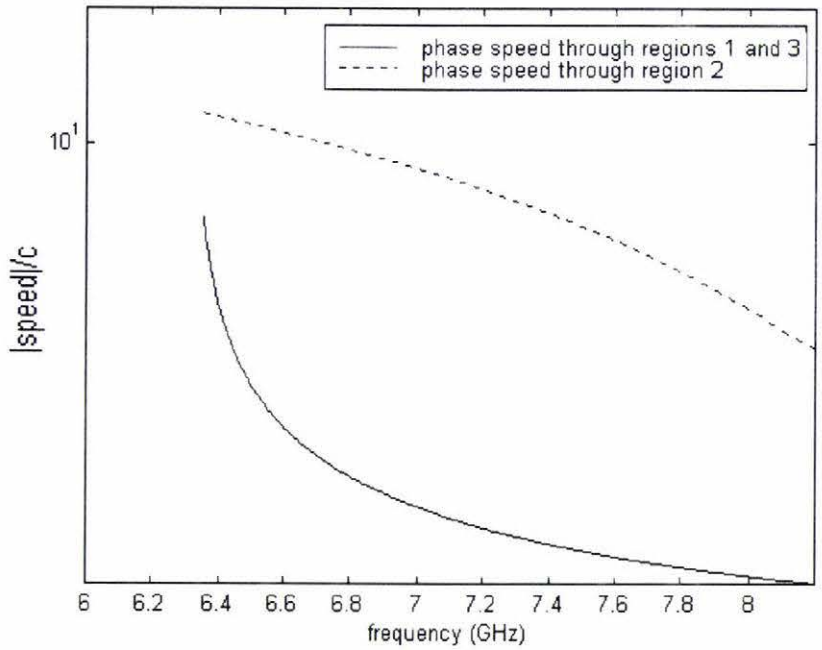

Figure 3.30: Magnitudes of the phase speeds through a dissipative barrier within a waveguide. The phase speed through region 1 is the same as that through region 3. Region 2 (the barrier) also has an associated phase velocity.

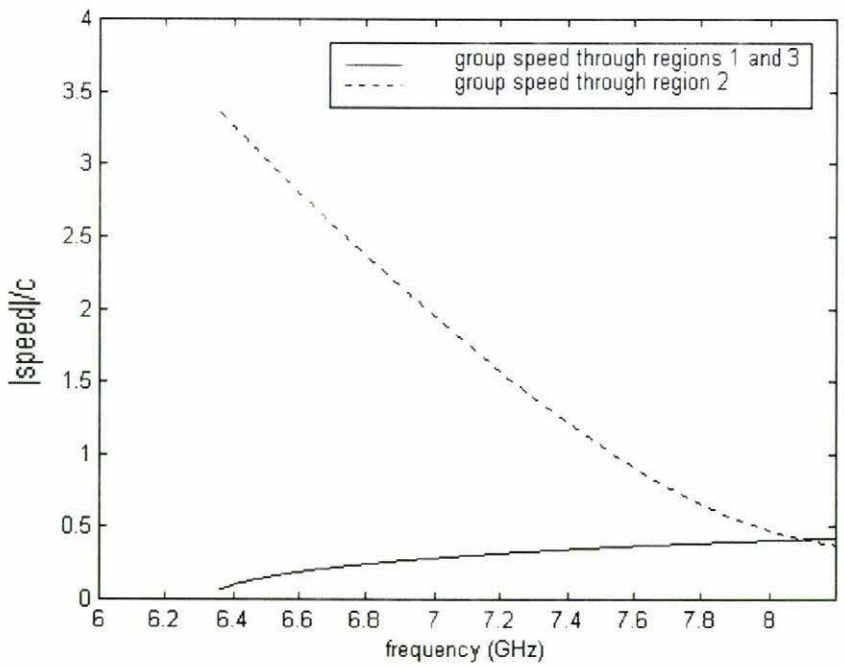

Figure 3.31: Magnitudes of the Group speeds through a dissipative barrier within a waveguide. The group speed through region 1 is the same as that through region 3. Region 2 (the barrier) also has an associated group velocity.

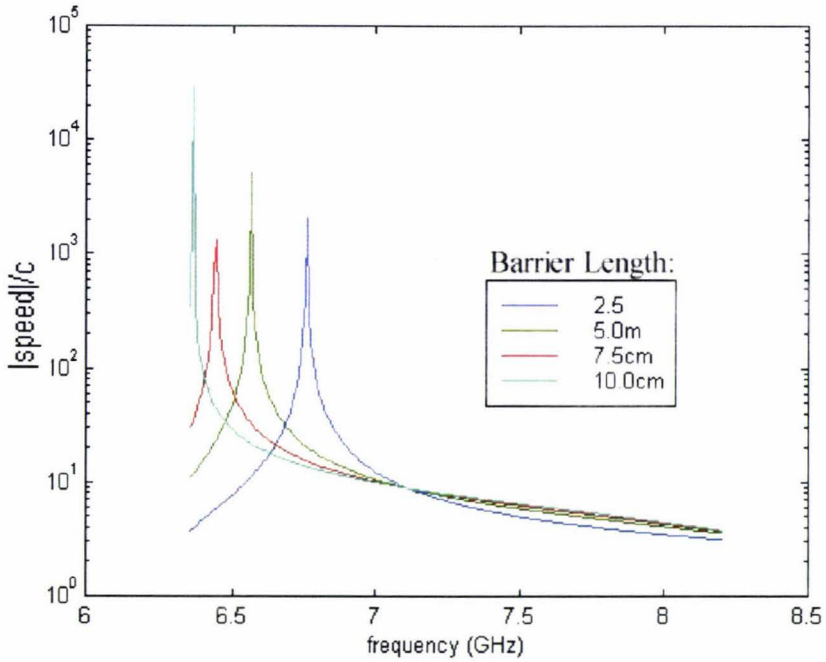

Figure 3.32: Hartman phase speeds as a function of frequency. Phases to the left of a peak are positive, while those to the right are negative. At barrier lengths greater than about 10cm, there is a negative phase shift at all frequencies.

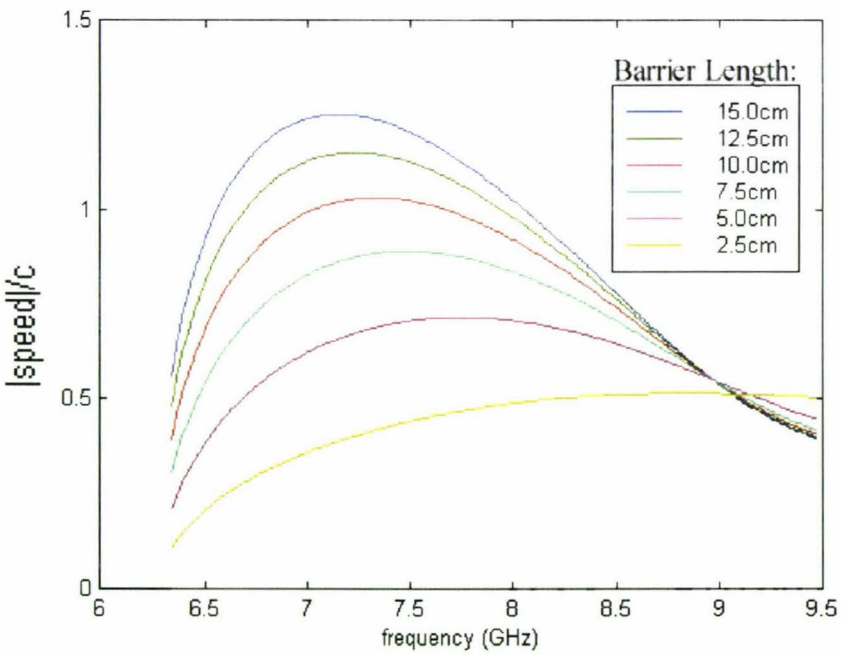

Figure 3.33: Hartman Group speeds as a function of frequency. All group speeds are subluminal for barrier lengths less than about 10cm.

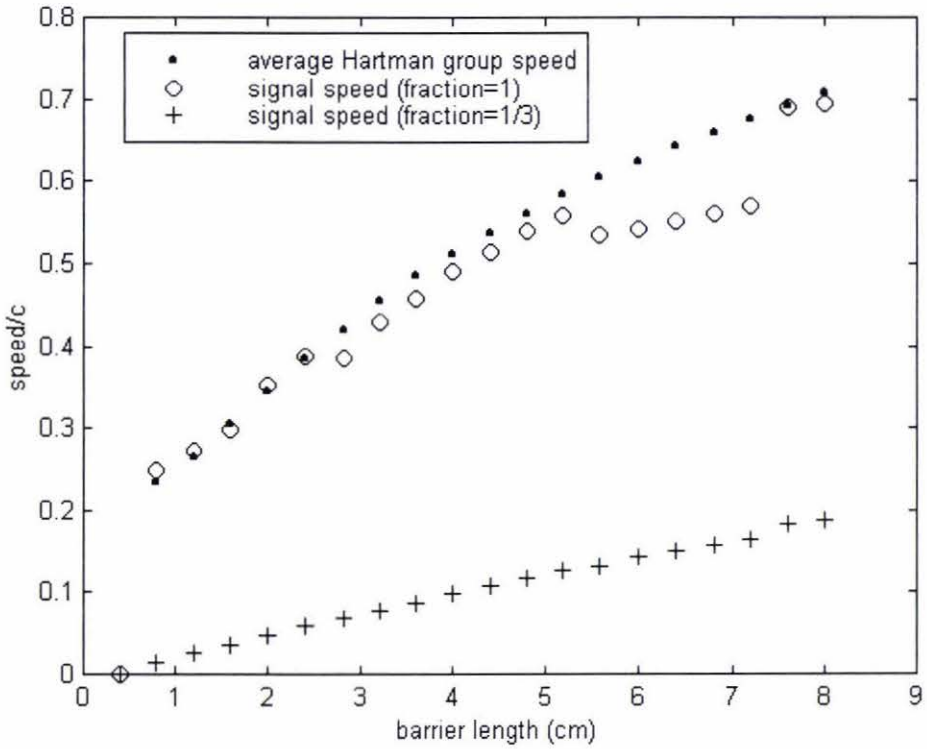

Figure 3.34: Speed as a function of barrier length for a Gaussian shaped signal penetrating a dissipative barrier. Similar results can be obtained from other investigated signals but not up to the barrier lengths shown above (due to significant signal distortion).

Chapter 4

Creation of matched incident signals able to penetrate long non-dissipative barriers

Only very short propagation delays occur through short barriers so propagation through long barriers is investigated theoretically even though considerable attenuation encountered would render long barriers impractical.

Barriers longer than a few centimeters can cause considerable pulse distortion such that propagation delay times are difficult if not impossible to assess. This problem is also faced in radar and seismic wave detection where a 'matched filter' is used to restore the detected pulse to an acceptable shape, see Bloch [45] for a discussion of matched filters. Skolnik [46] discusses matched filters designed to cancel some aspects of the distortion caused by propagation through a lossy dispersive medium. That particular solution is not appropriate here because the additional time delays introduce by the matched filter would be of the same order as those we are trying to measure through the barrier. However, we can use a 'matched signal'.

A matched signal is one that has a single peak incident on the barrier and a single peak emerging from the barrier. It is not a distortion free signal rather it is a controlled distortion. The barrier acts as a high pass filter of known parameters, see for example figure 1.2. In this study, the filter (the barrier) is specified so one must choose a signal that "matches" the filter parameters. The pertinent barrier parameters consist of a frequency dependent phase shift and a frequency dependent attenuation. If one limits one's attention to the middle region of the allowed frequency range for non-dissipative barriers with lengths greater than 2cm, one can model the barrier parameters as being a constant phase shift and an attenuation given by equation (4.2) in section 4.1.

4.1 *Piecewise linear Model for the attenuation as a function of frequency through a non-dissipative barrier*

$|T|$ is the magnitude of the transmission coefficient and is often referred to as the transfer function. It defines a family of curves that exponentially decrease with increasing barrier length. Plotting $\ln(|T|)$ against $\ln(f)$, where ln represents the natural logarithm, a number of characteristic attenuation curves for different barrier lengths can be compared, refer to figure 4.1.

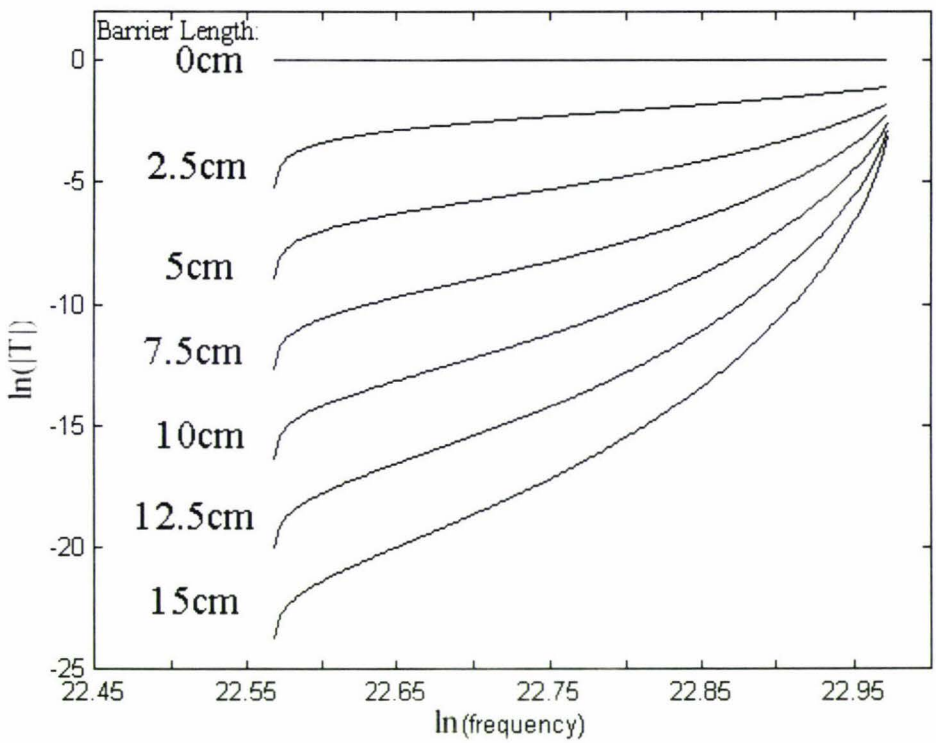

Figure 4.1: Curves showing the attenuation as a function of frequency for increasing non-dissipative barrier lengths.

There are three important regions for each of these curves, as an example refer to figure 4.2 which shows the attenuation curve for a 5cm non-dissipative barrier. Region [I] shows a very 'steep' increase of $\ln(|T|)$ with increasing frequencies close to ln(6.33GHz). Region [II] shows an approximately 'linear' increase of $\ln(|T|)$ over a large domain of $\ln(f)$. Region [III] shows a steeply rising 'non-linear' increase in $\ln(|T|)$ for $\ln(f)$ values approaching ln(9.49GHz). These regions, in particular region [II] can be approximated using a piece-wise linear model.

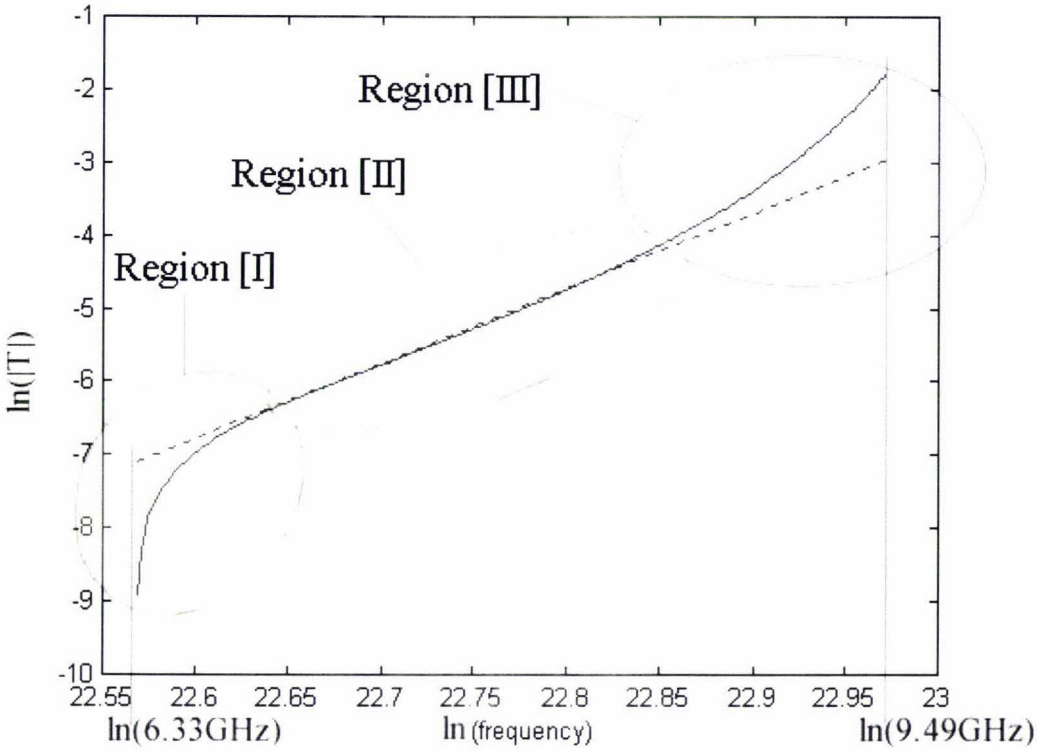

Figure 4.2: Regions of interest of a ln(|*T*|) against ln(*f*) graph. Region [I] shows that lower frequency components suffer highest attenuation. Region [III] shows that higher frequency components suffer less attenuation. Region [II] shows an approximate linear relationship between ln(|*T*|) and ln(frequency).

Comparing figure 4.1 with figure 4.2, it can be seen that region [III] becomes the dominant region at longer barrier lengths. The model that follows will therefore only apply to short barrier lengths.

As can be seen in Figure 4.2, many of the frequencies and therefore much of the signal information lies within the approximate linear region of region [II]. Using a piecewise linear approximation, this region will have an equation of the form

$$\ln(|T|) = m\ln(f) + c_1 \tag{4.1}$$

where m is the slope of the line and c_1 is the ln(|T|) axis intercept.

Equation 4.1 can be re-written as

$$|T| = c_2 f^m \tag{4.2}$$

where $c_1 = \ln(c_2)$. $|T|$ is an exponential function of f, and will henceforth be written as $|T(f)|$. m and c_1 (and therefore c_2) are dependent on barrier length and approximations of these values can be obtained from figure 4.1. An accurate method is required since small errors are greatly enlarged due to the logarithmic scale of this model. It can be shown that $m \approx a\ell$ and $c_1 \approx -b\ell$ where ℓ is the barrier length and a and b in this case are positive constants (not to be confused with the dimensions of the waveguide). This implies that c_2 has a value between 0 and 1 and exponentially decreases with increasing ℓ. f^m however, exponentially increases with ℓ. The constant c_2 is a 'scaling' factor which is independent of frequency and does not change the 'shape' of a curve at a given barrier length. It only causes attenuation at each frequency and is the same for all frequencies. The f^m part of equation (4.2) is a rapidly increasing curve and is the main cause of the transmitted amplitude spectrum distortion. Equation (4.2) can be used to predict the way in which the attenuation will affect the amplitude spectra for different barrier lengths, refer to section 4.4.

In terms of the spectral magnitudes,

$$|X_t(f)| = |T(f)||X_i(f)| \tag{4.3}$$

If significant shape differences between the incident and transmitted amplitude spectral curves exist, then the time signals will differ significantly. When comparing a transmitted time signal with the incident time signal, it is important that they are of similar shape and not heavily 'shape' distorted. For this to occur, the power spectra of $|X_i(f)|$ must be of the same shape as $|X_t(f)|$, with magnitudes that have been normalised accordingly. This condition is sufficient for the non-dissipative barrier regime since the phase shift becomes frequency independent for barrier lengths greater than about 2cm and there is no significant signal distortion from these 'initial' phase shifts.

The amplitude spectrum of a signal migrates to higher frequencies with increasing barrier length, see figure 3.12, so the matched signal is required to limit this migration otherwise the lesser-attenuated higher frequencies will dominate the transmitted amplitude spectrum. The matched signal is also required to have an amplitude spectrum that has a single peak that rapidly falls to zero, especially on the high frequency side. One can start

the search for the 'matched' signal by considering a Gaussian shaped signal since a Gaussian is the signal that suffers least distortion when traversing a non-dissipative barrier.

4.2 *A matched Gaussian signal*

A 'stretched Gaussian' time signal will have a 'narrowed Gaussian' amplitude spectrum. Likewise, a 'narrowed Gaussian' time signal will have a 'stretched Gaussian' amplitude spectrum, refer to appendix C.2 and C.3. A stretched spectrum has large non-zero magnitudes at high frequencies. These quickly dominate with increasing barrier length, refer once more to appendix C.3. Unfortunately, the 'narrowed Gaussian' amplitude spectrum created using the DFT has 'bumps'. These bumps are caused by the bandwidth, component and sampling limitations and truncation artifacts. At higher frequencies these bumps quickly dominate the spectrum with increasing barrier length, refer to appendix C.2. If these bumps did not exist, the narrowed amplitude spectrum would be an good spectrum to use to create a matched Gaussian time signal. A good amplitude spectrm can be formed by re-defining the bumpy amplitude spectrum to be that of an ideal Gaussian (eliminating the bumps), and shifting the spectrum to the lower end of the available frequency band. This would form a matched Gaussian time signal. Shifting the entire spectrum to lower frequencies prevents large frequency amplitude domination at larger barrier lengths. Any amplitude which is not zero, or close to zero within region [III] of figure 4.2 will become dominant at larger barrier lengths and the amplitude spectrum shape (in this case, a Gaussian) will be destroyed.

4.2.1 *Creating a matched Gaussian shaped amplitude spectrum*

Since the amplitude spectrum of interest will be shifted to lower frequencies, a spectrum of high upper frequency values (>9.49GHz) is required so that when shifted, low valued magnitudes close to zero will exist for frequencies up to 9.49GHz. Figure 4.3(a) shows the amplitude spectrum created between 6.33GHz and 15GHz. Due to the bandwidth limitations, bumps exist. The amplitude spectrum is then redefined to be the shape of an ideal Gaussian (eliminating the bumps) and is then shifted to lower frequency values, refer to figure 4.3(b). The phase for each amplitude is found from the DFT and although

the magnitudes have been redefined to be that of an ideal Gaussian, the phases have been left unaltered. The spectrum created in figure 4.3 is for illustrative purposes only. Although this amplitude spectrum is able to penetrate non-dissipative barrier lengths of up to 55cm without significant distortion, the amplitude spectrum investigated in the following section and used in the Matlab EBP simulation is narrower. This narrower amplitude spectrum results in a broader (stretched) Gaussian time signal. Ideally, a time window of about 8ns is required to visualize the entire signal, however a window of only 4ns is enough to visualise the beginning and the peak of the signal, refer to figure 4.4.

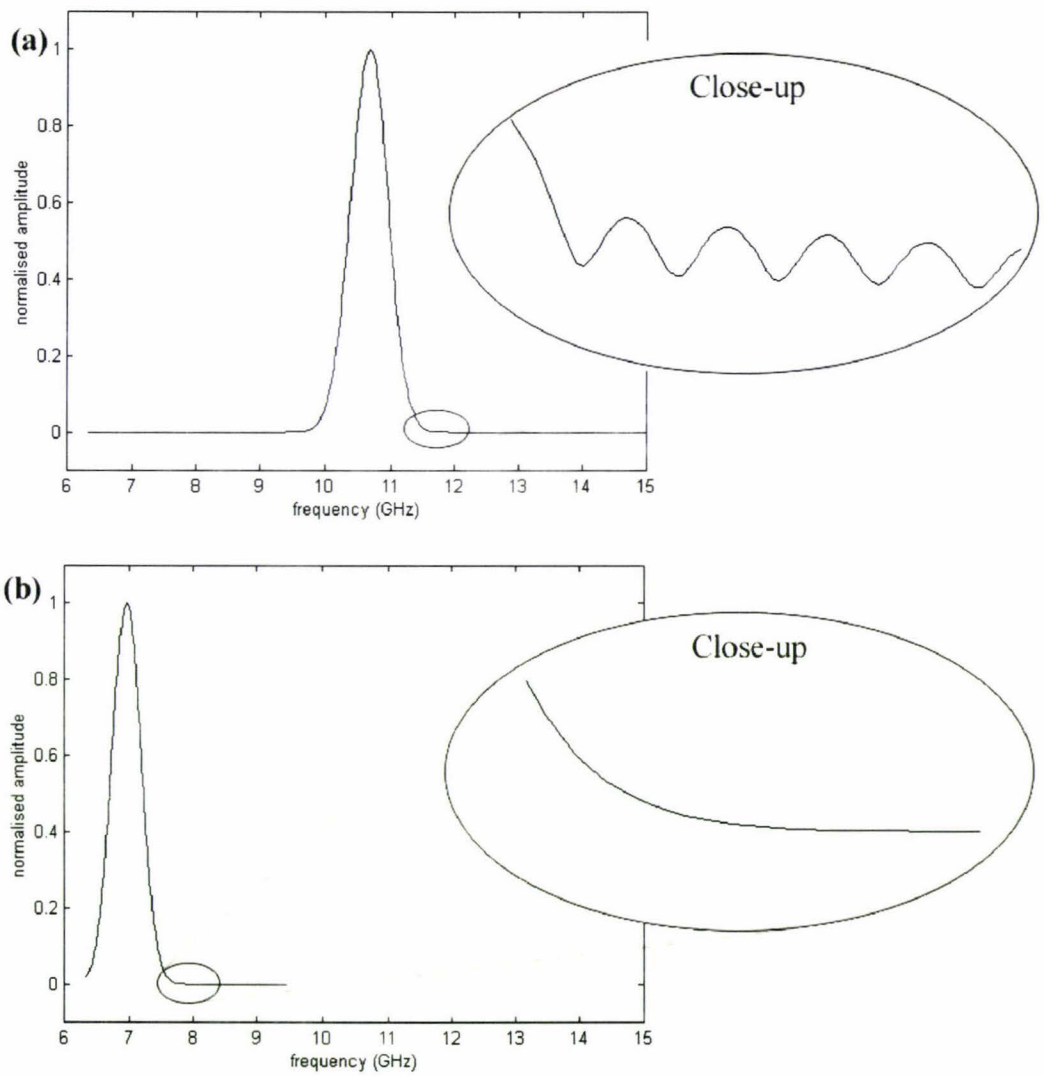

Figure 4.3: Creation of a 'matched' Gaussian amplitude spectrum. (a) shows a 'stretched' (time) Gaussian spectrum up to 15GHz. The "close up" shows that they spectrum is 'bumpy'. This is a result from the bandwidth limitations. (b) shows a Gaussian shaped approximation of the spectrum in (a) removing the bumps. The spectrum has been shifted so that it 'fits' between 6.33GHz and 9.49GHz. The peak is not centralised within these frequencies since amplitudes close to zero are required at higher frequencies.

4.2.2 *The matched Gaussian transmitted time signal and its associated amplitude spectrum*

Re-sampling the transmitted signal at the new centre frequency (the frequency at which the amplitude spectrum peaks) and allowing for the appropriate delay (start sampling at the first peak of the wavepacket), the transmitted signal shape is similar to that of the incident signal for barrier lengths over 150cm, refer to figure 4.4.

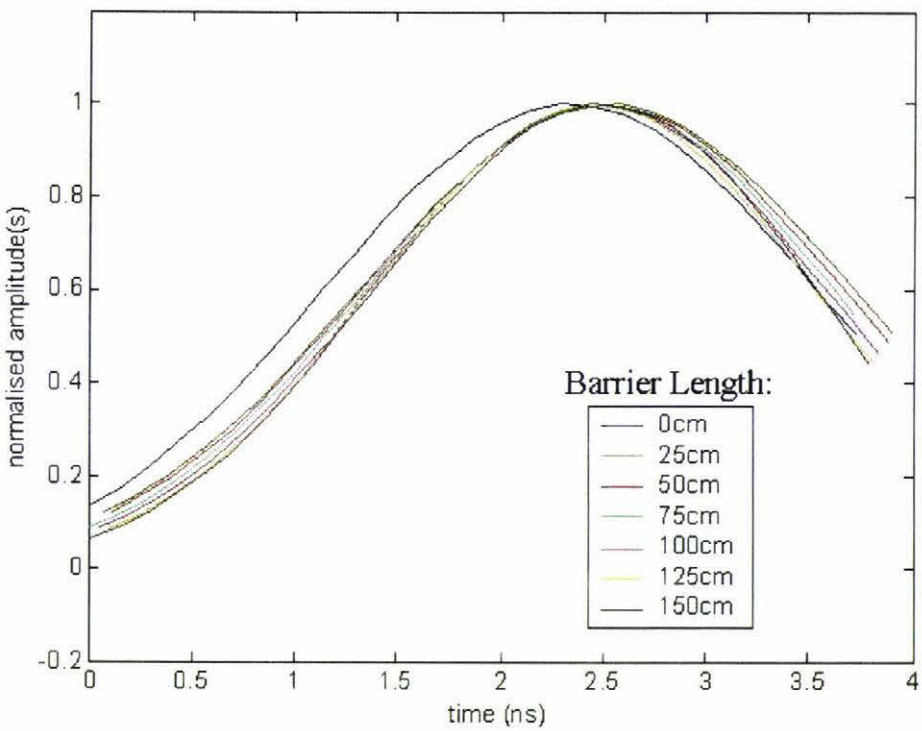

Figure 4.4: Transmitted envelope of a matched Gaussian incident signal through barriers up to 150cm. Notice the time delay between the incident signal (0cm barrier) and all the other lengths is approximately constant. This shows the independent nature of phase shift with increasing barrier length.

Figure 4.5 shows the transmitted amplitude spectra for barrier lengths up to 175cm. When the barrier length is greater than 150cm, significant amplitudes exist within region [III] of figure 4.2 and these amplitudes begin to dominate the entire amplitude spectrum and the time signal is destroyed. It is no longer representative of the incident signal shape.

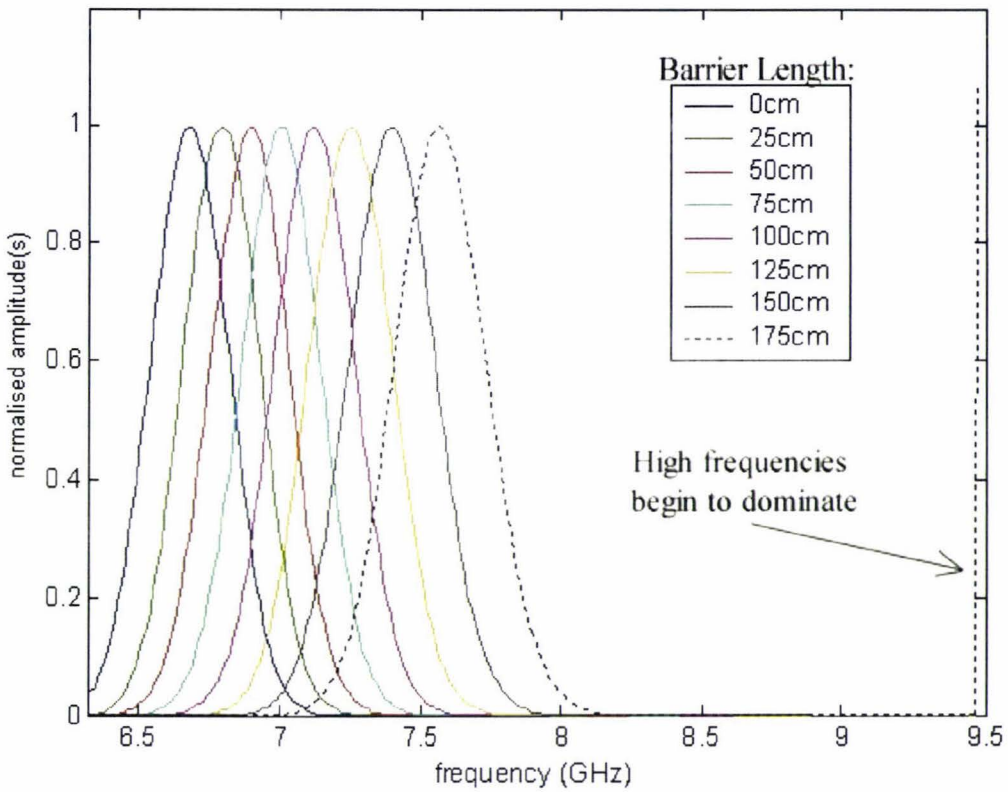

Figure 4.5: The transmitted amplitude spectra of a matched Gaussian time signal. At barrier lengths greater than 150cm, the dominant frequency is that of the upper cutoff frequency 9.49GHz. At barrier lengths greater than 150cm, the time signal is essentially destroyed (has no local peak representative of the incident signal shape).

Figure 4.5 shows the migration of the transmitted amplitude spectrum to higher frequencies with increasing barrier length. Figure 4.6 shows the frequency of the peak of the amplitude spectrum at different barrier lengths. It is these frequencies that are used to define the new time sampling rate for the transmitted time signal.

The transfer function $|T|$ used in this investigation is the actual transfer function rather than its piecewise linear approximation. If the approximation were used, then the spectrum would continue to migrate to higher frequencies without the higher frequency domination at larger barrier lengths.

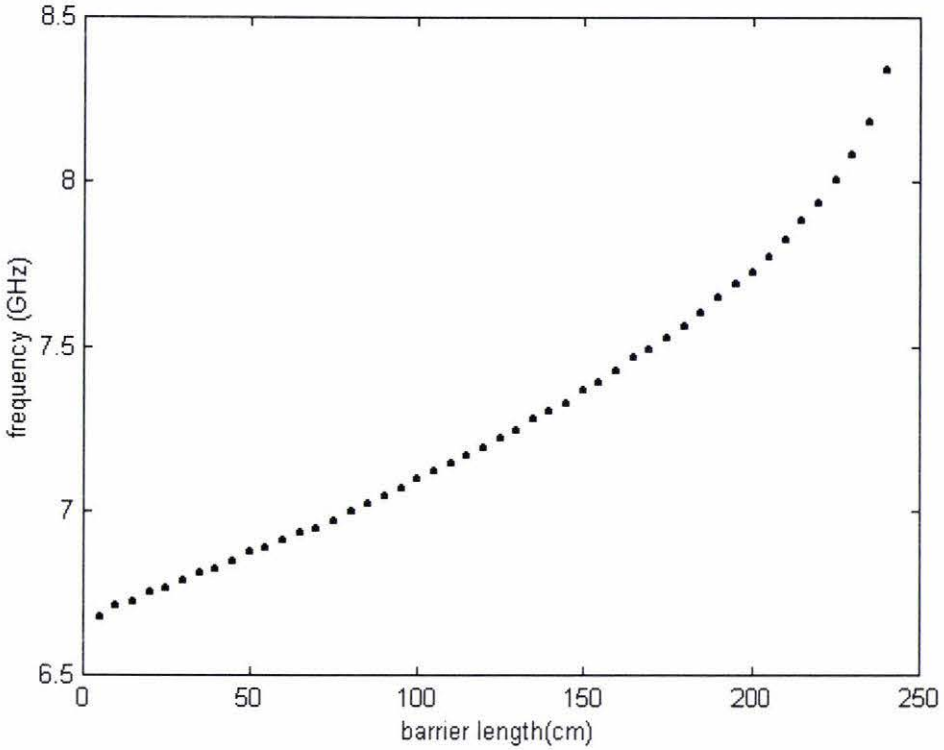

Figure 4.6: Migration of the peak of the amplitude spectrum with barrier length. For barrier lengths greater than 150cm, the peak represents a local maximum since higher frequencies dominate.

4.2.3 *Speeds of the matched Gaussian signal*

At larger barrier lengths, larger Hartman phase and group speeds are observed for all frequencies between the upper and lower cutoff frequencies, refer to figure 3.21. At a barrier length of 1.5m, a group speed of about $35c$ is predicted for the 7GHz frequency component of a matched Gaussian signal.

Since the transmitted matched Gaussian time signal does not have values close to zero near the beginning and end of the time signal (due to truncation), accurate cross-correlation and signal speeds will prove difficult if not impossible to calculate.

When finding the cross-correlation speed, the incident and transmitted signals were 'padded' with zeros, refer to figure 3.22. For cross-correlation purposes, the padding of the clipped signal results in the incident and transmitted signals resembling each other

more than they actually would if clipping had not occurred. As a result, small (even negligible) cross-correlation times giving very high (or infinite) cross-correlation speeds occur.

Since the time signal is truncated, the signal speed when the transmitted signal is a third of its incident signal shape cannot be found since these values have been truncated. The signal speed when the fraction is one (time between incident and transmitted peaks) can however be found. Figure 4.7 shows the average Hartman group speed and the signal speed when the fraction chosen is one for barrier lengths up to 150cm. A linear relationship appears to exist. Using linear regression, the average Hartman group speed can be given by $(0.257 \pm 0.002)\ell$ and the signal speed (fraction=1) can be given by $(0.24 \pm 0.2)\ell$, where the barrier length is measured in centimeters.

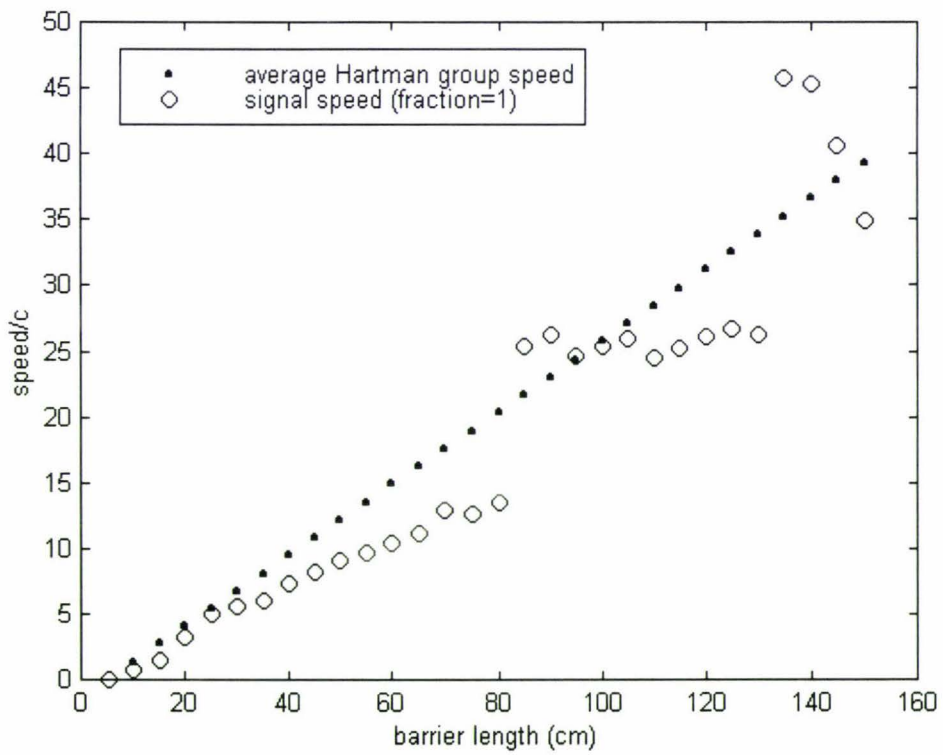

Figure 4.7: Graph showing the linearity of the average Hartman group speed and signal speed (fraction=1) for increasing barrier lengths. Average Hartman group and signal speeds of over 40 times the vacuum speed of light are predicted for barrier lengths over 150cm.

4.3 *An improved matched signal*

It has been shown in the previous sections that a Gaussian amplitude spectrum suffers less distortion in penetrating larger barrier lengths than other signal shapes investigated and can be used to find a matched signal. The distortion could be further reduced if the amplitude spectrum fell to zero more rapidly. Such a signal is algebraically simple to construct. Appendix D discusses analytically and graphically how to construct such curves. The family of curves created will be referred to as Shalav curves. Figure 4.8 shows a Gaussian curve and a similar shaped Shalav curve.

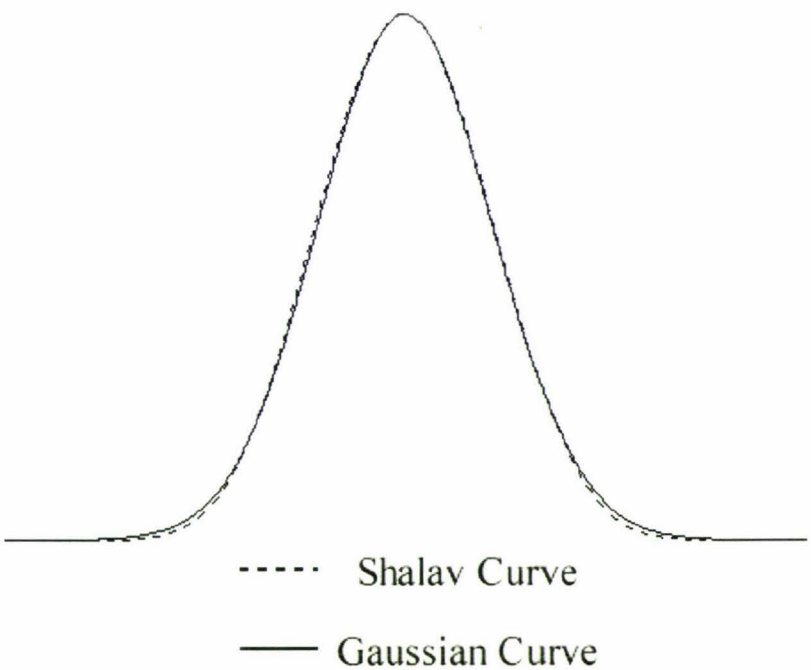

Figure 4.8: A Gaussian curve and a similar shaped Shalav curve. Notice the Shalav curve rises and drops more rapidly than a Gaussian.

4.3.1 *Creating a improved matched amplitude spectrum*

An improved matched amplitude spectrum can be obtained by replacing the Gaussian amplitude spectrum as defined in the previous section with a Shalav curve approximation. Again, only the respective magnitudes have been changed with the corresponding phases left unaltered. The amplitudes for the cosine components above about 8.2GHz have been defined to be zero. This essentially eliminates the effect of high amplitude domination since no significant amplitude exists within region [III] of figure 4.2.

4.3.2 *The improved matched transmitted time signal and its associated amplitude spectrum*

Re-sampling the transmitted signal at the appropriate frequency and allowing for the appropriate delay, the transmitted signal envelope is similar to that of the incident signal envelope for barrier lengths over 300cm, refer to figure 4.9. It can be seen that the signal broadens with increasing barrier lengths. It does however maintain a measurable peak representative of the shape of the incident signal over barrier lengths of 300cm. The broadening of the time signal is a result of the narrowing of the amplitude spectrum, refer to figure 4.10. It is the narrowing of the amplitude spectrum which causes the 'death' of the time signal. For very large barrier lengths, the amplitude spectrum will appear to consist of only a single frequency resulting in a 'flat line' envelope shape and a peak will no longer exist in the time domain.

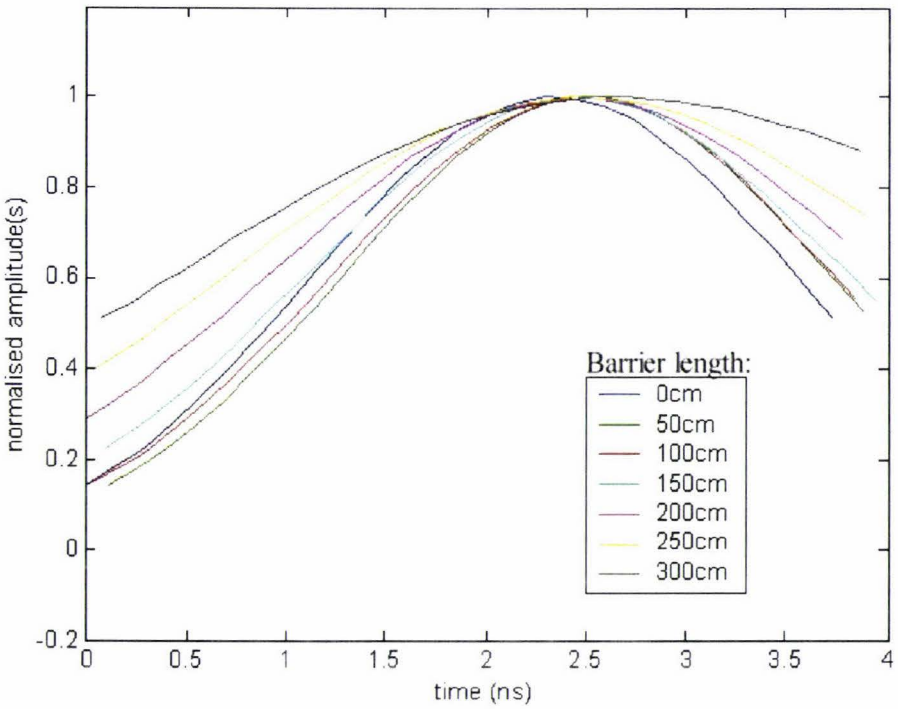

Figure 4.9: Transmitted envelope of an improved matched incident signal through barriers up to 300cm. Notice the signal broadens with increasing barrier length.

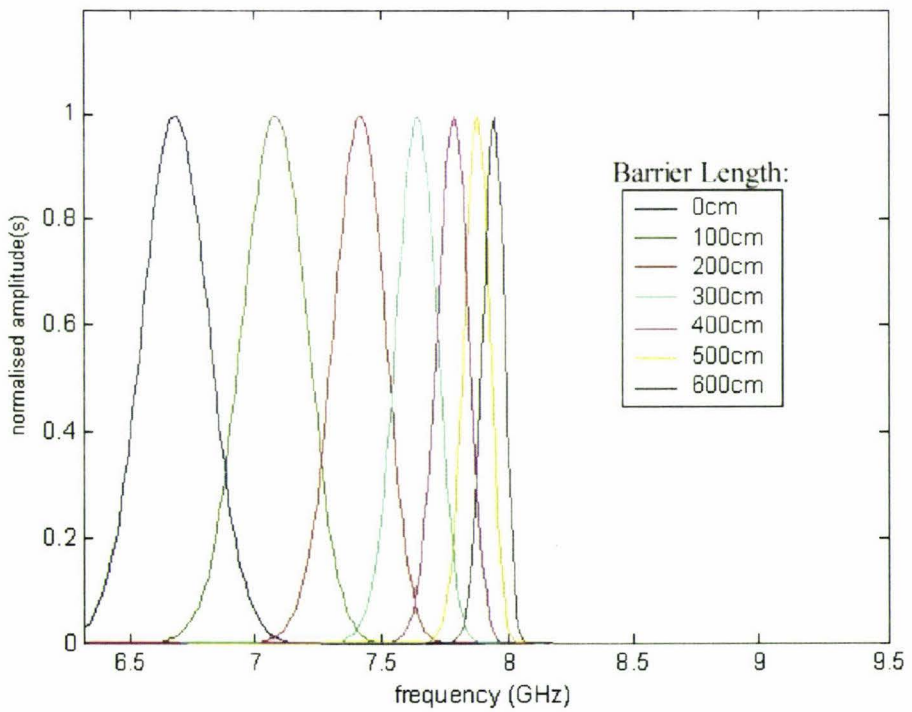

Figure 4.10: The transmitted amplitude spectra of a matched Shalav amplitude spectrum. The amplitude spectrum narrows with increasing barrier length. The narrower the amplitude spectrum, the broader the time signal, as expected.

Notice the migration of the peak of the amplitude spectrum slows with increasing barrier length. This is illustrated in figure 4.11.

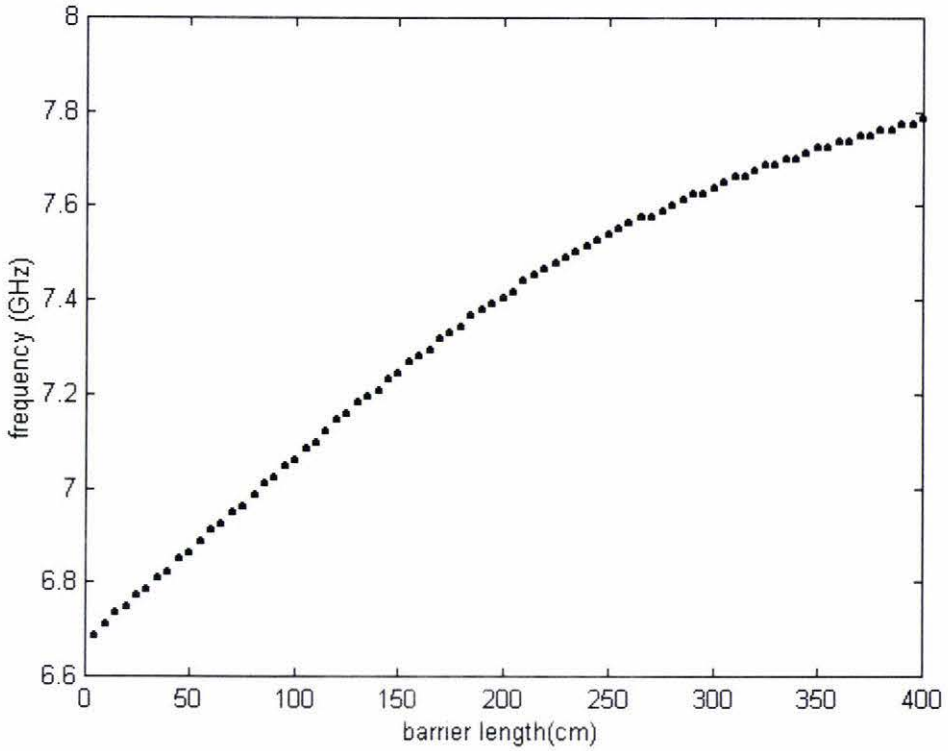

Figure 4.11: Migration of the peak of the amplitude spectrum with barrier length for matched Shalav curves.

4.3.3 *Speeds of the improved matched signal*

At a barrier length of 300cm, a group speed of 70*c* is predicted for the 7GHz frequency component of the improved matched signal.

Like the matched Gaussian transmitted time signal, the improved matched time signal does not have values close to zero near the beginning and end of the time signal (also due to truncation). The time signal broadens with increasing barrier lengths resulting in further truncation of the 'stretched' signal. Accurate cross-correlation and signal speeds will once more prove difficult to calculate.

The fraction for the signal speed to be calculated will again be taken to be unity (time between incident and transmitted peaks). Large errors exist at larger barrier lengths since the peak of the transmitted signal becomes more problematical to find due to the broadening of the transmitted signal. Figure 4.12 shows the average Hartman group speed and the signal speed when the fraction chosen is one for barrier lengths up to 300cm. Again, a linear relationship appears to exist. Using regression, the average Hartman group speed is again given by $(0.257 \pm 0.002)c\ell$ and the signal speed (fraction=1) can be given by $(0.24 \pm 0.04)c\ell$.

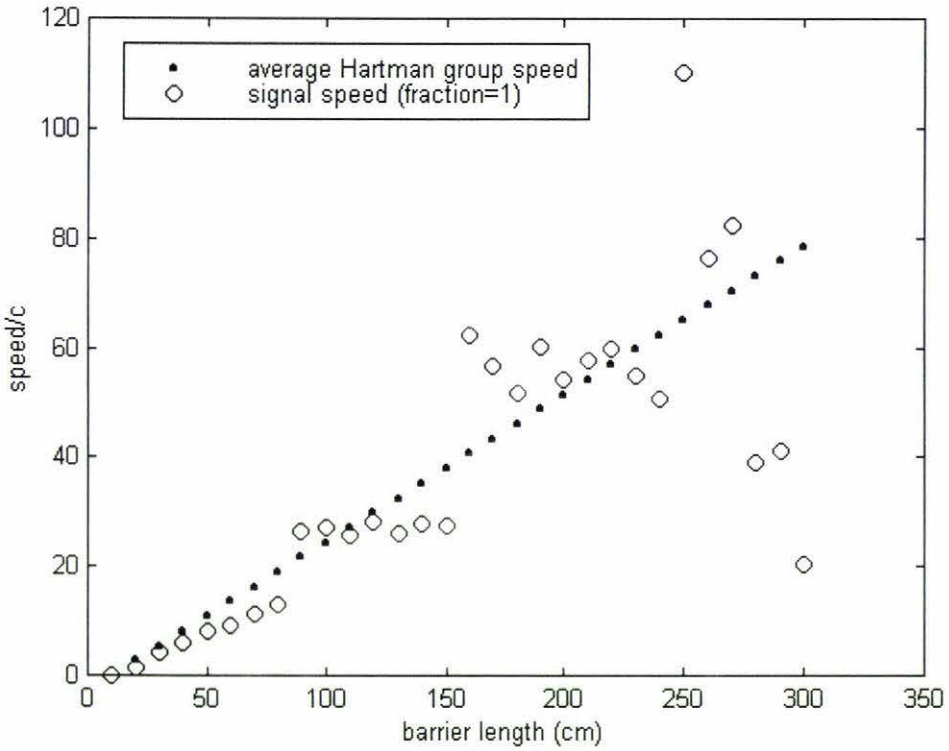

Figure 4.12: Average Hartman group speed and signal speed (fraction=1) for increasing barrier lengths for an improved matched signal. Average Hartman group and signal speeds of over 80 times the vacuum speed of light are predicted for barrier lengths over 300cm.

4.4 *Verification of the attenuation model*

Equation (4.2) can be used to predict how the peak of an amplitude spectrum migrates with increasing barrier lengths. Using Gaussian and Shalav curves to represent the shape of $|X_i(f)|$ and using the piece-wise linear approximation of $|T|$ for increasing barrier lengths results in a Gaussian curve being shifted, and a Shalav curve being shifted and narrowed, refer to figure 4.13. These results agree with the results of sections 4.2.1 and 4.3.1. Curves similar to that of figure 4.6 and 4.11 are also predicted.

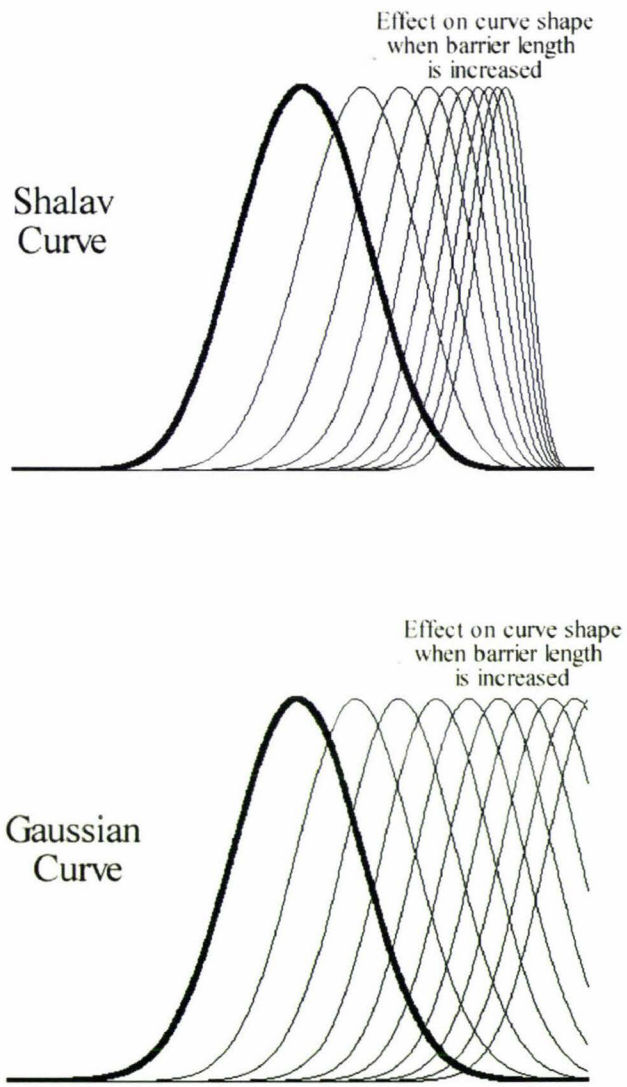

Figure 4.13: Effect on Shalav and Gaussian curve shapes when the barrier length is increased. These results are obtained by defining $|X_i|$ to be either a Shalav or Gaussian curve and then multiplying by f^m where $m \propto \ell$ for increasing ℓ. The x-axis represents the frequency domain.

4.5 *Gaussian and Shalav amplitude spectrum curves*

Taking consideration to avoid amplitude spectra that have significant magnitudes at higher frequencies has resulted in the creation of two different kinds of matched signal, the matched Gaussian signal and the improved matched signal. The matched Gaussian signal has a Gaussian amplitude spectrum whereas the improved matched signal has a Shalav curve amplitude spectrum. The migration of the peak of the amplitude spectra are described by the curves shown in figure 4.6 and 4.11 respectively.

All signal shapes investigated appear to have amplitude spectra that migrate either as a Gaussian curve amplitude spectrum or that of a Shalav curve amplitude spectrum. The 'Gaussian', 'narrowed Gaussian' and 'logarithmic Gaussian' time signals studied (refer to appendix B and C) have amplitude spectra which behave like a Gaussian curve amplitude spectrum, refer to figure 4.14.

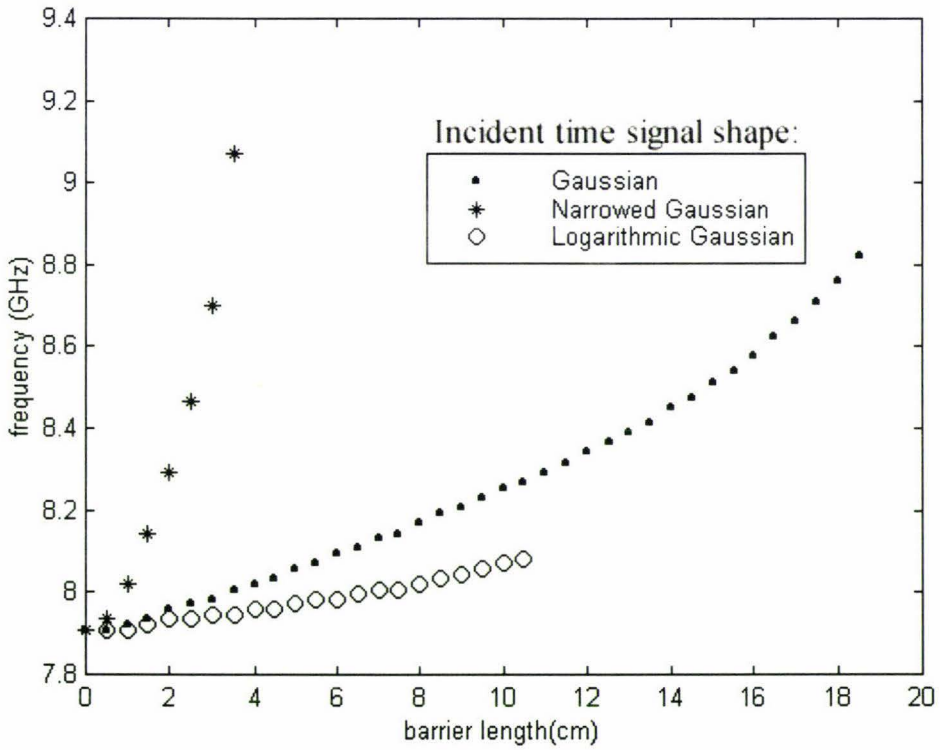

Figure 4.14: Graph showing at which frequency Gaussian shaped amplitude spectrum peaks for different barrier lengths. These curves are similar to the one shown in figure 4.6, though over a restricted range.

The 'double Gaussian', 'stretched Gaussian' and 'sinc' time signals studied (refer to appendix B and C) have amplitude spectrums which behave like a Shalav curve amplitude spectrum, refer to figure 4.15.

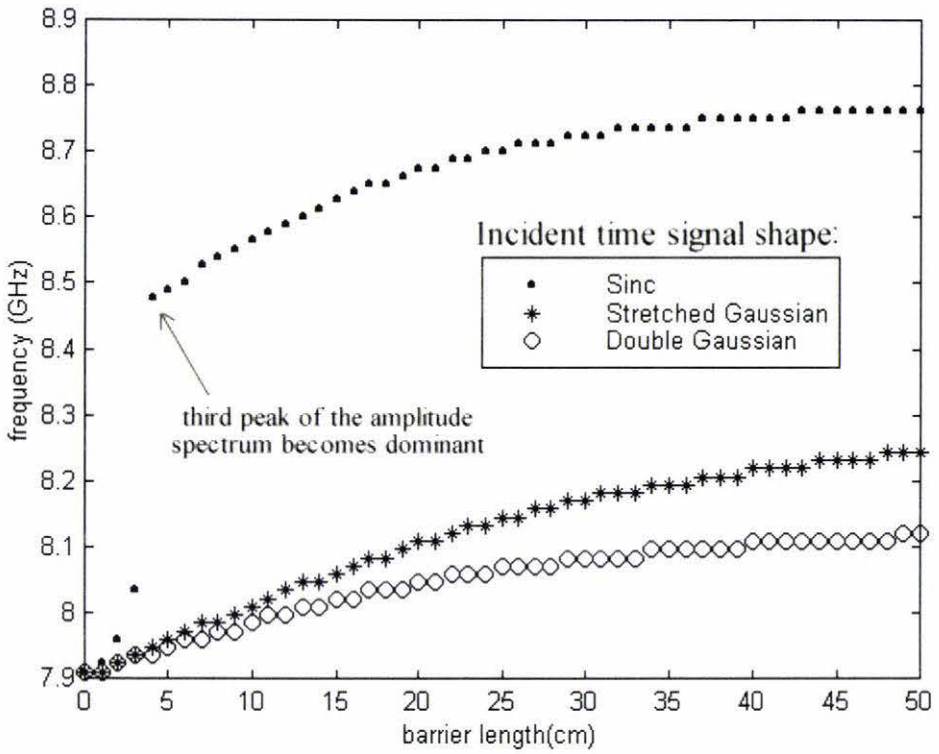

Figure 4.15: Graph showing at which frequency Shalav shaped amplitude spectrum peaks for different barrier lengths. These curves are similar to the one shown in figure 4.11. Notice the third peak of the amplitude spectrum for the Sinc curve becomes dominant at a barrier length of about 4cm (refer to appendix C.5).

Although the 'stretched Gaussian' amplitude spectrum is that of a narrowed Gaussian, bumps exist, refer to appendix C.3. These bumps behave like Shalav curves resulting in the amplitude spectrum behaving like a Shalav curve amplitude spectrum. All the peaks of the investigated amplitude spectra behave either as a Gaussian or Shalav curve with increasing barrier length.

Chapter 5

Conclusion

5.1 *Overview*

Chapter 2 compares the previously studied numerical electromagnetic penetration model with a transmission line model. Both these models yield the same numerical results and are validated since they accurately predict experimental data. The quantum model was also discussed and the analogy between quantum and electromagnetic barrier penetration has been further verified and appreciated.

Various incident time (and frequency) signal shapes have been created using the DFT. The distortion of these signals when penetrating both non-dissipative and dissipative barriers have been investigated using a transmission line model. All investigated signals were greatly attenuated in both barrier types.

5.1.1 *Non-dissipative barrier penetration*

For non-dissipative barrier penetration, the phase shift was shown to become independent of barrier length resulting in superluminal Hartman phase, Hartman group and correlation speeds for barrier lengths greater than about 4cm. Although the correlation and signal speeds were obtained from an incident Gaussian time signal, similar results from other incident shapes were also found. The only subluminal speed for the non-dissipative barrier was the signal speed (fraction=1/3). The signal speed is dependent on the fraction chosen. It was reassuring to find that the signal speed (fraction=1) is within uncertainty of the cross-correlation speed and also becomes superluminal at barrier lengths greater than about 4cm. This similarity is expected since the same data (the envelopes of the signals) have been used to calculate these speeds. Both the cross-correlation and the

signal speeds (fraction=1) were close to values predicted by the average Hartman group speed. The 7GHz component of an investigated signal gave a Hartman group speed similar to that of the average Hartman group speed, even though it is not necessarily the average frequency. The non-dissipative barrier acted as a high pass filter, and the amplitude spectrum was shown to migrate to higher frequencies for increasing barrier lengths. The transmitted time signals lost their incident time signal shape because high frequency components dominated at larger barrier lengths.

5.1.2 *Dissipative barrier penetration*

For dissipative barrier penetration, the phase shift was shown to be dependent on barrier length. This resulted in subluminal speeds being calculated for all investigated lengths. The dissipative barrier also acted as a high pass filter. Migration of the amplitude spectrum to higher frequencies for increasing barrier lengths was observed, but the high frequency components did not dominate.

5.1.3 *Matched Signals penetrating non-dissipative barriers*

The effect of the attenuation on the amplitude spectrum was analysed and a simplified model based on a piecewise approximation was suggested. From constraints introduced in the analysis, a matched Gaussian and an improved matched signal were created. These signals maintained their incident signal shape after penetrating non-dissipative barrier lengths of over 1.5m and 3m respectively. The speeds calculated at these larger lengths were a linear projection of the speeds calculated from the un-matched investigated signals. Signal (fraction=1) and average Hartman Group speeds were found to be a maximum of about 35c for a matched Gaussian signal penetrating a barrier of 1.5m and about 70c for an improved matched signal penetrating a barrier of 3m.

5.2 *Signal Limitations and improvements*

5.2.1 *Bandwidth constraints and wavepackets*

Due to the bandwidth restrictions, the components obtained from the DFT resulted in the creation of a wave-packet incident signal. The wave-packet of the transmitted signal had a higher number of waves within the wave-packet implying a form of high pass filtering had occurred upon penetration of the barrier. This effect may not have been so obvious

if the signal was not a wavepacket. Using a wave-packet signal also emphasised the importance of sampling at an appropriate frequency when high pass filtering is present within a given system.

5.2.2 *Matched signal limitations*

Due to the broadness of the matched time signals, accurate correlation and signal speeds proved difficult to obtain since the time signal was truncated within the 4ns time window. A matched time signal could be redefined to be a signal that has a single 'narrow' peak incident on the barrier and a single 'narrow' peak emerging from the barrier. This would allow the cross-correlation and signal speeds to be easily and accurately calculated since significant truncation of the time signal would be avoided. The improved matched time signal was labeled 'improved' because it had a measurable peak for non-dissipative barrier lengths over 3m. However, the broadening of the signal made it 'un-improved' to analyse.

The matched Gaussian signal cannot be improved by defining amplitudes at higher frequencies to be zero (as was done for the improved matched signal). This is because distortion of the transmitted time signal will occur due to truncation of the transmitted amplitude spectrum, refer to figure 3.27 showing truncation of the amplitude spectrum for a Gaussian signal penetrating a dissipative barrier.

When developing a useful matched signal, the developer is placed in a 'catch-22' scenario. The ideal signal will be that of a narrow time signal with a narrow amplitude spectrum. Since this is not possible, a compromise has to be made since narrowing a time signal broadens the amplitude spectrum and vice versa.

5.3 *Is causality violated?*

The theoretical superluminal results obtained for non-dissipative barrier penetration are in agreement with practical experiments. The question remains, has causality been violated? And if so, can a waveguide with a barrier be used to test causality? Most arguments for testing causality can be put into one of the two categories: practical and theoretical.

5.3.1 *A practical approach to casuality*

Taking a practical approach, the signals studied in this thesis can be created and sent through a non-dissipative barrier faster than the vacuum speed of light. The attenuation in the waveguide walls because of their finite conductivity means no truly non-dissipative barrier exists. Information can be sent from one point of space to another faster than light. The transmitted signal has however been heavily distorted. This distortion can be predicted and a signal similar (if not identical) to the incident signal can be restored. Cramer [47] suggests that a waveguide with a single barrier can be viewed as one element of a multi-stage device. Each stage would provide barrier transmission elements alternating with short fast amplification and pulse restoration elements. A transmitted signal would be restored and then transmitted through the next barrier element. Signal information should not therefore be lost from stage to stage. Such an apparatus it is believed could provide a practical test for causality. Unfortunately, amplification takes time and any superluminal signal may lose its superluminal properties from these time delays.

5.3.2 *A theoretical approach to causality*

In this study, the actual incident signal (and therefore the actual transmitted signal) is periodic. It has been assumed that the time between each pulse is such that interference from one pulse on another is negligible. This may not be a valid assumption.

Theorists argue that a signal that could be used to test causality must have a distinct beginning and end. It has also been warned that nothing should precede the signal that can be used to detect the arrival of the signal. The waveform therefore needs to be zero before it 'starts'. A periodic signal does not satisfy these conditions and can therefore not be used to test causality. The ideal signal required could not be created in the waveguide regime since the limited bandwidth will always result in a periodic signal. Practically, the ideal signal requires an infinite number of frequencies, and such a signal could not be created.

In summary, from a theorists approach, it is possible to send information 'faster than light', but causality would not have been violated since the transmitted information is not considered to be an ideal signal. Theoretically, causality will never be violated since creation of the required signal is not possible.

5.4 *Future developments*

5.4.1 *Further investigations*

5.4.1.1 Utilising the Matlab EBP simulation

The Matlab EBP simulation could prove very useful for future theoretical investigations. The toolbox has been designed to allow the user to define a number of important parameters within the simulation. For example, the upper and lower cut-off frequencies, the number of time samples and the number of frequency components can be changed within the main menu of the simulation. Other parameters such as the barrier dimensions, refractive index and time constraints can be changed manually within the appropriate sub-routines.

Accurate correlation and signal speeds could be found from the signals created in this study by extending the time domain to include a larger proportion of the broader time signals. The simulation could also be used to test other signal shapes in the hope of finding a 'best' matched signal. The search for an ideal non-dissipative barrier for a given signal could be investigated by changing the barrier parameters. An ideal barrier would be one that would allow penetration through long barrier lengths with minimum attenuation and minimum phase shifting.

5.4.1.2 Other matched signals

The matched Gaussian amplitude spectrum migrates to higher frequencies for increasing barrier lengths and it is this migration that results in signal distortion at large barrier lengths. The modified matched amplitude spectrum is the shape of a Shalav curve and does not migrate to the same higher frequencies as the Gaussian amplitude spectrum. It does however narrow resulting in a broad time signal. An amplitude spectrum that has the properties of both a Gaussian and Shalav curve may give an improved measurable time signal representative of the incident time signal shape at larger barrier lengths. Such an amplitude spectrum could have a peak that shifts linearly to higher frequencies when the barrier length is increased. This 'linear' result lies between the rapidly increasing and slowly increasing peak shifts of the Gaussian and Shalav curves, refer to figures 4.6 and 4.11. A Hubbert curve is used to model oil production and is a curve that decreases rapidly like a Shalav curve but 'levels out' more quickly than a Shalav curve. At points

away from the peak, the Hubbert curve resembles a Gaussian curve. One could start the search for a 'better' matched signal by investigating Hubbert shaped amplitude spectra.

5.4.2 *Applications*

Superluminal signals could be used in the development of super fast computers. The ideal signal used to relay computational information would have a narrow peak like a Gaussian signal. A narrow peak would allow more peaks to exist within a given time and therefore having a greater bit rate. The peak could be used to represent the bits of the signal, for example 0 (non peak) and 1 (peak). Unfortunately, digital signals will not propagate through a waveguide, although a DFT version of one may prove a useful signal to investigate.

Superluminal signals could also prove useful in the telecommunication industry. Unfortunately, massive attenuation at longer barrier lengths makes longer barriers impractical. Shorter barriers (as would be used in a computer) are however useful.

For any theoretical study, the development of a practical device demonstrating the theory is always a possibility for future study and development. The waveguide used by Nimtz *et al.* [8] could be used to test the validity of the matched signals. A multi-stage amplification regime as mentioned by Cramer [47] would need to be introduced to account for the large attenuation and restore the transmitted signal back in to something physically measurable. Some would argue that such device could be used to test causality.

Appendix A

Selected Mathematical Calculations and Proofs

A.1 Finding the α and β coefficients which define the propagation constant γ_2 through a dissipative barrier

From Chapter 2: $\gamma_2 = \alpha + i\beta$ and $\gamma_2 = \sqrt{k^2 + i\omega\mu_0(\sigma + i\omega\varepsilon)}$ [A1.1]

[Note: the medium is dissipative, $\sigma \neq 0$ in which case, we can use the formula(s) for a non-dissipative medium but $\varepsilon - \frac{i\sigma}{\omega}$ replaces ε .]

[A1.1] implies $(\alpha + i\beta)^2 = k^2 + i\omega\mu_0(\sigma + i\omega\varepsilon)$

$$\Rightarrow \alpha^2 + 2i\alpha\beta - \beta^2 = k^2 + i\omega\mu_0\sigma - \omega^2\mu_0\varepsilon \qquad [A1.2]$$

Both the left hand side and right hand side of [A1.2] have real and imaginary components. Both the real components must equal, as must the imaginary components.

Real components: $\alpha^2 - \beta^2 = k^2 - \omega^2\mu_0\varepsilon$ [A1.3]

Imaginary components: $2\alpha\beta = \omega\mu_0\sigma$ [A1.4]

Rearranging [A1.4] gives us an expression for β in terms of α, namely:

$$\boxed{\beta = \frac{\omega\mu_0\sigma}{2\alpha}} \qquad [A1.5]$$

From [A1.3], $\alpha^2 = k^2 - \omega^2\mu_0\varepsilon + \beta^2$. Substituting in [A1.5] and multiplying by α^2 gives

$$a^2 - ba - c^2 = 0 \qquad [A1.6]$$

Where $a = \alpha^2 ; b = k^2 - \omega^2\mu_0\varepsilon$ and $c = \frac{\omega\mu_0\sigma}{2}$.

Completing the square for [A1.6] and solving for a yields

$$a = \sqrt{\frac{1}{4}b^2 + c^2} + \frac{1}{2}b \qquad [A1.7]$$

Substituting back the original variables and solving for α leaves

$$\boxed{\alpha = \tfrac{1}{2}\left\{k^2 - \omega^2\mu_0\varepsilon_2 + \sqrt{\left(k^2 - \omega^2\mu_0\varepsilon_2\right)^2 + \left(\omega\mu_0\sigma\right)^2}\right\}^{1/2}}$$

A.2 Calculation of the transmission coefficient T through a potential barrier within a waveguide

There are two interfaces of interest. These are the barrier interfaces. The transmission coefficient at the first interface can be given by the Fresnel equation (for example, from [24])

$$T_1 = \frac{E_1}{E_i} = \frac{2Z_2}{Z_1 + Z_2} \qquad \text{[A2.1]}$$

where T_1 is the transmission coefficient through the first interface, E_1 is the transmitted field, E_i is the field incident on the first interface and Z_1 and Z_2 are the wave impedances of the appropriate regions.

The transmission coefficient at the second interface

$$T_2 = \frac{E_t}{E_2} = \frac{2Z_1}{Z_2 + Z_1} \qquad \text{[A2.2]}$$

where T_2 is the transmission coefficient through the second interface only, E_t is the transmitted field and E_2 is the field incident to the second interface. E_2 does not equal E_1 since attenuation occurs within the barrier of length ℓ and multiple reflections of E_1 occur within the barrier. This implies that

$$E_2 = E_1 \exp(-\alpha\ell) + R^2 E_1 \exp(-3\alpha\ell) + R^4 E_1 \exp(-5\alpha\ell) + \ldots\ldots\ldots \qquad \text{[A2.3]}$$

which simplifies to

$$E_2 = \frac{E_1 \exp(-\alpha\ell)}{1 - R^2 \exp(-2\alpha\ell)} \qquad \text{[A2.4]}$$

The reflection coefficient R within the barrier is equal to (also a Fresnel equation)

$$R = \frac{Z_2 - Z_1}{Z_2 + Z_1} \qquad \text{[A2.5]}$$

From Equations [A2.1] and [A2.2], $E_1 = T_1 E_i$ and $E_t = T_2 E_2$, implying

$$E_t = E_i \left(\frac{2Z_1}{Z_2 + Z_1} \right) \left(\frac{2Z_2}{Z_1 + Z_2} \right) \left(\frac{\exp(-\alpha\ell)}{1 - R^2 \exp(-2\alpha\ell)} \right) \qquad \text{[A2.6]}$$

The transmission coefficient T written in terms of E_t and E_i is given as

$T = \frac{E_t}{E_i}$ which will be identical to the solution obtained by Rulf [28].

A.3 Showing that the magnitude of the transmission coefficient $|T|$ using a transmission line model is identical to that calculated from the numerical model used by Cuevas et al.

Dividing Equation (2.36) by $2\alpha\beta$ gives the transmission coefficient T to be

$$T = \frac{1}{z} \qquad [A3.1]$$

where z is complex and of the form $a + ib$. In this case

$$\begin{aligned} a &= \cosh(\alpha\ell) \\ b &= \left(\frac{\beta^2 - \alpha^2}{2\alpha\beta} \right) \sinh(\alpha\ell) \end{aligned} \qquad [A3.2]$$

The magnitude of T will be given by

$$|T| = \left| \frac{1}{a+ib} \times \frac{a-ib}{a-ib} \right| = \frac{1}{\sqrt{a^2 + b^2}} \qquad [A3.3]$$

Substituting in [A3.2] yields

$$|T| = \frac{1}{\sqrt{\cosh^2(\alpha\ell) + \left(\frac{\beta^2 - \alpha^2}{2\alpha\beta} \right)^2 \sinh^2(\alpha\ell)}} \qquad [A3.4]$$

Substituting $1 + \sinh^2(\alpha\ell)$ for $\cosh^2(\alpha\ell)$ and expanding the brackets, it is easy to show that [A3.4] can be re-written as

$$|T| = \frac{1}{\sqrt{1 + \left[\left(\frac{\alpha^2 + \beta^2}{2\alpha\beta} \right) \sinh(\alpha\ell) \right]^2}} \qquad [A3.5]$$

This is equal to the result obtained using the model presented by Cuevas *et al.* [26].

Appendix B

Selected transmitted time signal envelopes after penetrating a non-dissipative barrier

Transmission through a non-dissipative barrier with a:

GAUSSIAN

Incident Signal

number of time samples n=31.64
number of components N=256

```
%*****MATLAB instructions to create incident signal*****
%t is the time interval [0 4] ns with n samples
t1=((2*(10^9)*t)-4);
for bbb=1:length(t);
  %*****characteristic gaussian equation*****
  x(1,bbb)=exp(-0.5*(t1(1,bbb))^2);
end
```

Transmission through a non-dissipative barrier with a:

'NARROWED' GAUSSIAN

Incident Signal

number of time samples n=31.64
number of components N=256

```
%*****MATLAB instructions to create incident signal*****
%t is the time interval [0 4] ns with n samples
t1=((2*(10^9)*t)-4)*3;
for bbb=1:length(t);
  %*****characteristic gaussian equation*****
  x(1,bbb)=exp(-0.5*(t1(1,bbb))^2);
end
```

Transmission through a non-dissipative barrier with a:

'STRETCHED' GAUSSIAN

Incident Signal

number of time samples n=31.64
number of components N=256

```
% *****MATLAB instructions to create incident signal*****
%t is the time interval [0 4] ns with n samples
t1=((2*(10^9)*t)-4)*0.5;
for bbb=1:length(t);
  %*****characteristic gaussian equation*****
  x(1,bbb)=exp(-0.5*(t1(1,bbb))^2);
end
```

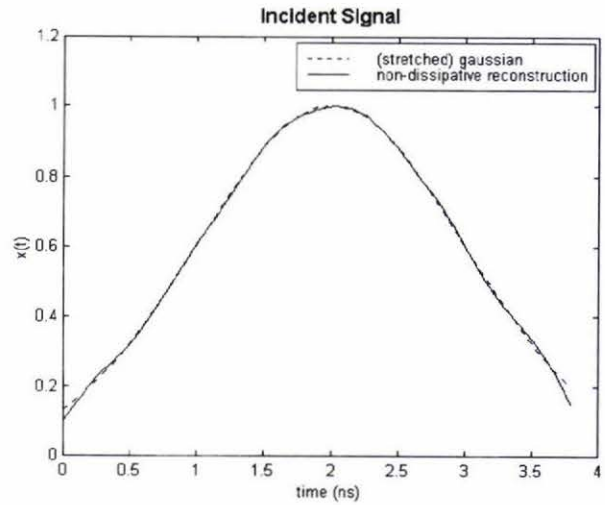

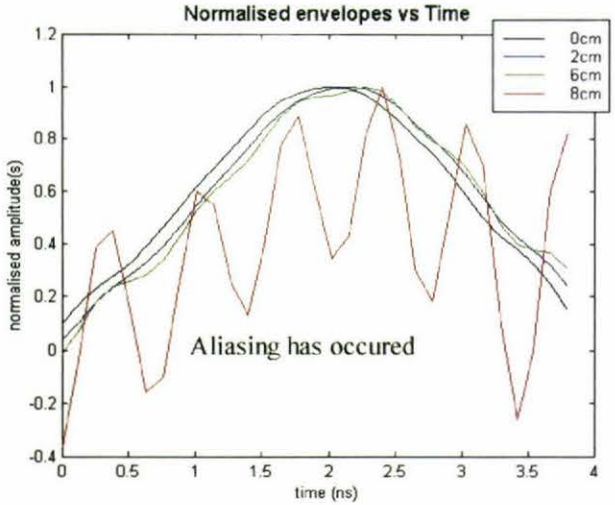

Wavepacket peak differences

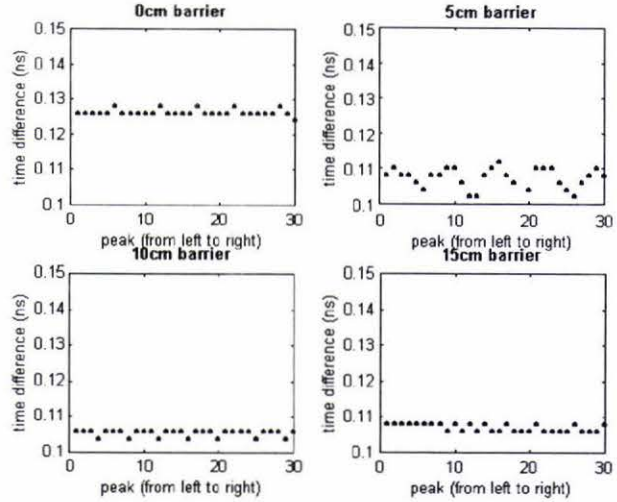

Transmission through a non-dissipative barrier with a:

'DOUBLE' GAUSSIAN

Incident Signal

number of time samples n=31.64
number of components N=256

```
%******MATLAB instructions to create incident signal******
%t is the time interval [0 4] ns with n samples
t1=((2*(10^9)*t)-5.7)*2;
for bbb=1:length(t);
  %*****characteristic gaussian equation*****
  x(1,bbb)=exp(-0.5*(t1(1,bbb))^2);
end
x(1,1:16)=x(1,16:31);
```


Wavepacket peak differences

Transmission through a non-dissipative barrier with a:

'LOGARITHMIC' GAUSSIAN

Incident Signal

number of time samples n=31.64
number of components N=256

```
%*****MATLAB instructions to create incident signal*****
%t is the time interval [0 4] ns with n samples
t1=t*1.6*10^9;
for bbb=1:length(t);
  %*****characteristic log-gaussian equation*****
  x(1,bbb)=exp(-1*(log(t1(1,bbb)))^2);
end
```

Transmission through a non-dissipative barrier with a:

SINC

Incident Signal

number of time samples n=31.64
number of components N=256

```
%*****MATLAB instructions to create incident signal*****
%t is the time interval [0 4] ns with n samples
t1=((750*10^6)*t)-1.5;
for bbb=1:length(t);
  %*****characteristic sinc equation*****
  x(1,bbb)=(1/t1(1,bbb))*sin(t1(1,bbb)*2*pi);
end
```


Wavepacket peak differences

Appendix C

Amplitude spectra for selected signal shapes at different non-dissipative barrier lengths

Transmission through a non-dissipative barrier with a:

GAUSSIAN
Incident Signal

*IMPORTANT NOTE:
The 'relative amplitude' is a 'normalised' signal, divided by a maximum. This maximum is taken to be the 'local maximum' which is closest to the maximum of the incident signal spectrum.

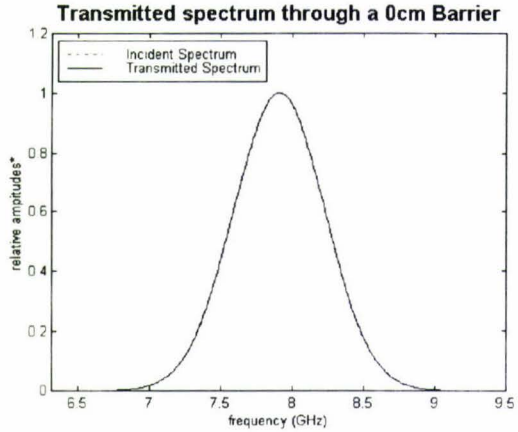

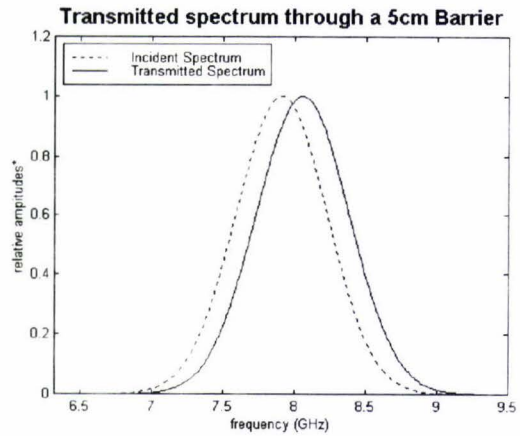

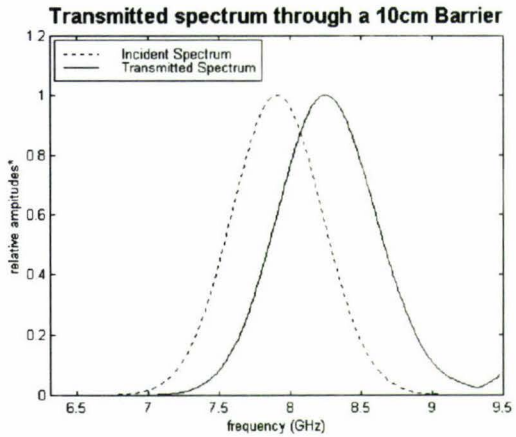

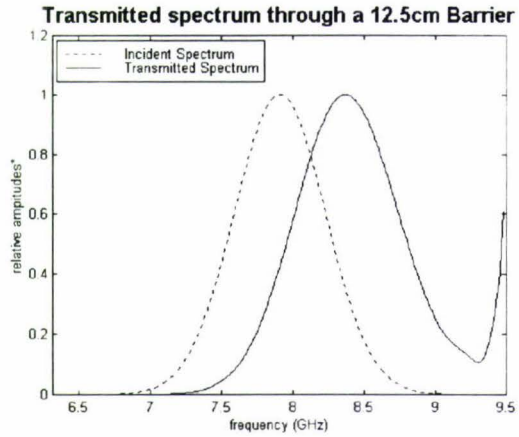

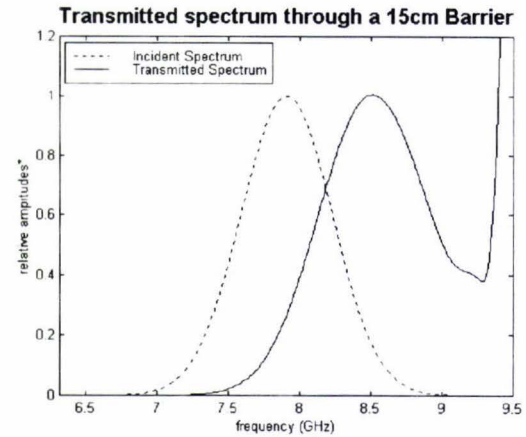

Transmission through a non-dissipative barrier with a:

'NARROWED' GAUSSIAN

Incident Signal

*IMPORTANT NOTE:
The 'relative amplitude' is a 'normalised' signal, divided by a maximum. This maximum is taken to be the 'local maximum' which is closest to the maximum of the incident signal spectrum.

(There is no 'local maximum after barrier lengths of about 5cm for the 'Narrowed' Gaussian.)

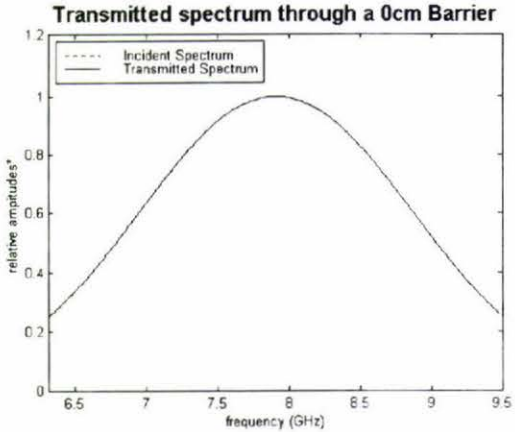

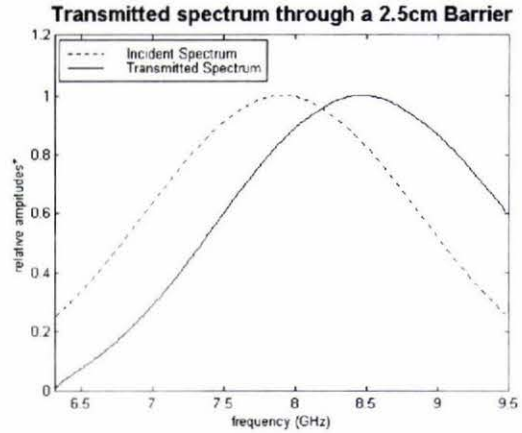

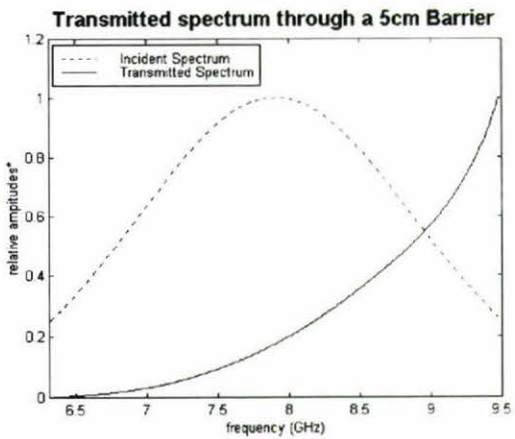

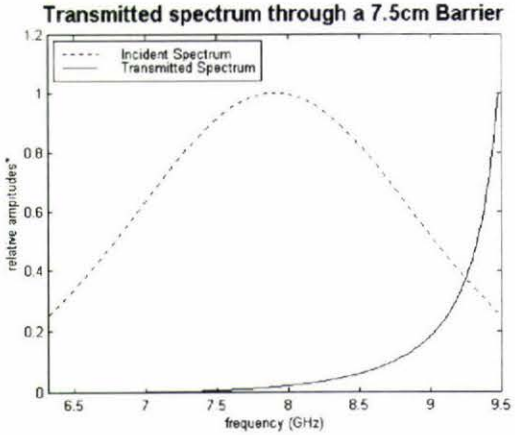

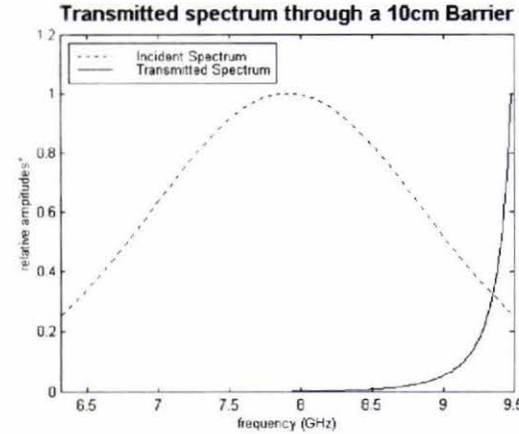

Transmission through a non-dissipative barrier with a:

'STRETCHED' GAUSSIAN Incident Signal

*IMPORTANT NOTE:
The 'relative amplitude' is a 'normalised' signal, divided by a maximum. This maximum is taken to be the 'local maximum' which is closest to the maximum of the incident signal spectrum.

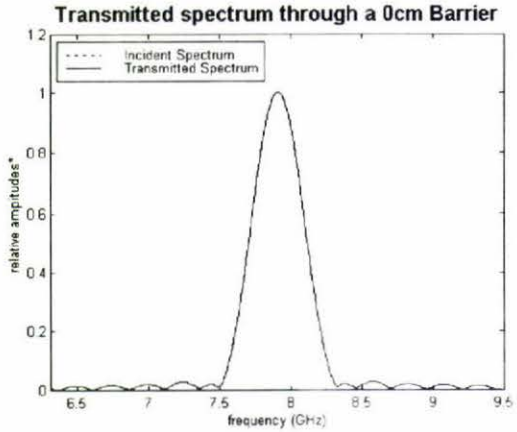

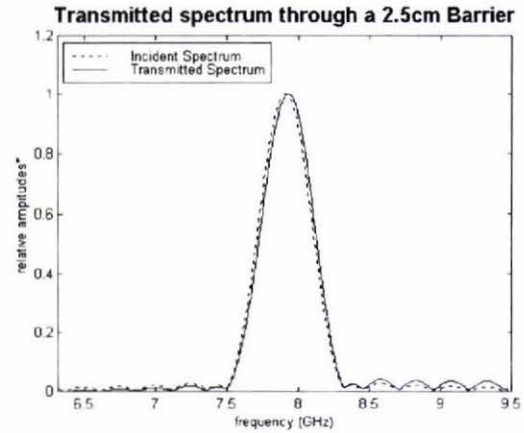

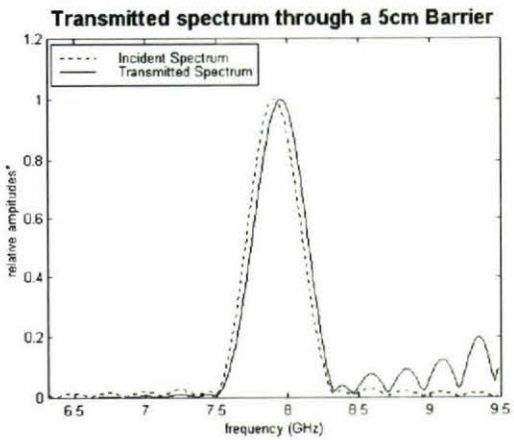

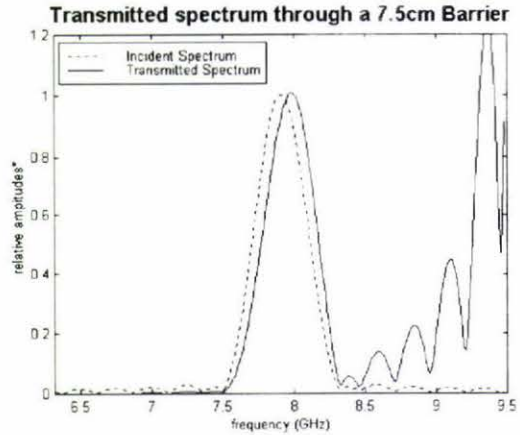

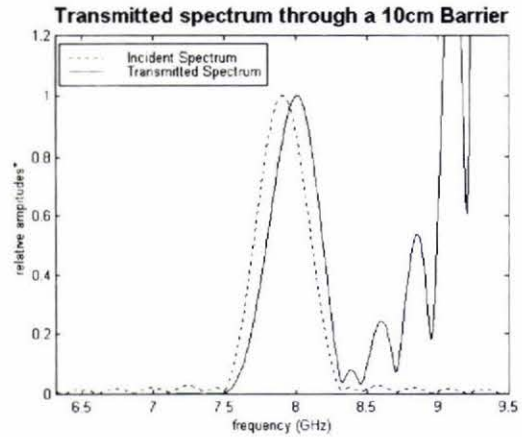

Transmission through a non-dissipative barrier with a:

'DOUBLE' GAUSSIAN
Incident Signal

*IMPORTANT NOTE:
The 'relative amplitude' is a 'normalised' signal, divided by a maximum. This maximum is taken to be the 'local maximum' which is closest to the maximum of the incident signal spectrum.

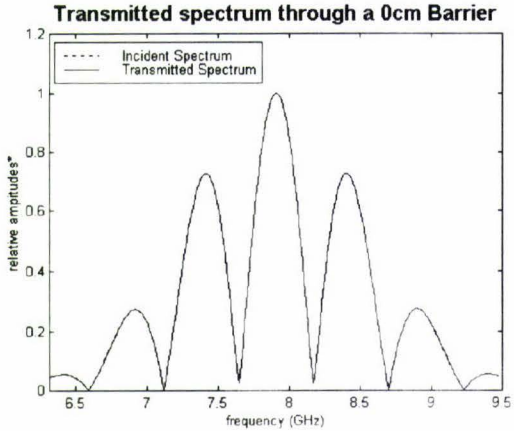

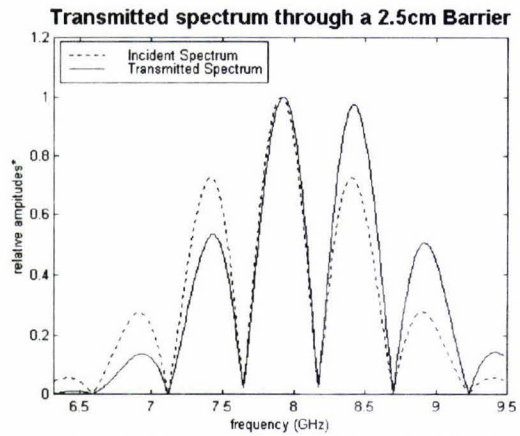

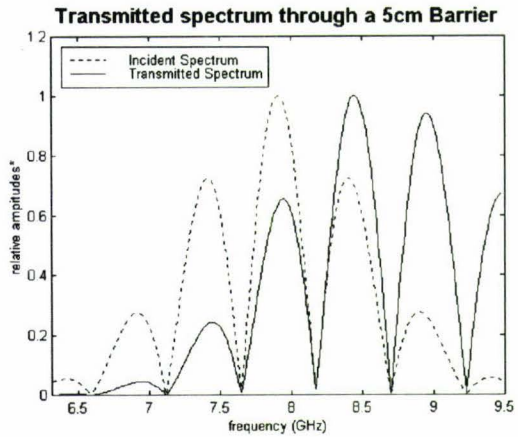

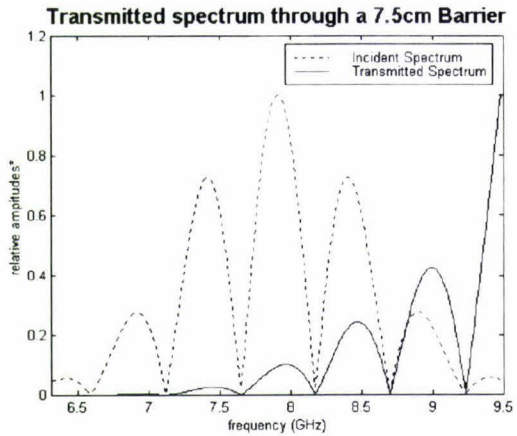

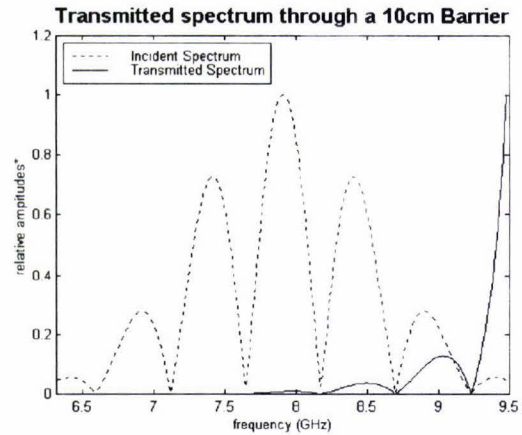

Transmission through a non-dissipative barrier with a:

'LOGARITHMIC' GAUSSIAN Incident Signal

*IMPORTANT NOTE:
The 'relative amplitude' is a 'normalised' signal, divided by a maximum. This maximum is taken to be the 'local maximum' which is closest to the maximum of the incident signal spectrum.

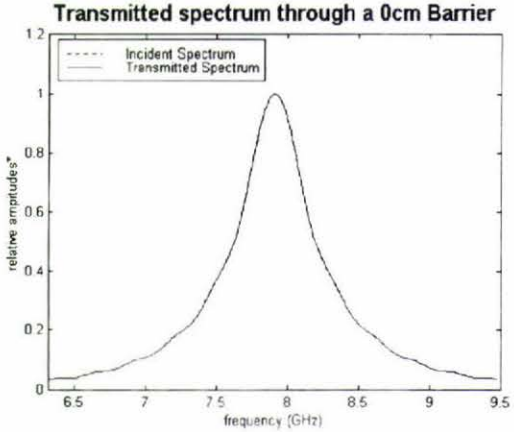

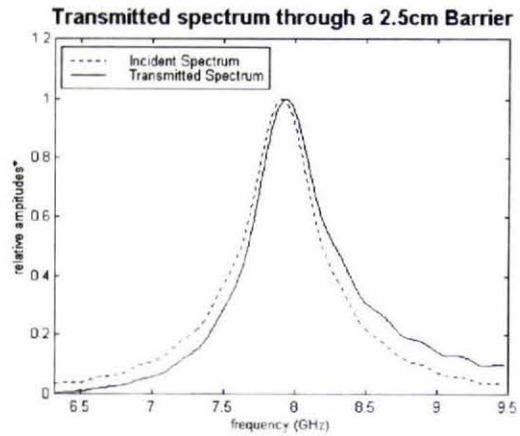

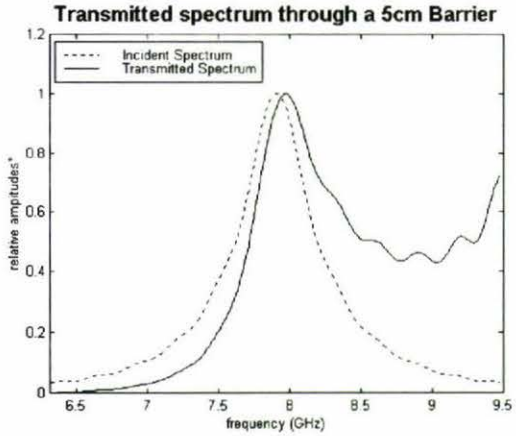

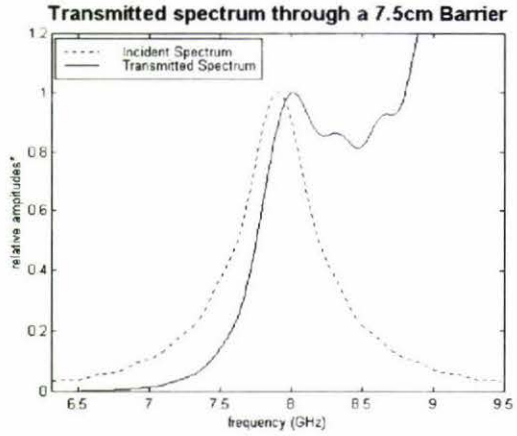

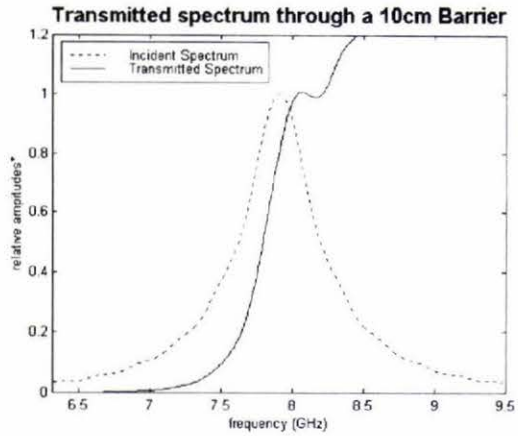

Transmission through a non-dissipative barrier with a:

SINC
Incident Signal

*IMPORTANT NOTE:
The 'relative amplitude' is a 'normalised' signal, divided by a maximum. This maximum is taken to be the 'local maximum' which is closest to the maximum of the incident signal spectrum.

Transmitted spectrum through a 0cm Barrier

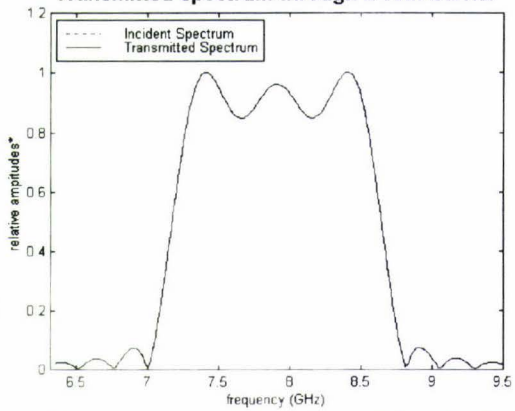

Transmitted spectrum through a 2.5cm Barrier

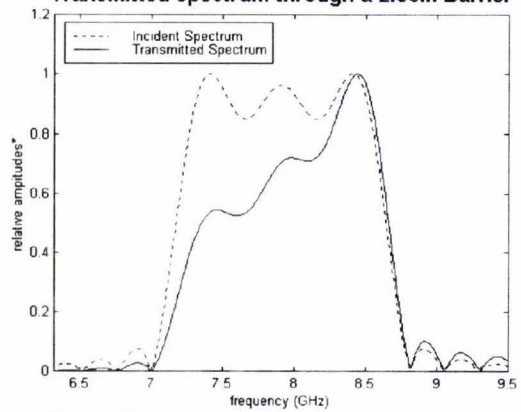

Transmitted spectrum through a 5cm Barrier

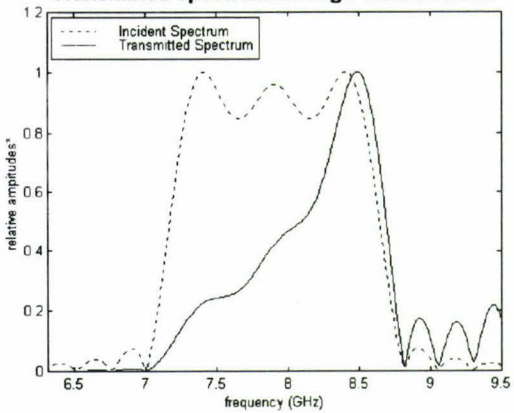

Transmitted spectrum through a 7.5cm Barrier

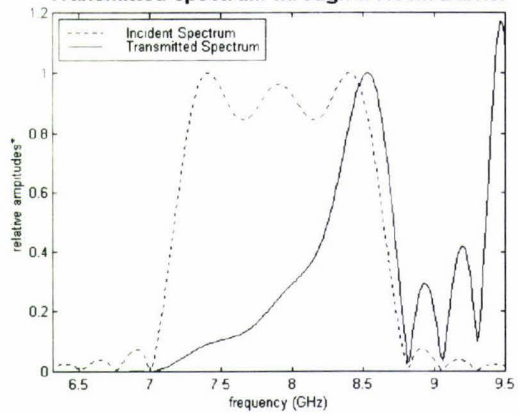

Transmitted spectrum through a 10cm Barrier

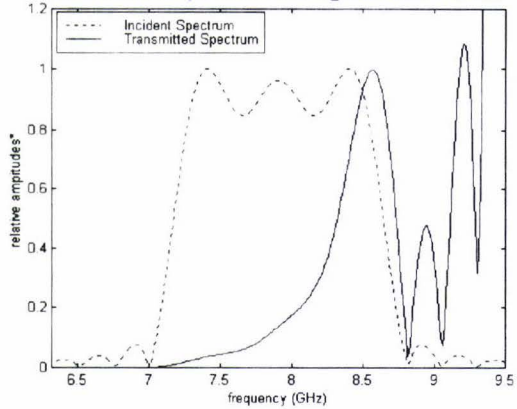

Appendix D

Construction of a Shalav curve

A curve which is rapidly inceasing or rapidly decreasing can be created graphically from a 'linear' basis set. For example, let  represent a set of points in Cartesian co-ordinates with a slope of +1 and  represent a set of points with a slope of –1.

Let n be a binary operation such that:

$$(i, j) \otimes (k, l) = (i \times k,\ j \times l) \qquad \text{[D1.1]}$$

where (i, j) and (k, l) are Cartesian co-ordinates. The functional Cartesian forms of these curves would be $y = x^n$ and $y = (A - x)^n$ respectively where $0 < x < A$.

It is easy to show

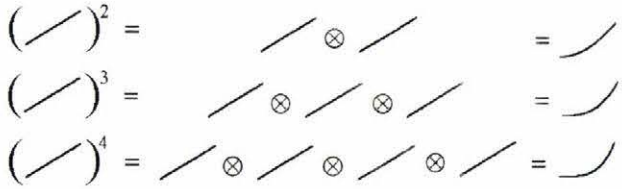

A product of the form where n is a positive integer greater than one, creates a rapidly increasing curve .

Likewise, a product of the form  creates rapidly decreasing curve.

For example:

More complicated curves can be created by combining an exponential growth and exponential decay curve together using the binary multiplication operator $\otimes$. Using the above notation, an expression of the form 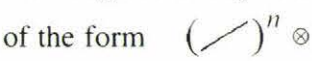 with n and m being positive integers, will create a curve with a maximum (for example a pulse). If $n = m$, then this curve is symmetrical. For example:

If $n \neq m$, then a similar type curve is still created, but will not be symmetrical. If the rapidly increasing curve dominates ($n > m$) then the center of the curve shifts to the left. If the rapidly decreasing term dominates ($n < m$) then the center shifts to the right. Such curves will be called 'Shalav' curves. A number of different Shalav curves can be seen in table D1.1. This table is a Group and has been created with $n, m = 1, 2, 3, 4, 5$.

Each column has been operator multiplied by $(\diagup)^n$ where n is the column number.
Each row has been operator multiplied by $(\diagdown)^m$ where m is the row number.

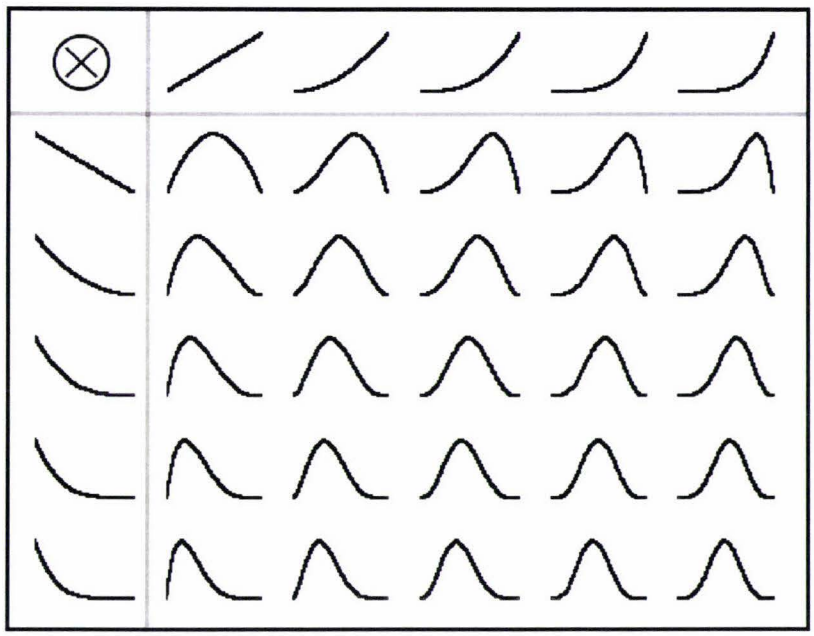

Table D1.1: Group multiplication (by the binary operator $\otimes$) table using a graphical representation of different Shalav type curves

Figure D1.1 shows a resulting Shalav curve from the following Matlab commands:

```
» x=0:0.1:10;        % increasing curve with slope +1
» y=10:-0.1:0;       % decreasing curve with slope -1
» xn=x.^5;           % rapidly increasing curve (n=5)
» yn=y.^5;           % rapidly decreasing curve (m=5)
» shalav=xn.*yn;
» plot(x,shalav)
```

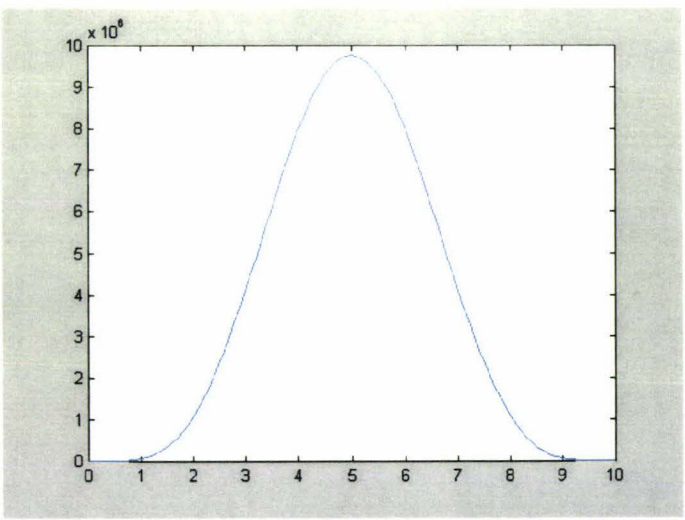

Figure D1.1: Shalav curve created from simple Matlab instructions

Appendix E

Matlab Electromagnetic Barrier Penetration (EBP) simulation user guide

E.1 The Main Menu

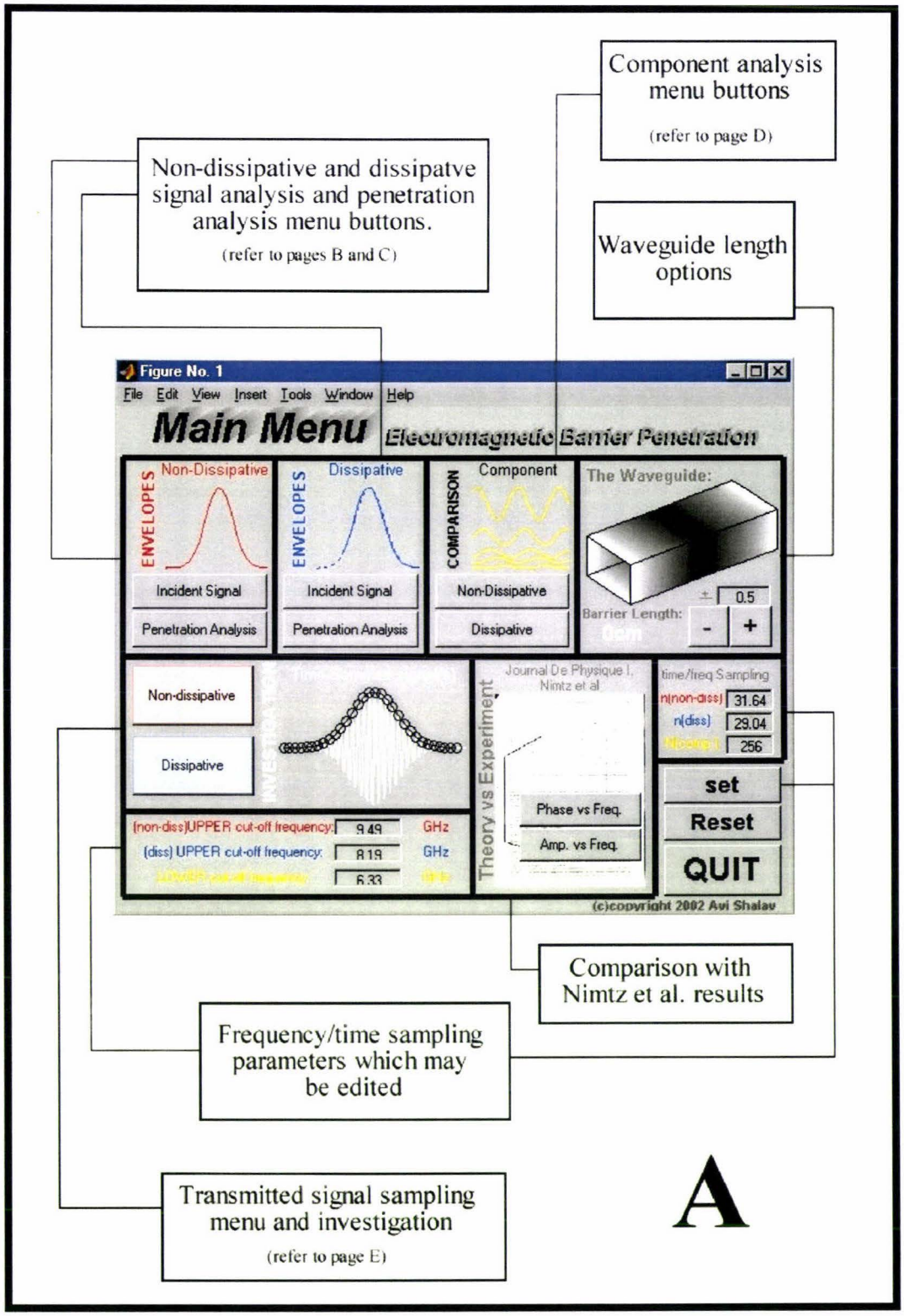

E.2 Incident Pulse Analysis

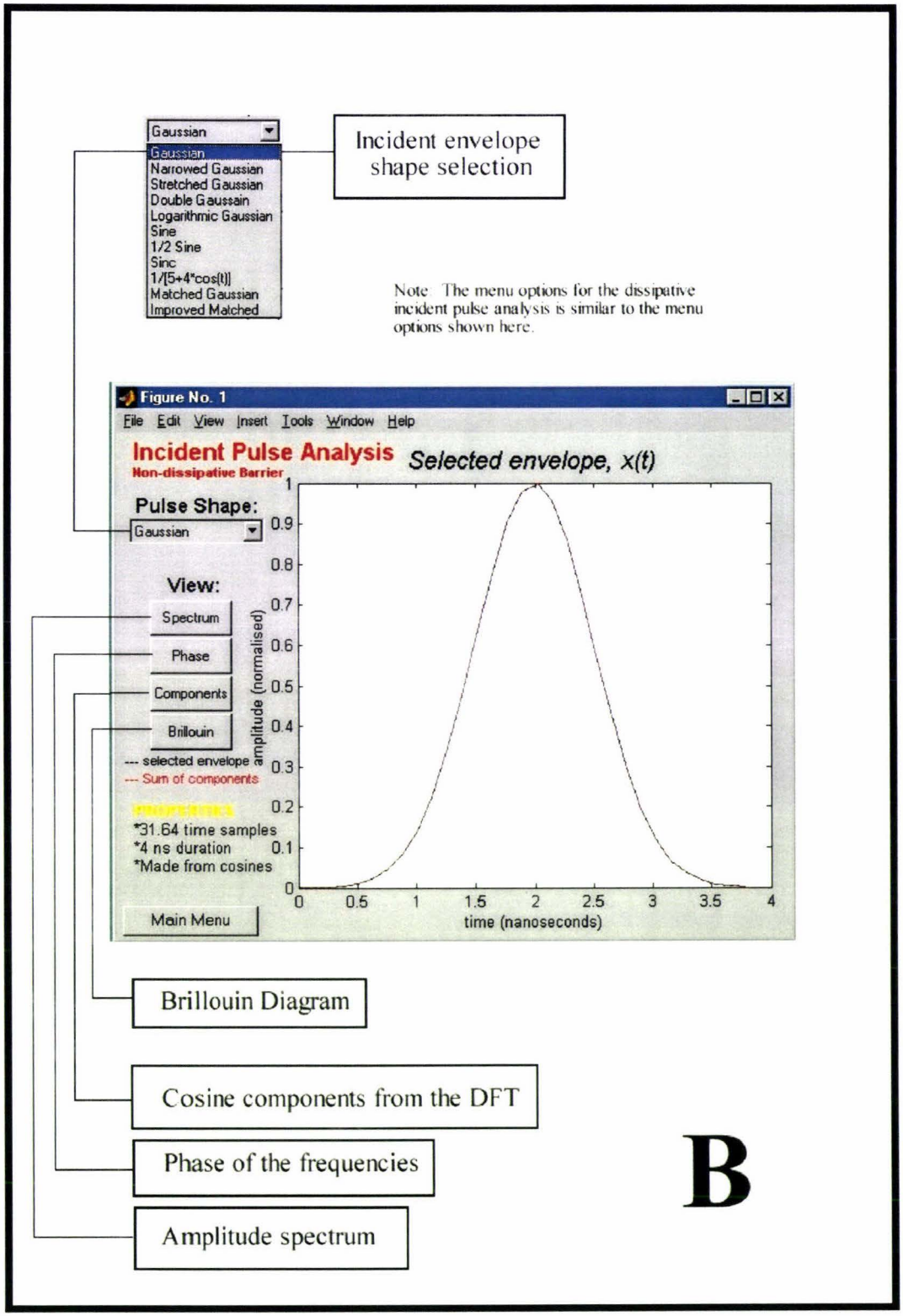

E.3 Penetration Analysis

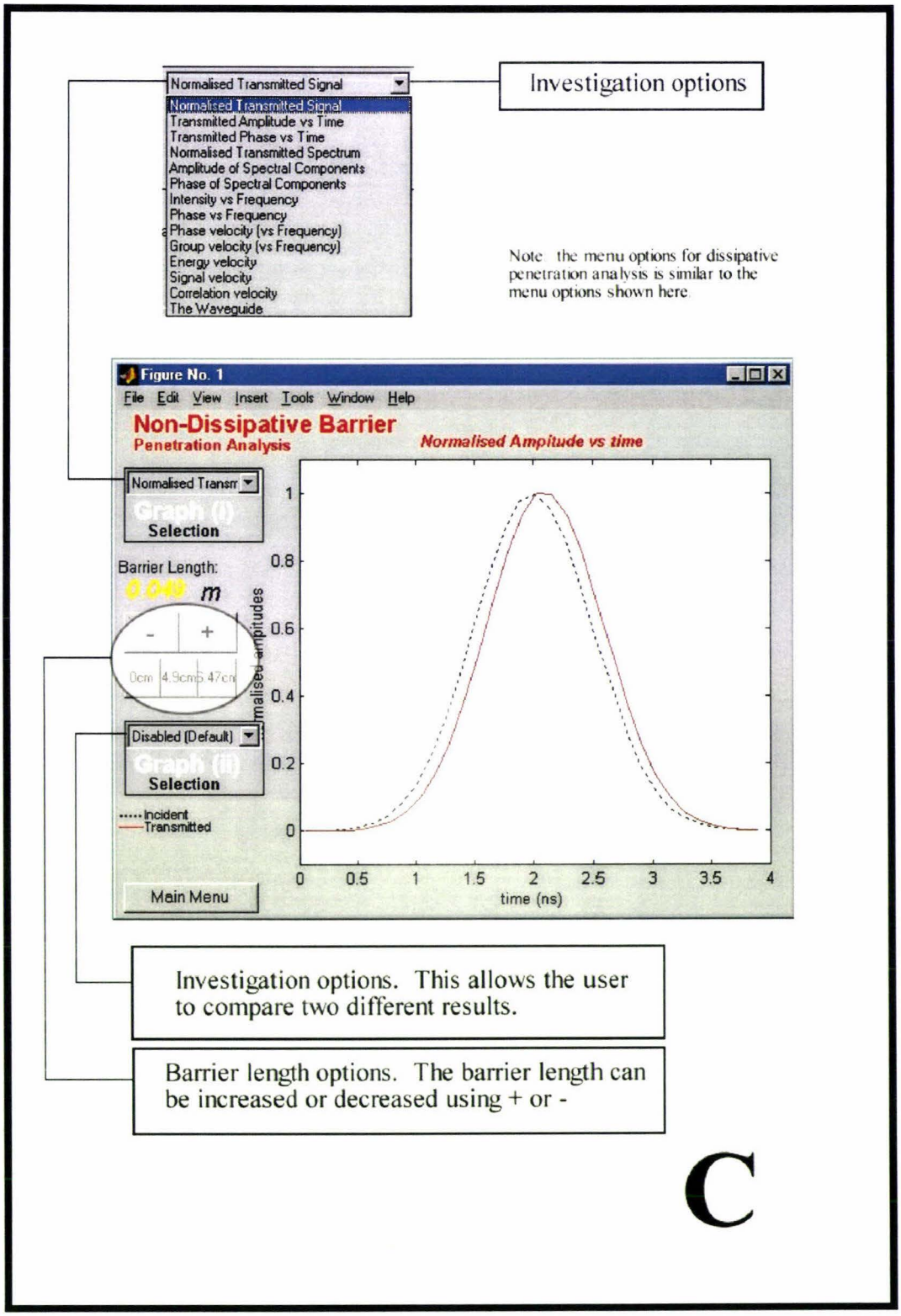

E.4 Speed/Phase Analysis

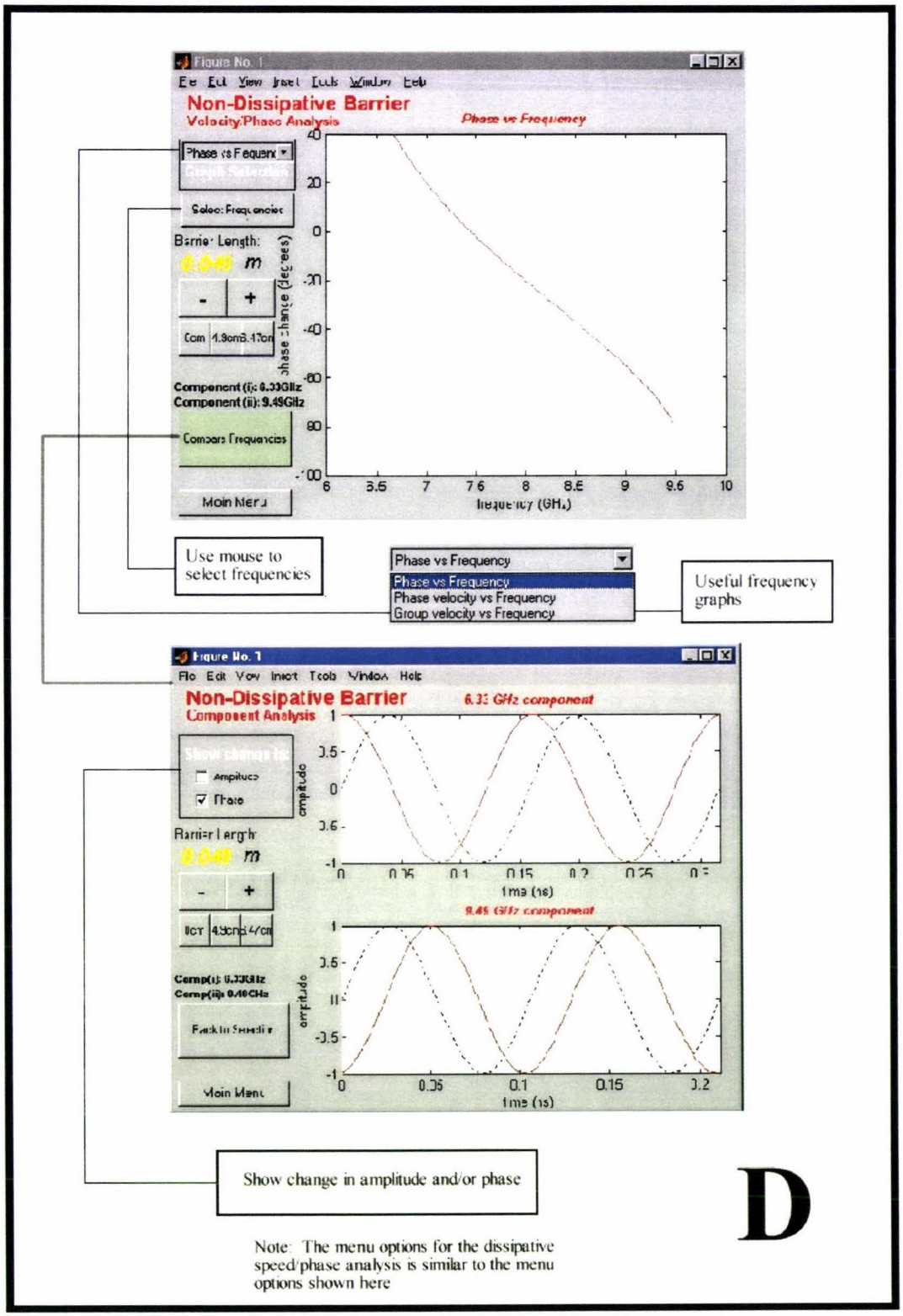

E.5 Transmitted Signal Time-Sampling

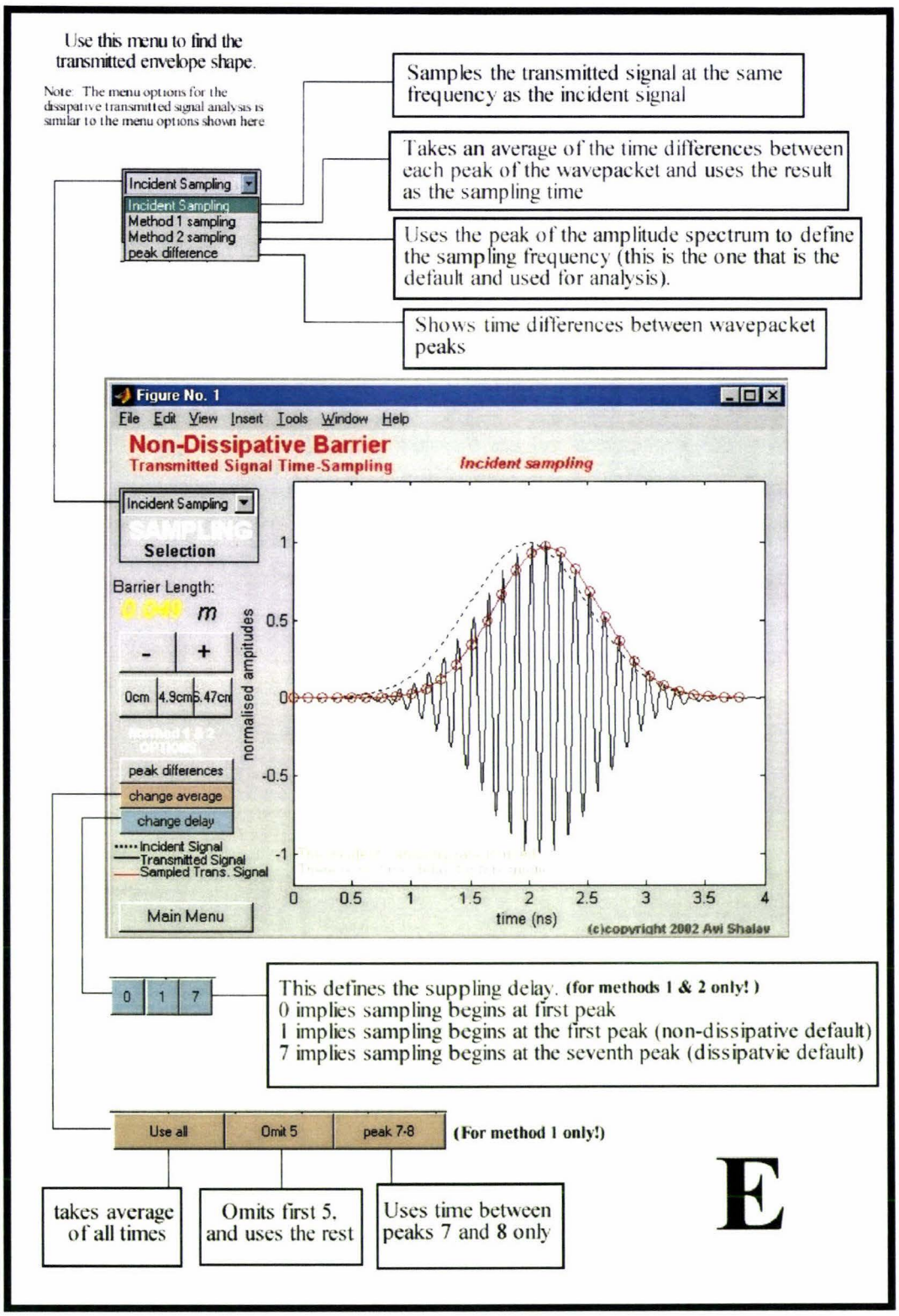

References

1. Sartori, L., *Understanding Relativity.* 1996, Los Angeles: University of California Press.

2. Brown, J., *Faster than the speed of light.* New Scientist, 1995. **145**(1971): p. 26-30.

3. Landauer, R., *Light faster than light?* Nature, 1993. **365**.

4. Steinberg, A.M., P.G. Kwiat, and R.Y. Chiao, *Measurement of the Single-Photon Tunneling time.* Physical Review Letters, 1993. **71**(5): p. 708-711.

5. Chiao, R.Y., *Tachyonlike excitations in inverted two-level media.* Physical Review Letters, 1996. **77**(7): p. 1254-1257.

6. Chiao, R.Y., *Superluminal (but causal) propagation of wave packets in transparent media with inverted atomic populations.* Physical Review A, 1993. **48**(1): p. 34-37.

7. Ranfagni, A.,P. Fabeni, G.P. Pazzi, and D. Mugnai, *Anomalous pulse delay in microwave propagation: A plausible connection to the tunneling time.* Physical Review E, 1993. **48**(2): p. 1453-1460.

8. Nimtz, G., H. Spieker, and H.M. Brodowsky, *Tunneling with dissipation.* Journal De Physique I, 1994. **4**(10): p. 1379-1382.

9. Enders, A. and G. Nimtz, *On superluminal barrier traversal.* Journal De Physique I, 1992. **2**(8): p. 1693-1698.

10. Enders, A. and G. Nimtz, *Photonic-tunneling experiments.* Physical Review B, 1993. **47**(15): p. 9605-9609.

11. Enders, A. and G. Nimtz, *Zero-time tunneling of evanescent mode packets.* Journal De Physique I, 1993(3): p. 1089-1092.

12. Enders, A. and G. Nimtz, *Evanescent-mode propagation and quantum tunneling.* Physical Review E, 1993. **48**(1): p. 632-634.

13. Pelster, R., V. Gasparian, and G. Nimtz, *Propagation of plane waes and of waveguide modes in quasiperiodic dielectric heterostructures.* Physical Review E, 1997. **55**(6): p. 7645-7655.

14. Haibel, A. and G. Nimtz, *Universal relationship ot time and frequency in photonic tunneling.* Annals of Physics (Leipzig), 2001. **9**(1): p. 1-5.

15. Ragfagni, A., D. Mugnai, F. Fabeni, G.P. Pazzi, G. Naletto, C. Sozzi, *Optical-tunneling time measures: a microwave model.* Physica B, 1991(175): p. 283-286.

16. Chiao, R.Y., P.G. Kwiat, and A.M. Steinberg, *Analogies between electron and photon tunneling.* Physica B, 1991(175): p. 257-262.

17. Nimtz, G. and W. Heitmann, *Superluminal photonic tunneling and quantum electronics.* Progress in Quantum electronics 1997(21): p. 81-108.

18. Martin, T. and R. Landauer, *Time delay of evanescent electromagnetic waves and the analogy to particle tunneling.* Physical Review A, 1992. **45**(4): p. 2611-2617.

19. Hartman, T.E., *Tunneling of a Wave Packet.* Journal of Applied Physics, 1962. **33**(12): p. 3427-3433.

20. Aephraim, M.S., *Conditional probabilities in quantum theory and the tunneling-time controversy.* Physical Review A, 1995. **52**(1): p. 32-42.

21. Aephraim, M.S., *How much time does a tunneling particle spend in the barrier region?* Physical Review Letters, 1995. **74**(13): p. 2405-2409.

22. Deutch, J.M. and F.E. Low, *Barrier penetration and superluminal velocity.* Annals of Physics (NY), 1993. **228**(5): p. 184-202.

23. Krauss, J., *Electromagnetics*. 4 ed. 1992: McGraw-Hill, Inc.

24. Lorrain, P., D.R. Corson, and F. Lorrain , *Electromagnetic Fields and Waves*. third edition 1988: W.H Freeman and Comapany.

25. Gasiorowicz, S., *The Potential Barrier*, in *Quantum Physics*. 1996, John Wiley & Sons, Inc. p. 79-82.

26. Cuevas, E., V. Gasparian, M. Ortuno, and J. Ruiz, *Traversal time in periodically loaded waveguides.* Zeitshrift Fur Physik B, 1996(100): p. 595-599.

27. Emig, T., *Propagation of an electromagnetic pulse through a waveguide with a barrier:A time domain solution within classical electrodynamics.* Physical Review E, 1996. **54**(5): p. 5780-5787.

28. Rulf, B., *Transmission of microwaves through layered dielectrics-Theory, experiment, and application.* American Journal of Physics, 1988. **56**(1): p. 76-80.

29. Brillouin, L., *Wave propagation and group velocity*. 1960, New York: Academic Press Inc.

30. Oughstun, K.E. and G.C. Sherman, *Electromagnetic Pulse Propagation in Causal Dielectrics*. 1994, Berlin: Springer-Verlag.

31. Loudon R., *The propagation of electromagnetic energy through an absorbing dielectric.* Journal of Physics A:General physics, 1970. **3**: p. 233-245.

32. Smith, R.L., *The Velocities of Light.* American Journal of Physics, 1970. **38**(8): p. 978-984.

33. Bloch, S.C., *Eighth velocity of light.* American Association of Physics Teachers, 1977. **45**(6): p. 538-549.

34. Bosov, N.G., R.V. Ambartsumyam, V.S. Zuer, P.G. Kryukov, and V.W. Letolshev. Dokl. Akad. Nauk SSSR, 1965. **165**(58).

35. Klapka, J.L., Czech. J. Phys., 1967. **B17**(203).

36. Mugnai, D., A. Ragfagni, and R. Ruggeri, *Path-Integral Solution of the Telegrapher equation: An Application to the Tunnelling Time Determination.* Physical Review Letters, 1992. **68**(3): p. 259-262.

37. Olum, K.D., *Superluminal travel requires negative energies.* Physical Review Letters, 1998. **81**(17): p. 3567-3570.

38. Huxley, L.G.H., in *A Survey of the Principles and Practice of Wave Guides.* 1947, University Press: Cambridge. p. 47-60.

39. Pinder, N., *Electromagnetic Barrier Penetration (unpublished).* 1998.

40. Landauer, R. and T. Martin, *Time delay in wave packet tunneling.* Solid State Communications, 1992. **84**(1/2): p. 115-117.

41. Harris, R.W. and T.J. Ledwidge, *chapter 5*, in *Introduction to Noise Analysis.* 1974, Pion Limited: London.

42. Champeney, D.C., *Some Applications*, in *Fourier Transforms in physics.* 1985, Adam Hilger Ltd. p. 24-38.

43. James, J.F., *The Discrete Fourer transform*, in *A student's guide to Fourier transforms.* 1995, Cambridge University Press: Melbourne. p. 113-114.

44. Brodowsky, H.M., W. Heitmann, and G. Nimtz, *Comparison of Experimental Microwave Tunnelling Data with Calcualtions based on Maxwell's equations.* Physics Letters [A], 1996(222): p. 125-129.

45. Bloch, S.C., *SSP: The Spreadsheet Signal Processor.* 1992, New Jersey: Prentice Hall, Inc.

46. Skolnik, M.I., *Introduction to Radar Systems.* 1962, McGraw Hill: New York. p. chapters 9 and 10.

47. Cramer, J.G., *Tunneling through the lightspeed barrier.* Analog Science Fiction & Fact, 1995. December.